Electronic Supplementary Material (ESI) for Journal of Materials Chemistry C.

SUPPORTING INFORMATION

Intramolecular Non-Covalent Interactions as a Strategy Towards Controlled Photoluminescence in Copper(I) Complexes

Georgy A. Filonenko,[†] Robert R. Fayzullin[‡] and Julia R. Khusnutdinova[*,†]

[†]Coordination Chemistry and Catalysis Unit, Okinawa Institute of Science and Technology Graduate University, 1919-1 Tancha, Onna-son, Kunigami-gun, Okinawa, 904-0495 Japan

[‡]A.E. Arbuzov Institute of Organic and Physical Chemistry, Kazan Scientific Center, Russian Academy of Sciences, Arbuzov Street, 8, Kazan 420088, Russian Federation

Corresponding author: Julia Khusnutdinova (juliak@oist.jp)

Contents

S0. General

All manipulations unless stated otherwise were performed using Schlenk or glovebox techniques under dry argon atmosphere. Anhydrous solvents were dispensed from an MBRAUN solvent purification system and degassed prior to use. Anhydrous deuterated solvents were purchased from Eurisotop and stored over 4Å molecular sieves. All chemicals unless noted otherwise were purchased from major commercial suppliers (TCI, Sigma-Aldrich and Nacalai Tesque) and used without purification. Ligand **L1**,[1] 2,11-diaza[3.3](2,6)pyridinophane (**L$_{\mathbf{NH}}$**)[2] and NaBArF (sodium tetrakis[3,5-bis(trifluoromethyl) phenyl]borate)[3] were prepared according to literature procedures. $[Cu(MeCN)_4]^+$ precursors were prepared by dissolving Cu_2O in acetonitrile solutions in the presence of aqueous HBF_4 or HPF_6 followed by two consecutive recrystallizations from cold acetonitrile.[4]

Polymer blends of complexes **4-6** were prepared by mixing saturated solution of 2-3 mg of the corresponding complex in CH_2Cl_2 with 1 mL of PMMA (poly(methyl methacrylate)) solution in CH_2Cl_2 containing ca. 100 mg of the polymer. The films were prepared from these blends by drop casting in a rectangular PTFE mold followed by drying in vacuo.

Instrumentation: NMR spectra were measured on JEOL ECZ600R 600MHz, JEOL ECZ400S 400 MHz and Bruker Avance II 400 MHz spectrometers. Full spectra are available from the Supporting Information. Electrospray Ionization Mass Spectrometry (ESI-MS) measurements were performed on a Thermo Scientific ETD apparatus. Elemental analyses were performed using an Exeter Analytical CE440 instrument.

The photoluminescence measurements in degassed dichloromethane solutions at varying concentrations were performed using a Hitachi F7000 apparatus. Absorbance spectra were collected using an Agilent Cary 60 machine. Photoluminescence lifetime measurements were performed using the second harmonics of Spectra-Physics Mai Tai pulsed laser and a Hamamatsu Photonics Streak Scope camera. The decay data were fitted with a single exponential decay function unless specified otherwise. The same laser light source equipped with a Thorlabs IS236A integrating sphere and an OceanOptics USB4000-ES spectrometer was used for quantum yield measurements in solutions (CH_2Cl_2, $c = 0.5$-1 μM) and in the solid state. The accuracy of quantum yield data was confirmed using a Hamamatsu Photonics Quantaurus-QY system that established the variations in absolute QY to be within 5% for solid and solution samples.

Cyclic voltammetry (CV) studies were performed with an ALS/CHI Electrochemical Analyzer 660E. Electrochemical grade NBu_4ClO_4 supplied by Sigma-Aldrich was used as the supporting electrolyte. Electrochemical measurements were performed under nitrogen after the sample solutions were purged with nitrogen for 10 minutes. A glassy carbon disk electrode (GCE; $d = 1.6$ mm) was used as the working electrode, and a Pt wire as the auxiliary electrode. The non-aqueous Ag-wire reference electrode assembly was filled with 0.01 M $AgNO_3$/0.1 M NBu_4ClO_4/MeCN solution. The reference electrodes were calibrated against ferrocene. The ferrocene peak separation in acetonitrile and in CH_2Cl_2 solution was 105 and 210 mV at 23 °C, respectively.

X-ray diffraction data for single crystal samples was collected on a Rigaku XtaLab PRO instrument using graphite monochromated MoKα radiation (0.71073 Å) at -180 °C. Fragments of the main residues of complexes **2**, **3** and **6** and anionic fragments in **3** and **6** were disordered and reported in full in the Supporting information. Complex **2** crystallizes as an acetonitrile solvate. Complex **3** contained two independent molecules in the asymmetric cell. Section S5 of the Supporting Information contains full experimental details regarding data collection and structure refinement.

S1. Synthesis and characterization of new compounds

Ligand **L2**:

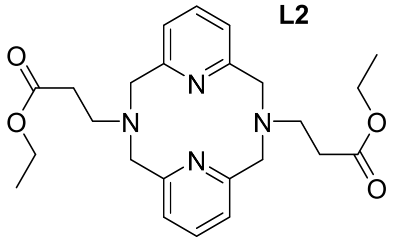

L2

2,11-diaza[3.3](2,6)pyridinophane (**L^{NH}**) (1.23 g, 5.12 mmol, 1 eq.) was suspended in 20 mL EtOH followed by 0.1 mL NEt_3 ethyl acrylate (4.1 g, ca. 20.5 mmol, 8 eq.). The mixture was heated in a sealed container for 16 h at 50 °C. The solution was concentrated to dryness and the coloured impurities were removed by pre-adsorption on silica and elution with DCM/NEt_3 (100/5). Evaporation yields 1.83 g of spectroscopically pure white solid **L2** (83%).

Characterization done at 25°C:

^{1}H NMR (400 MHz, $CDCl_3$) δ 7.05 (t, $^3J_{HH}$ = 7.6 Hz, p-H_{Py}, 1H), 6.71 (d, $^3J_{HH}$ = 7.6 Hz, m-H_{Py}, 2H), 4.20 (q, $^3J_{HH}$ = 7.1 Hz, -C(O)-C$\boldsymbol{H}_2$-CH_3, 2H), 3.88 (s, -Py-C$\boldsymbol{H}_2$-N-, 4H), 3.20 (t, $^3J_{HH}$ = 6.9 Hz, -N-C$\boldsymbol{H}_2$-CH_3-C(O)-, 2H), 2.67 (t, $^3J_{HH}$ = 6.8 Hz, -N-CH_2-C$\boldsymbol{H}_3$-C(O)-, 2H), 1.30 (t, $^3J_{HH}$ = 7.1 Hz, -C(O)-CH_2-C$\boldsymbol{H}_3$, 3H).

^{13}C NMR (101 MHz, $CDCl_3$) δ 172.82 (acyl C_q), 157.60 (Py-C_q), 135.56 (p-C_{Py}), 122.78 (p-C_{Py}), 63.75 (-C(O)-CH_2-$\boldsymbol{C}$$H_3$), 60.56 (-N-$\boldsymbol{C}$$H_2$-$CH_3$-C(O)-), 56.10 (-Py-$\boldsymbol{C}$$H_2$-N-), 33.61 (-N-$CH_2$-$\boldsymbol{C}$$H_3$-C(O)-), 14.42 (-C(O)-$\boldsymbol{C}$$H_2$-$CH_3$).

ESI-MS: Found (Calcd): $H^+ + C_{24}H_{33}N_4O_4$: 441.36 (441.25)

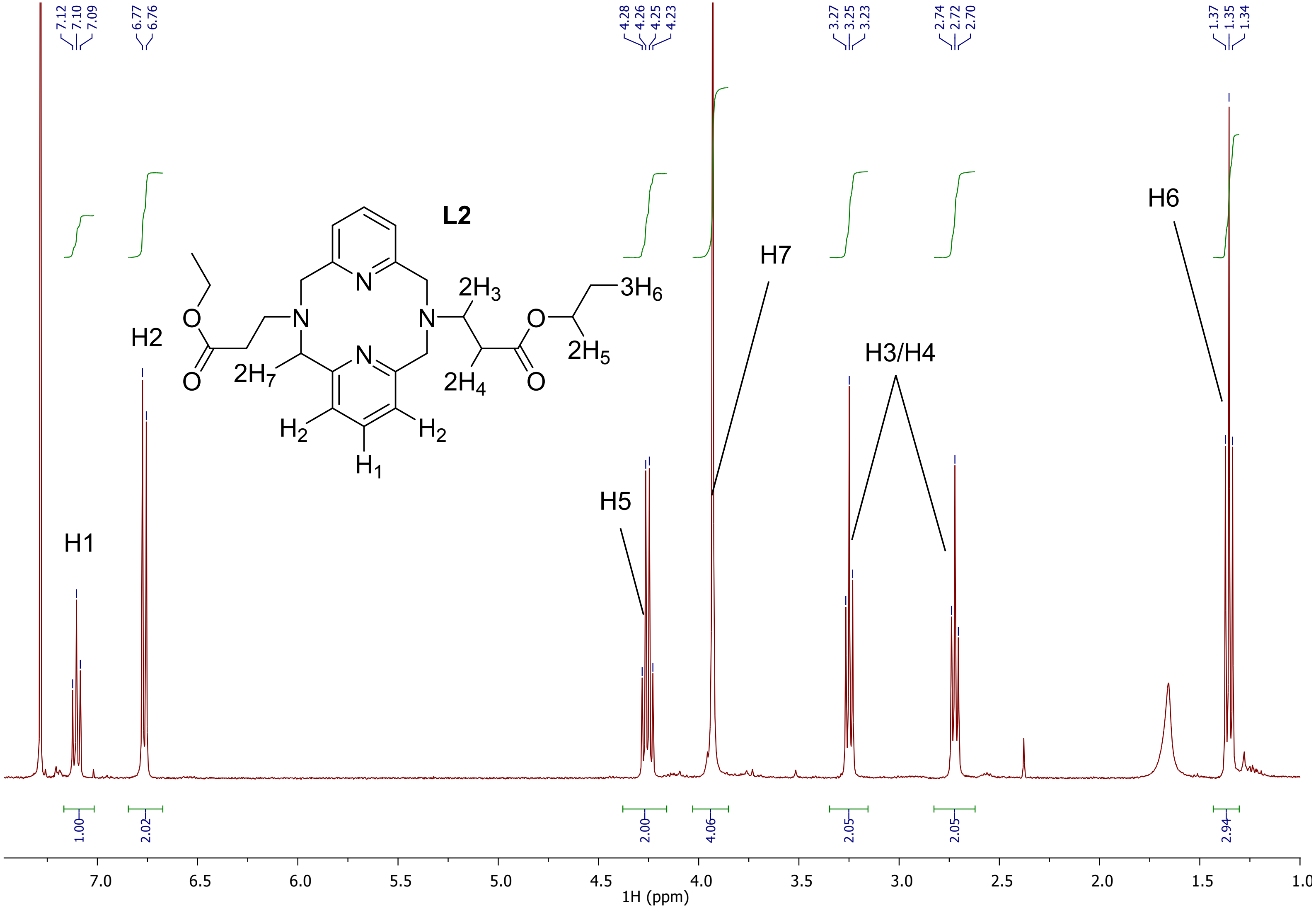

Figure S1 ^{1}H NMR spectrum of **L2** in $CDCl_3$ at 25 ^{o}C.

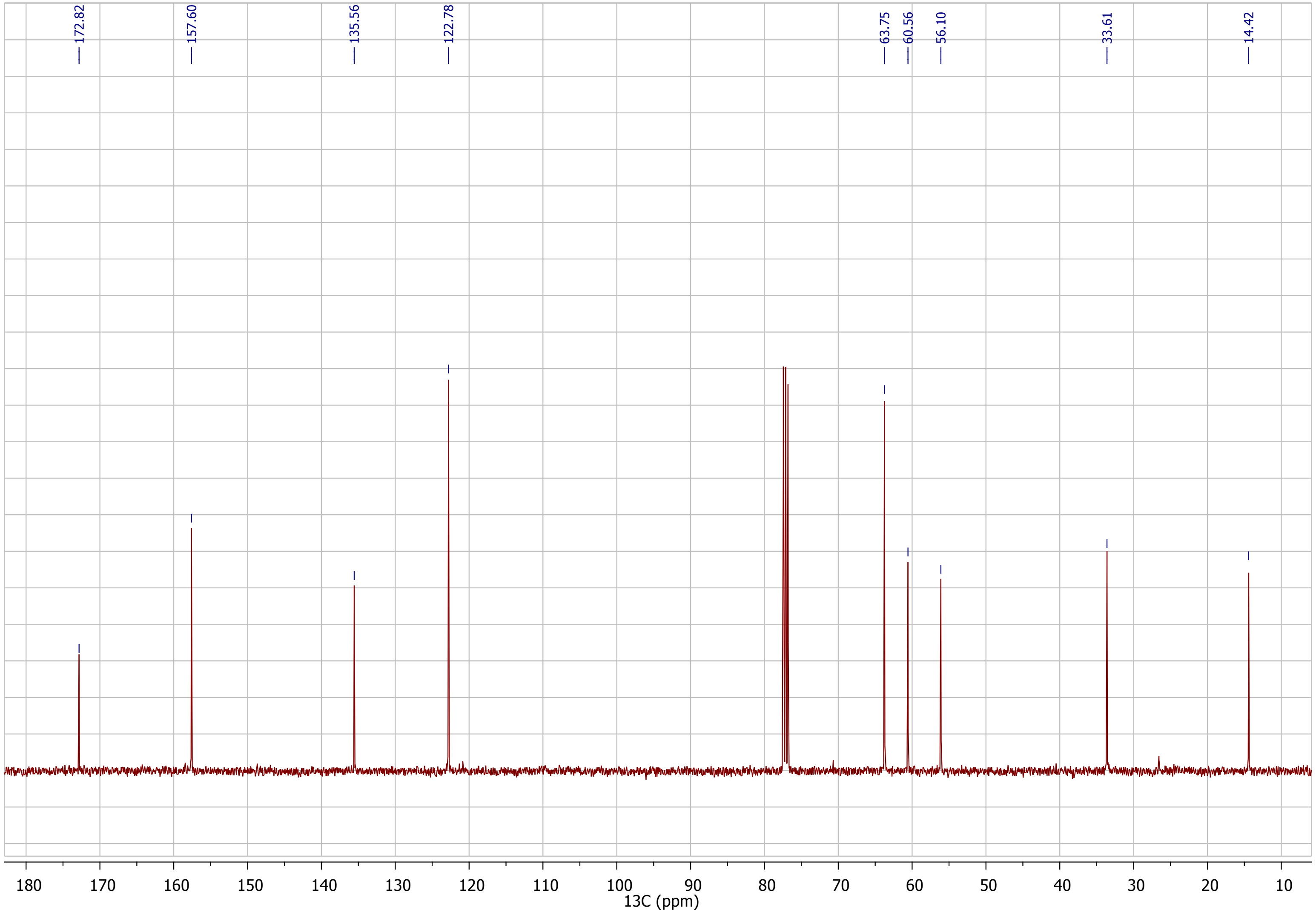

Figure S2 ^{13}C NMR spectrum of **L2** in $CDCl_3$ at 25 ^{o}C.

Ligand **L3**:

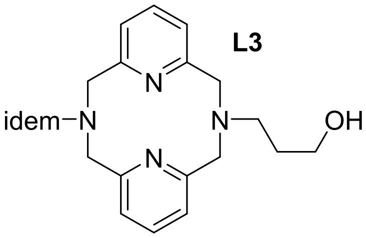

L3 was prepared from **L2**: 1.5 g of **L2** (3.41 mmol, 1eq.) in 100 mL of dry EtOH were treated with 3.081 g (81.48 mmol, 23.9 eq.) of solid sodium borohydride added in five portions. After addition the stirring continued for 30 min at 23 °C followed by a 20h incubation at 50 °C. Cooled reaction mixture was quenched with 5 mL H_2O followed by 5 mL of 0.1 M HCl. The liquid is decanted from the solid lump formed and concentrated to dryness. The residues are combined, treated with 10 mL water and few drops of 12M KOH until dissolution and the pH is then adjusted to 10-11 by addition of KOH. Extraction with $CHCl_3$ (5 X 60 mL) followed by drying and concentration to dryness yields waxy residue that solidifies upon co-evaporation with toluene. Yield 1.2 g (98.6%), pure by NMR.

Characterization done at 25°C:

^{1}H NMR (400 MHz, $CDCl_3$) δ 7.09 (t, $^3J_{HH}$ = 7.6 Hz, p-H_{Py},1H), 6.74 (d, $^3J_{HH}$ = 7.6 Hz, m-H_{Py}, 1H), 4.03 (q, $^3J_{HH}$ = 4.7 Hz, -N-CH_2-CH_2-C$\boldsymbol{H}_2$-OH,2H), 3.94 (s, 4H), 3.07 (t, $^3J_{HH}$ = 5.5 Hz, -N-C$\boldsymbol{H}_2$-CH_2-CH_2-OH,2H), 1.92 (quint, $^3J_{HH}$ = 5.3 Hz, -N-CH_2-C$\boldsymbol{H}_2$-CH_2-OH, 2H).

^{13}C NMR (101 MHz, $CDCl_3$) δ 157.08 (Py-C_q), 136.09 (p-C_{Py}), 122.09 (m-C_{Py}), 64.76 (-Py-$\boldsymbol{C}H_2$-N-), 64.46 (-N-$\boldsymbol{C}H_2$-CH_2-CH_2-OH), 60.94 (-N-CH_2-CH_2-$\boldsymbol{C}H_2$-OH), 28.95 (-N-CH_2-$\boldsymbol{C}H_2$-CH_2-OH).

ESI-MS: Found (Calcd): $H^+ + C_{20}H_{29}N_4O_2$: 357.36 (357.23)

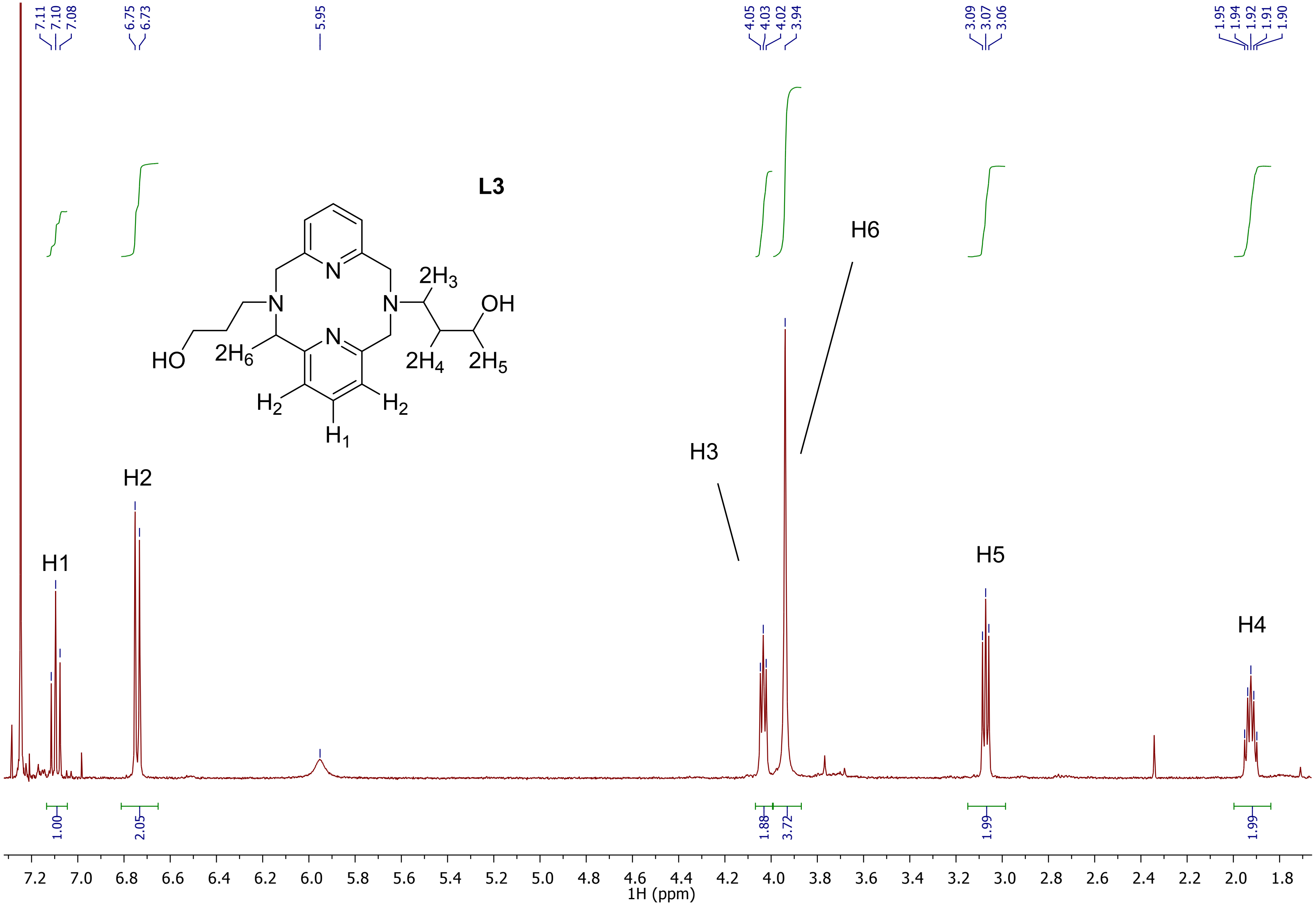

Figure S3 ^{1}H NMR spectrum of **L3** in $CDCl_3$ at 25 °C.

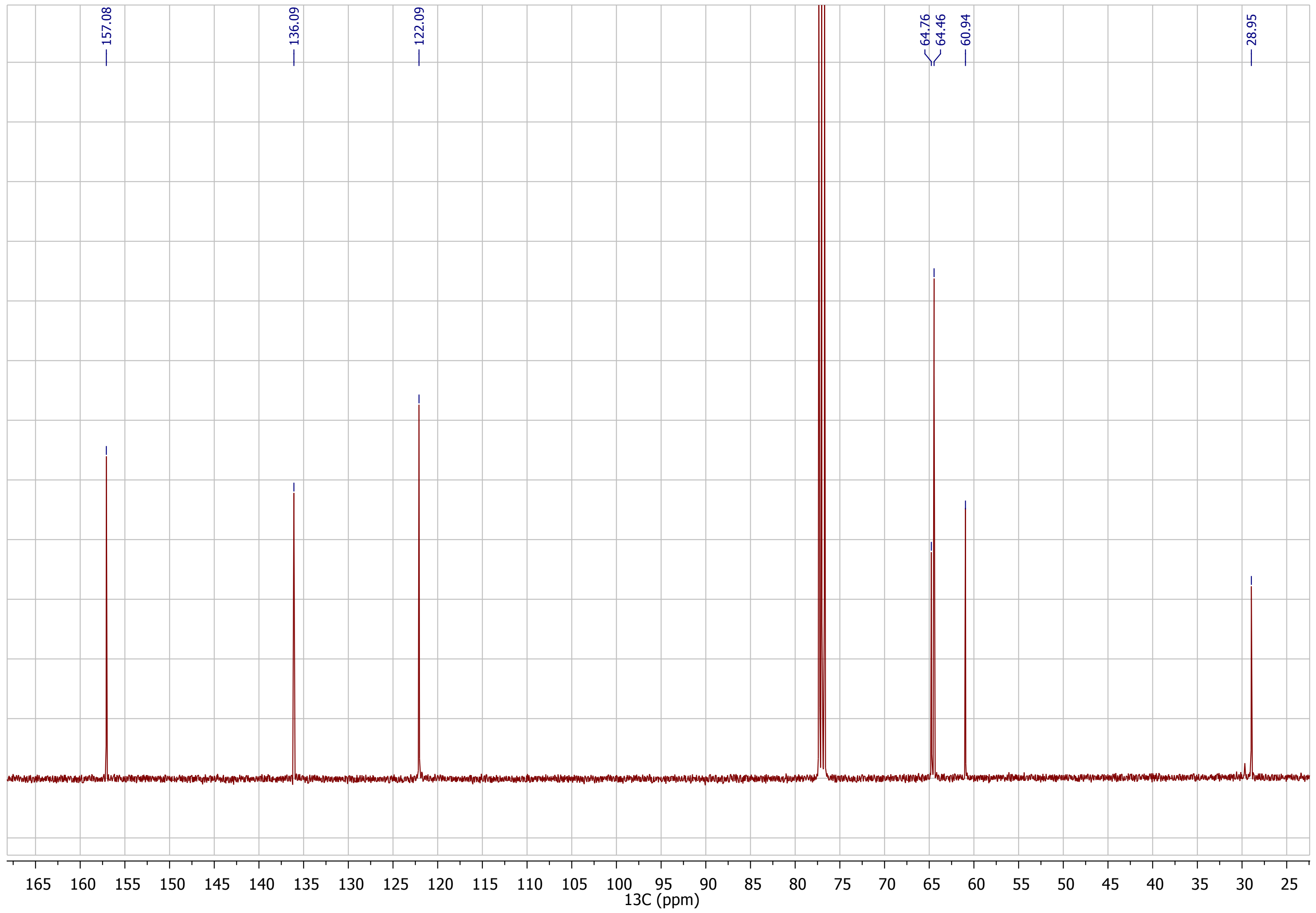

Figure S4 ^{13}C NMR spectrum of **L3** in $CDCl_3$ at 25 °C.

Complex 1 PF_6:

1 PF_6

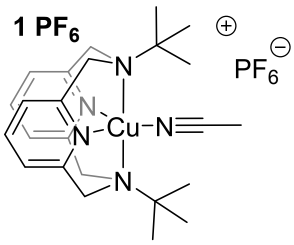

35.3 mg of **L1** (0.1 mmol, 1 eq.) in 2 mL CH_3CN were treated with 37.2 mg of $[Cu(CH_3CN)_4]PF_6$ to immediately produce red-orange solution. The stirring continued for 30 min, solution was filtered through celite plug and allowed to crystallize by ether vapour diffusion over 2 days. Orange crystals of X-ray quality were collected, washed with ether and dried in vacuum. Yield: 48.5 mg (80.5%) of analytically pure solid.

Complex **1 PF_6** is dynamic in acetonitrile at room temperature due to the presence of two conformers in which the ligand is coordinated in κ^4 and κ^3 fashion. At -5 ^{o}C, the ratio of two conformers is κ^3/κ^4=28.5/71.5. Peak assignments and NMR characterization were performed at -5 °C.

^{1}H NMR (400 MHz, -5 °C , CD_3CN) (κ^4-**L1**)Cu(MeCN)](PF_6) (κ^4-**1 PF_6**), major conformer: δ 7.32 (t, $^3J_{HH}$ = 7.7 Hz, *p*-H_{Py}, 1H), 6.77 (d, $^3J_{HH}$ = 7.7 Hz, *m*-H_{Py}, 2H), 4.50 (d, $^2J_{HH}$ = 15.3 Hz, methylene CH_2, 2H), 3.43 (d, $^2J_{HH}$ = 15.3 Hz, methylene CH_2, 2H), 1.58 – 1.32 (br s, overlap with ^{t}Bu-C$\boldsymbol{H}_3$ of k κ conformation).

[(κ^3-**L1**)Cu(MeCN)](PF_6) (κ^3-**1 PF_6**), minor conformer: δ 7.41 (t, $^3J_{HH}$ = 7.7 Hz, *p*-H_{Py}, 1H), 6.99 (d, $^3J_{HH}$ = 7.8 Hz, *m*-H_{Py}, 1H), 6.82 (d, $^3J_{HH}$ = 7.6 Hz, *m*-H_{Py}, 1H), 4.65 (overlap of doublets, methylene CH_2, 2H), 3.91 (d, $^2J_{HH}$ = 13.0 Hz, methylene CH_2, 1H), 3.61 (d, $^2J_{HH}$ = 15.2 Hz, methylene CH_2, 1H), 1.58 – 1.32 (br s, overlap with ^{t}Bu-C$\boldsymbol{H}_3$ of κ 4 conformation).

^{13}C NMR (101 MHz, -5 °C, CD_3CN): (κ^4-**L1**)Cu(MeCN)](PF_6), major conformer: δ 157.94 (quaternary C_{Py}), 137.27 (*p*-C_{Py}), 122.92 (*m*-C_{Py}), 58.08 (C_q-^{t}Bu), 57.15 (methylene *C*H_2), 26.82 (br s, *C*H_3-^{t}Bu).

[(κ^3-**L1**)Cu(MeCN)](PF_6), minor conformer: δ 159.83 (quaternary C_{Py}), 155.92 (quaternary C_{Py}), 138.17 (*p*-C_{Py}), 124.63 (*m*-C_{Py}), 122.20 (*m*-C_{Py}), 60.83 (methylene *C*H_2), 59.36 (C_q-^{t}Bu), 58.97 (methylene *C*H_2), 27.59 (*C*H_3-^{t}Bu); only one resonance was observed for C_q-^{t}Bu or *C*H_3-^{t}Bu in κ3 conformation instead of expected two resonances due to severe broadening associated with chemical exchange.

EA Found (Calcd): $C_{24}H_{35}N_5CuPF_6$: C 47.90 (47.88), H 5.80 (5.86), N 11.43 (11.63)

QY (Solid, 400 nm) 34.75%

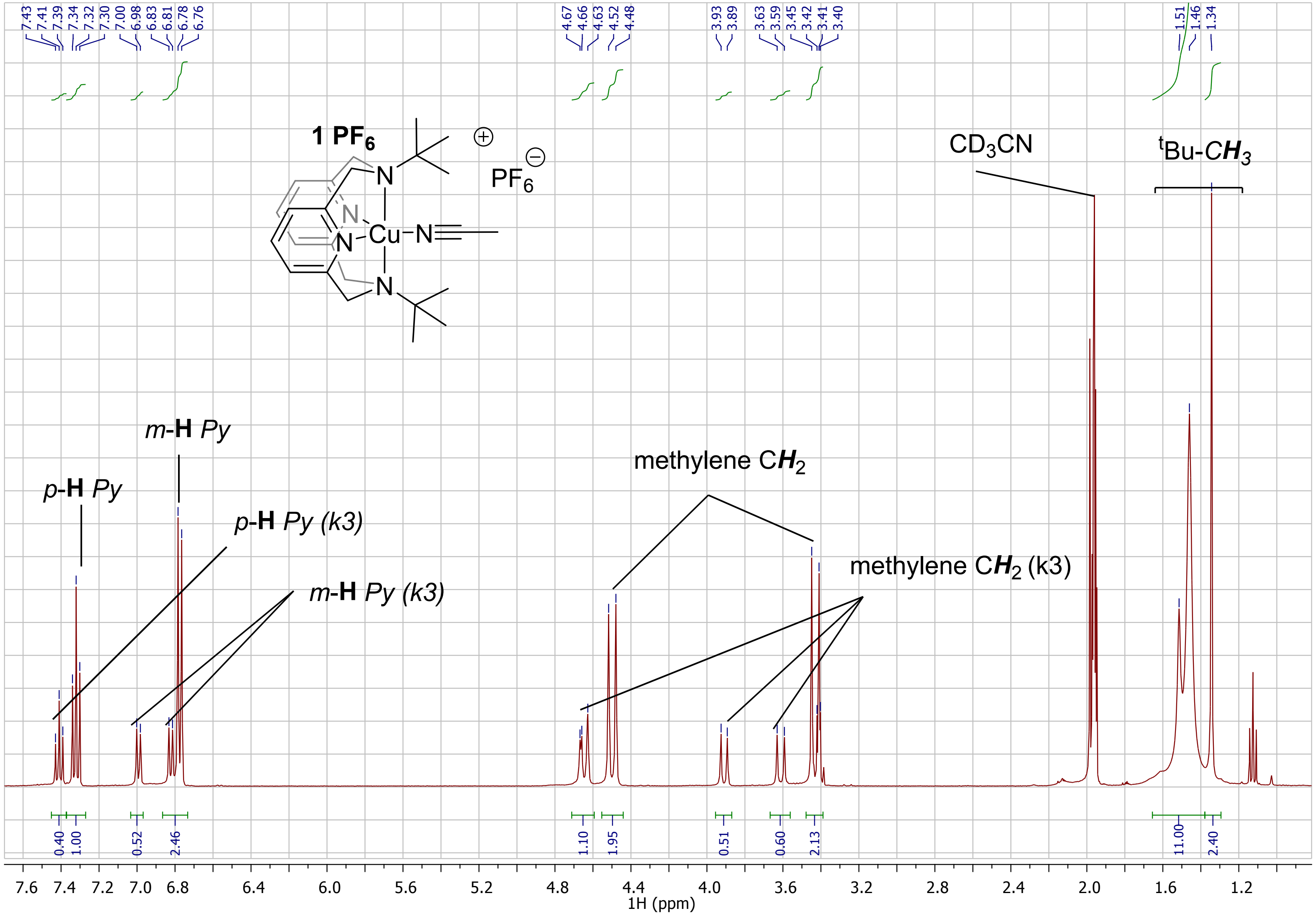

Figure S5. ^{1}H NMR spectrum of **$1PF_6$** in CD_3CN at -5 °C

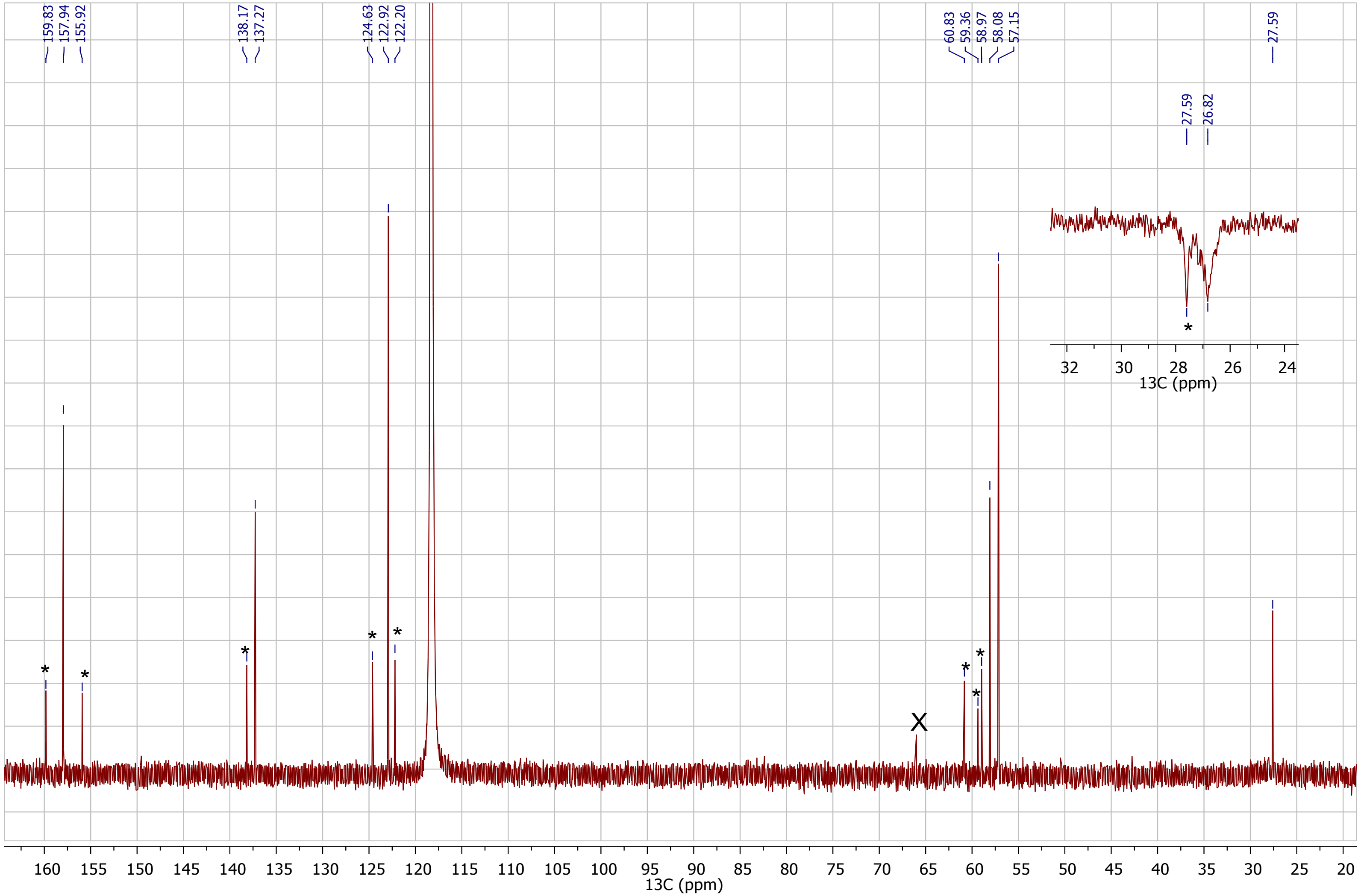

Figure S6. ^{13}C NMR spectrum of **1PF$_6$** in CD$_3$CN at -5 °C. Peaks of minor κ^3-**1 PF$_6$** conformer are labelled with an asterisk (*****), diethyl ether impurity labelled with X. An insert shows a section of DEPT 135 measurement used to detect the broadened ^{t}Bu-CH3 resonances at room temperature.

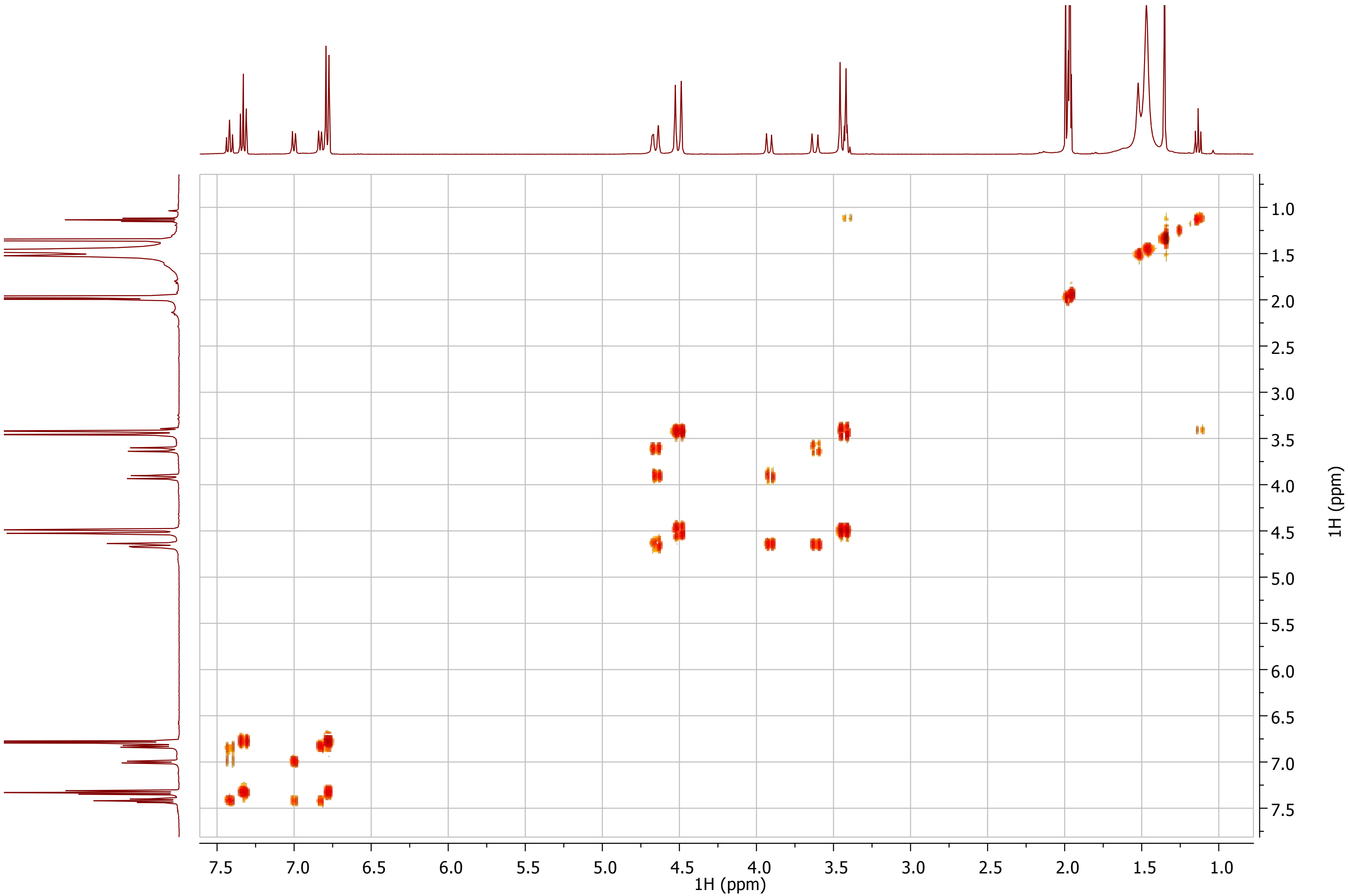

Figure S7. gCOSY spectrum of $\mathbf{1PF_6}$ in CD_3CN at -5 °C

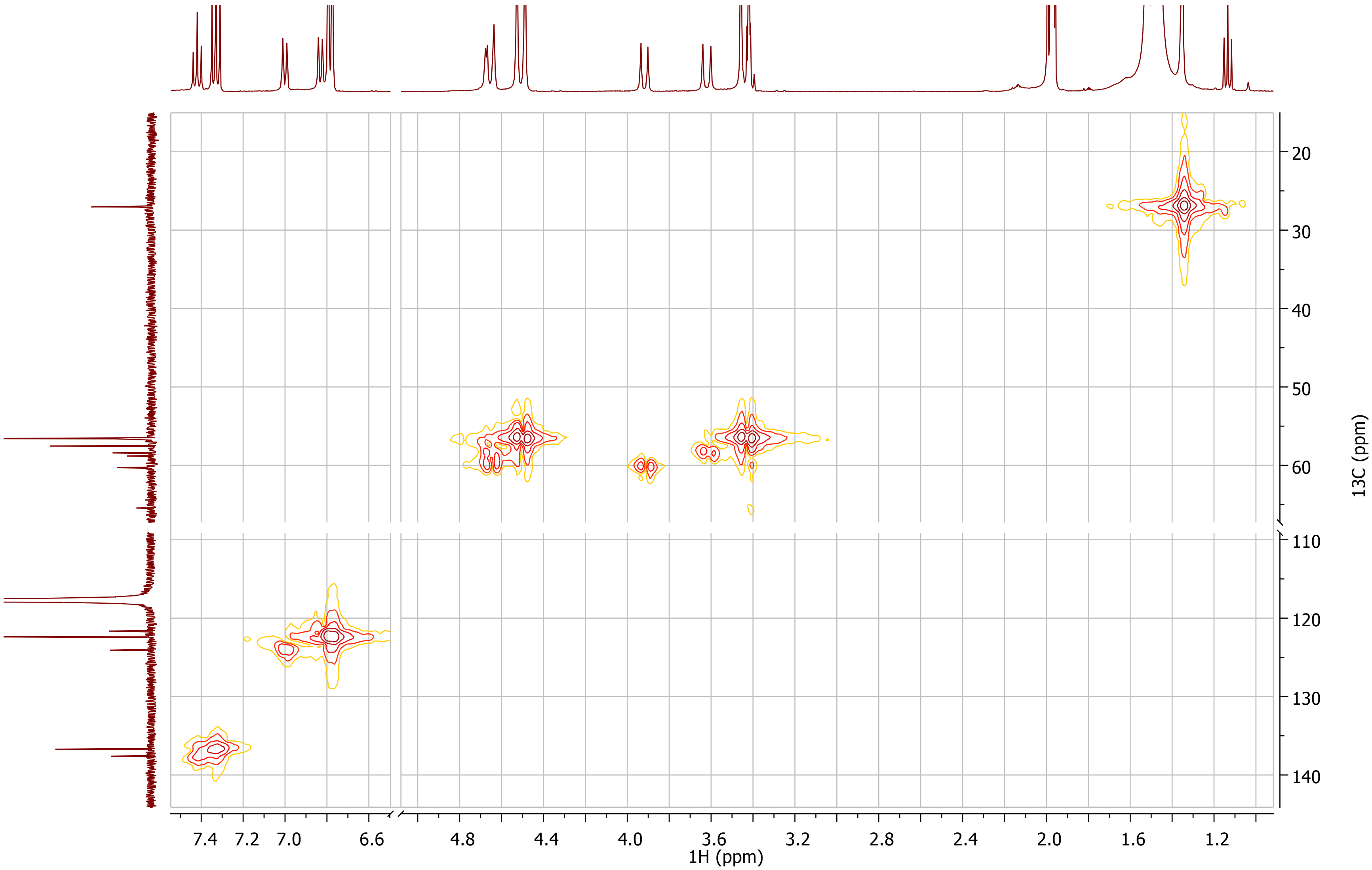

Figure S8. gHMQC spectrum of **$1PF_6$** in CD_3CN at -5 °C

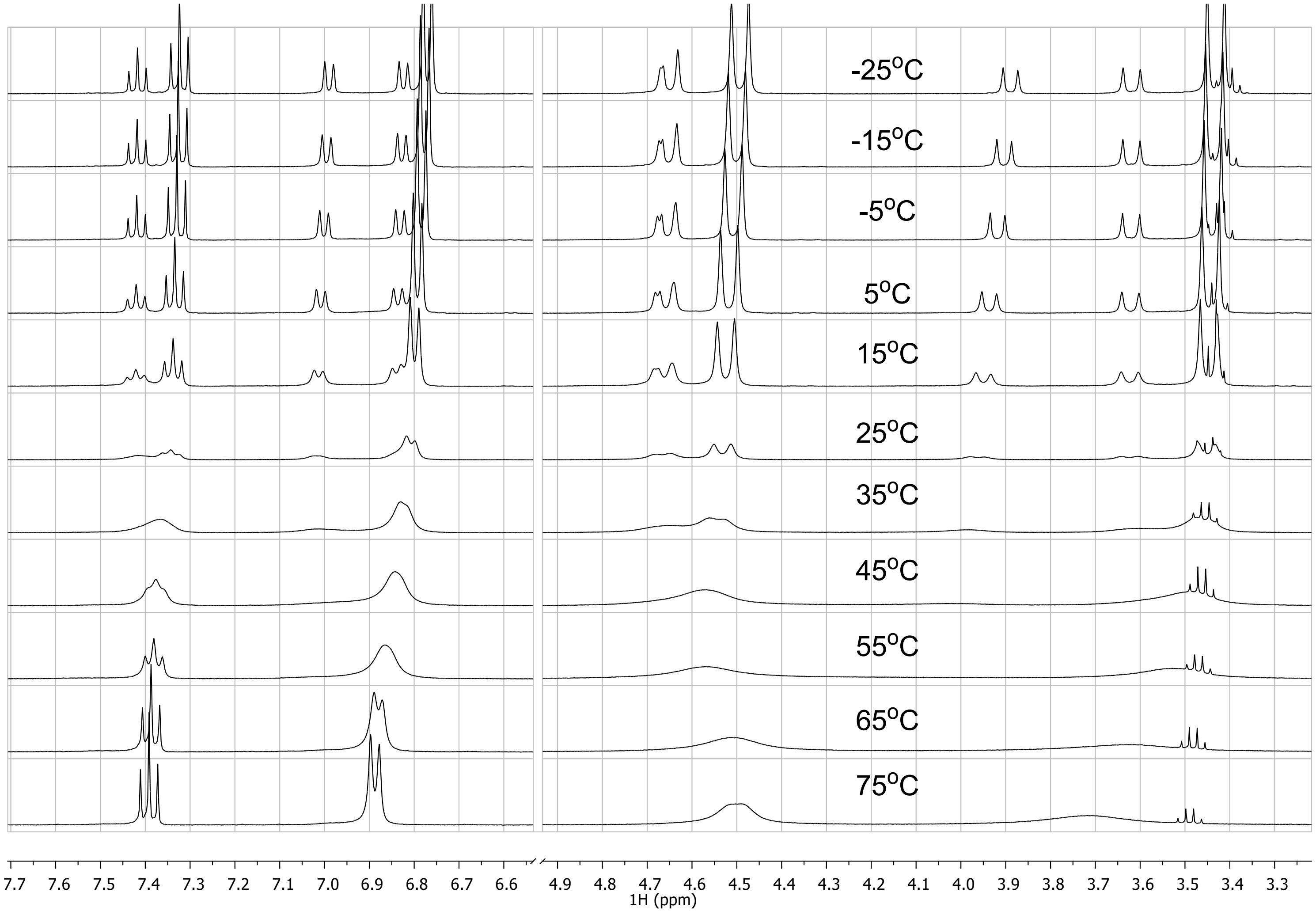

Figure S9. Section of ^{1}H VT NMR spectra of **$1PF_6$** in CD_3CN

Complex 1 BF_4:

1 BF_4

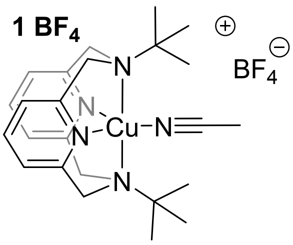

Prepared via previous procedure on the same scale in 79% yield with $[Cu(MeCN)_4](BF_4)$ precursor. Orange crystalline analytically pure solid. Due to fast exchange at 25°C, the peak assignement was performed at -30 °C. Two conformers, $[(\kappa^4$-**L1**$)Cu(MeCN)](BF_4)$ (κ^4-**1 BF_4**) and $[(\kappa^3$-**L1**$)Cu(MeCN)](BF_4)$ (κ^3-**1 BF_4**) were present in κ^3/κ^4=31.3/68.7 ratio at this temperature.

^1H NMR (600 MHz, -30 °C, CD_3CN): κ^4-**1 BF_4**, major conformer: δ 7.29 (t, $^3J_{HH}$ = 7.6 Hz, *p*-H_{Py}, 1H), 6.74 (d, $^3J_{HH}$ = 7.7 Hz, *m*-H_{Py}, 2H), 4.47 (d, $^2J_{HH}$ = 15.2 Hz, methylene CH_2, 2H), 3.40 (d, $^2J_{HH}$ = 15.3 Hz, methylene CH_2, 2H), overlap of singlet at 1.48, broad singlet at 1.43 and singlet at 1.31 (combines resonances of tBu-C$\boldsymbol{H}_3$ in both complexes).

κ^3-**1 BF_4**, minor conformer: δ 7.38 (t, $^3J_{HH}$ = 7.6 Hz, *p*-H_{Py}, 1H), 6.96 (d, $^3J_{HH}$ = 7.8 Hz, *m*-H_{Py}, 1H), 6.79 (d, $^3J_{HH}$ = 7.8 Hz, *m*-H_{Py}, 1H), 4.61 (overlap of doublets, methylene CH_2, 2x1H), 3.88 (d, $^2J_{HH}$ = 13.0 Hz, methylene CH_2, 1H), 3.58 (d, $^2J_{HH}$ = 15.2 Hz, methylene CH_2, 1H), overlap of singlet at 1.48, broad singlet at 1.43 and singlet at 1.31 (combines resonances of tBu-C$\boldsymbol{H}_3$ in both complexes).

^{13}C NMR (151 MHz, -30 °C, CD_3CN) κ^4-**1** BF_4, major conformer: δ 157.43 (quaternary C_{Py}), 136.78 (*p*-C_{Py}), 122.43 (*m*-C_{Py}), 57.58 (C_q-^tBu), 56.64 (methylene *C*H_2), 27.08 (s, *C*H_3-^tBu).

κ^3-**1 BF_4**, minor conformer: δ 159.29 (quaternary C_{Py}), 155.43 (quaternary C_{Py}), 137.69 (*p*-C_{Py}), 124.13 (*m*-C_{Py}), 121.71 (*m*-C_{Py}), 60.34 (methylene *C*H_2), 58.86 (C_q-^tBu), 58.45 (methylene *C*H_2), 28.85 (br s, *C*H_3-^tBu), only one resonance was observed for C_q-^tBu or *C*H_3-^tBu in κ3 conformation instead of expected two resonances due to severe broadening associated with chemical exchange.

EA Found (Calcd): $C_{24}H_{35}N_5CuBF_4$: C 52.84 (53.00), H 6.46 (6.49), N 12.64 (12.88)

QY (Solid, 400 nm) 30.21%

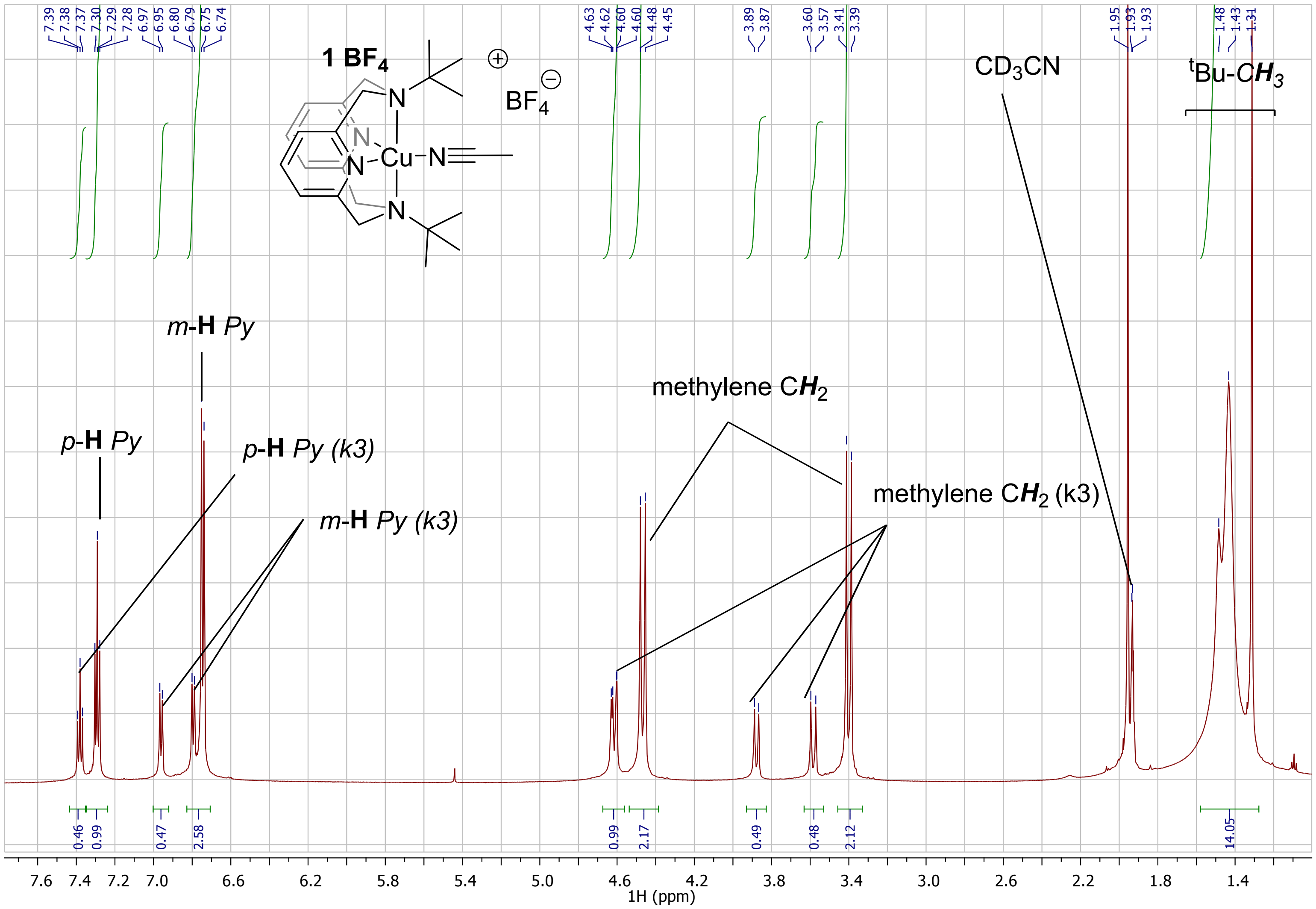

Figure S10. ^{1}H NMR spectrum of **$1BF_4$** in CD_3CN at -30 °C

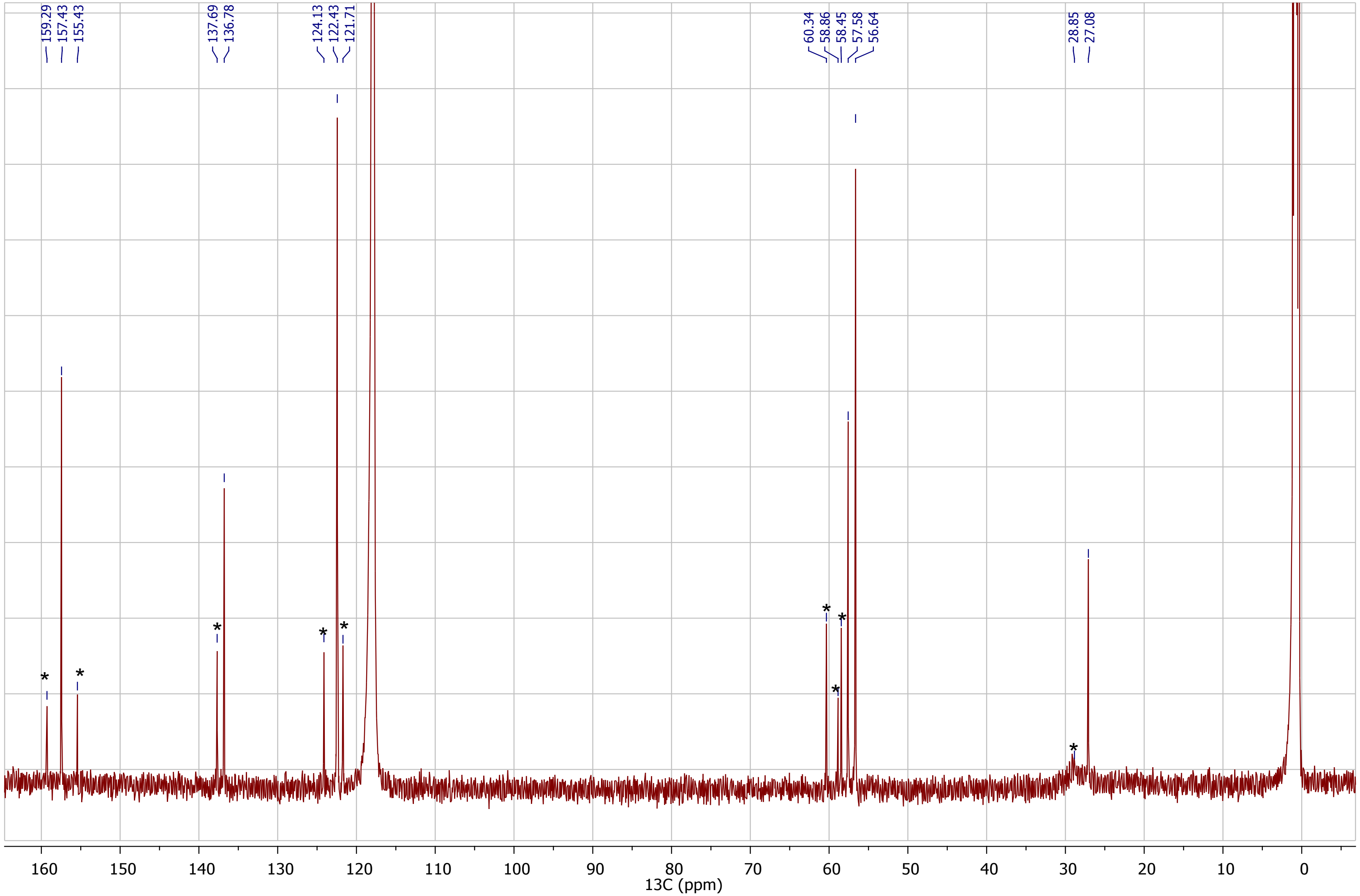

Figure S11. ^{13}C NMR spectrum of **1BF$_4$** in CD$_3$CN at -30 °C. Peaks of minor (κ^3-**1 BF$_4$**) conformer are labelled with an asterisk (*).

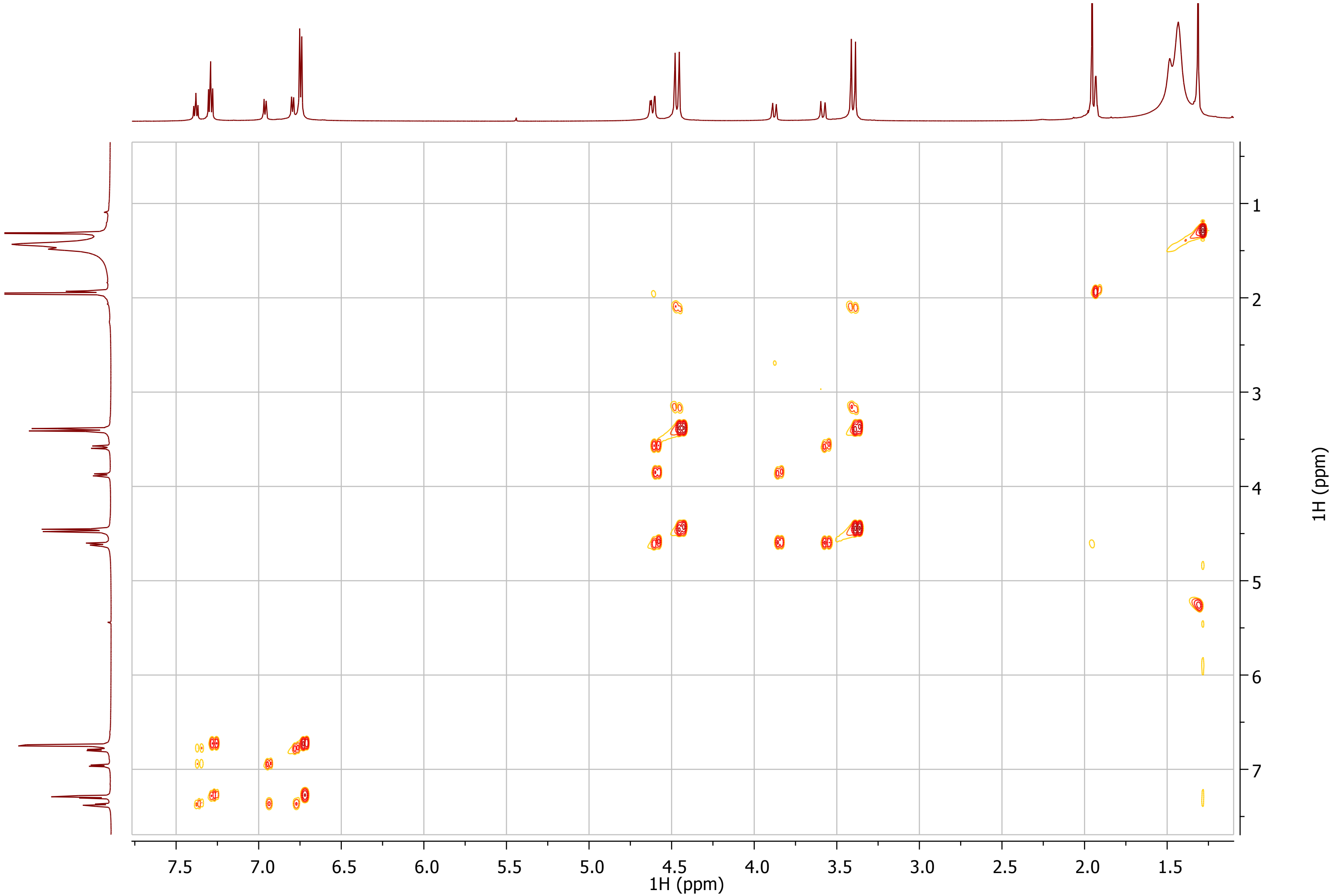

Figure S12. gCOSY spectrum of $\mathbf{1BF_4}$ in CD_3CN at -30 °C

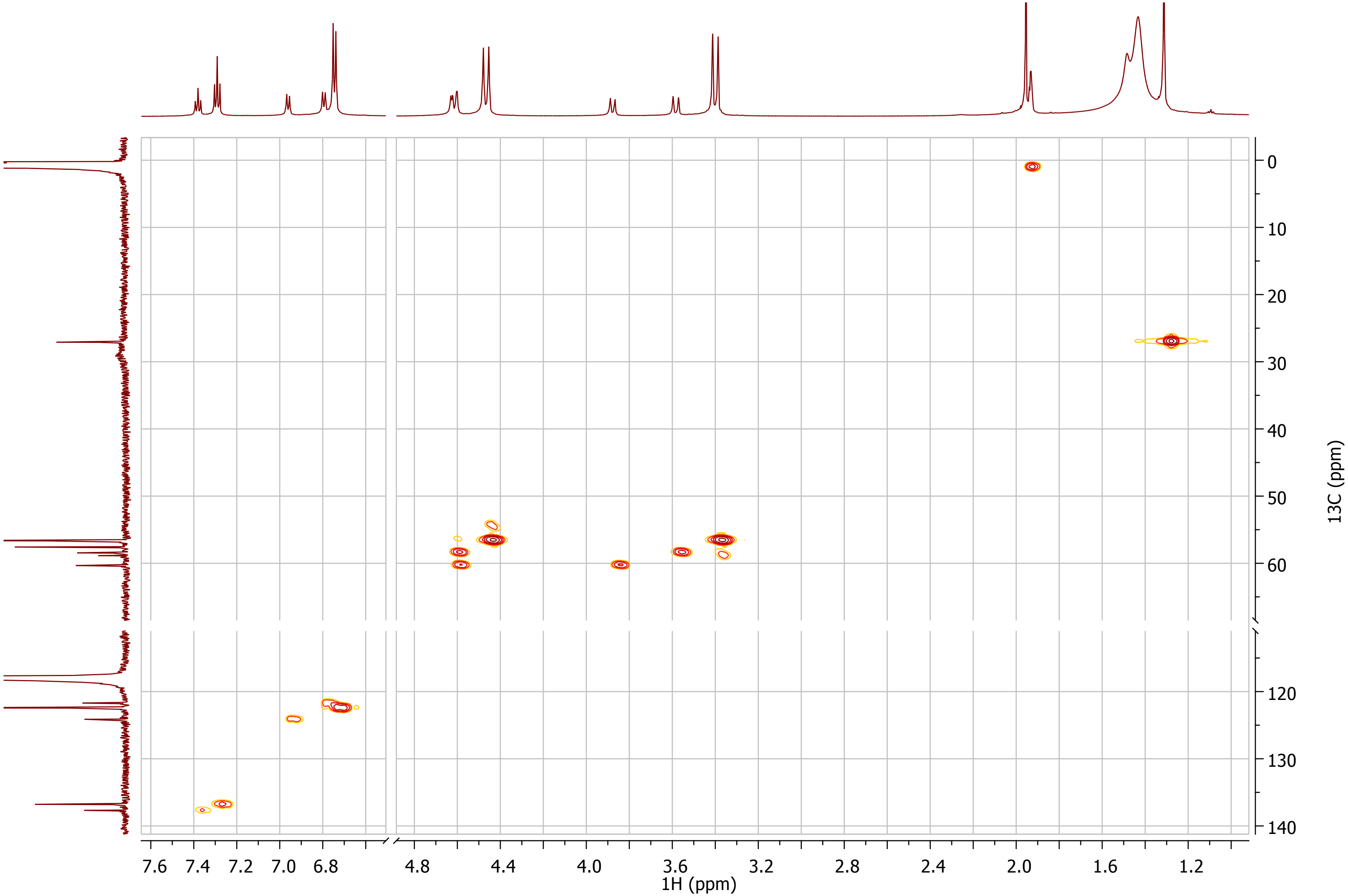

Figure S13. gHMQC spectrum of **1BF$_4$** in CD$_3$CN at -30 °C

Complex 2:

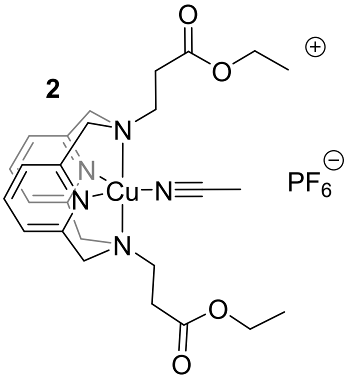

2

Identical synthetic procedure as for complexes **1** above using 3 mL CH_3CN, 100 mg of **L2** (0.227 mmol, 1 eq.) and 37.2 mg of $[Cu(CH_3CN)_4PF_6]$. Yellow crystals of X-ray quality. Yield: 127 mg (81.1%) of analytically pure solid.

Complex **2** was characterized at 23 °C.

^{1}H NMR (400 MHz, CD_3CN): δ 7.35 (t, $^3J_{HH}$ = 7.6 Hz, *p*-H_{Py}, 1H), 6.79 (d, $^3J_{HH}$ = 7.4 Hz, *m*-H_{Py}, 2H), 4.19 (q, $^3J_{HH}$ = 7.1 Hz, -C(O)-C$\boldsymbol{H}_2$-CH_3, 2H), 4.14 (d, $^2J_{HH}$ = 12.7 Hz, methylene CH_2, 2H), 3.69 (d, $^2J_{HH}$ = 15.0 Hz, methylene CH_2, 2H), 3.55 (t, $^3J_{HH}$ = 7.3 Hz, N-C$\boldsymbol{H}_2$-CH_2-C(O)R-, 2H), 2.85 (t, $^3J_{HH}$ = 7.5 Hz, N-CH_2-C$\boldsymbol{H}_2$-C(O)R-, 2H), 1.29 (t, J = 7.1, -C(O)-CH_2-C$\boldsymbol{H}_3$, 3H).

^{13}C NMR (101 MHz, CD_3CN): δ 172.95 (-C(O)-), 156.90 (quaternary C_{Py}), 137.99 (*p*-C_{Py}), 123.23 (*m*-C_{Py}), 61.85 (methylene *C*H_2), 61.38 (-C(O)-$\boldsymbol{C}H_2$-CH_3), 56.92 (N-$\boldsymbol{C}H_2$-CH_2-C(O)R-), 32.01 (N-CH_2-$\boldsymbol{C}H_2$-C(O)R-), 14.49 (-C(O)-CH_2-$\boldsymbol{C}H_3$).

EA Found (Calcd): $C_{26}H_{35}N_5O_4CuPF_6$: C 45.33 (45.25), H 5.08 (5.11), N 9.92 (10.15)

IR(ATR, cm^{-1}): υ 1722 (ester -C=O)

QY (Solid, 400 nm) 3.23%

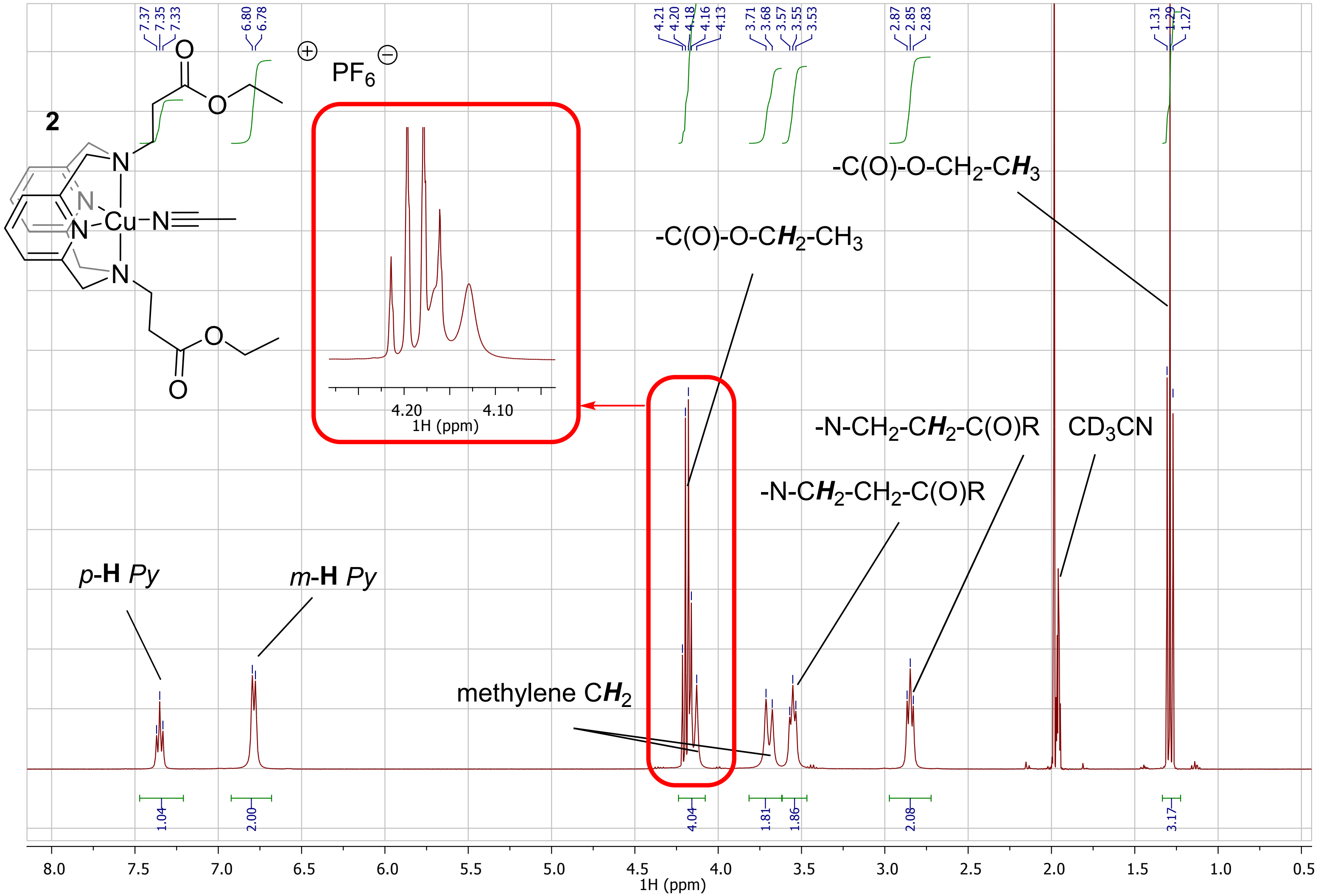

Figure S14. ^{1}H NMR spectrum of **2** in CD_3CN at 23 °C. An insert shows overlapping alkoxy and pyridilmethylenic unit resonances.

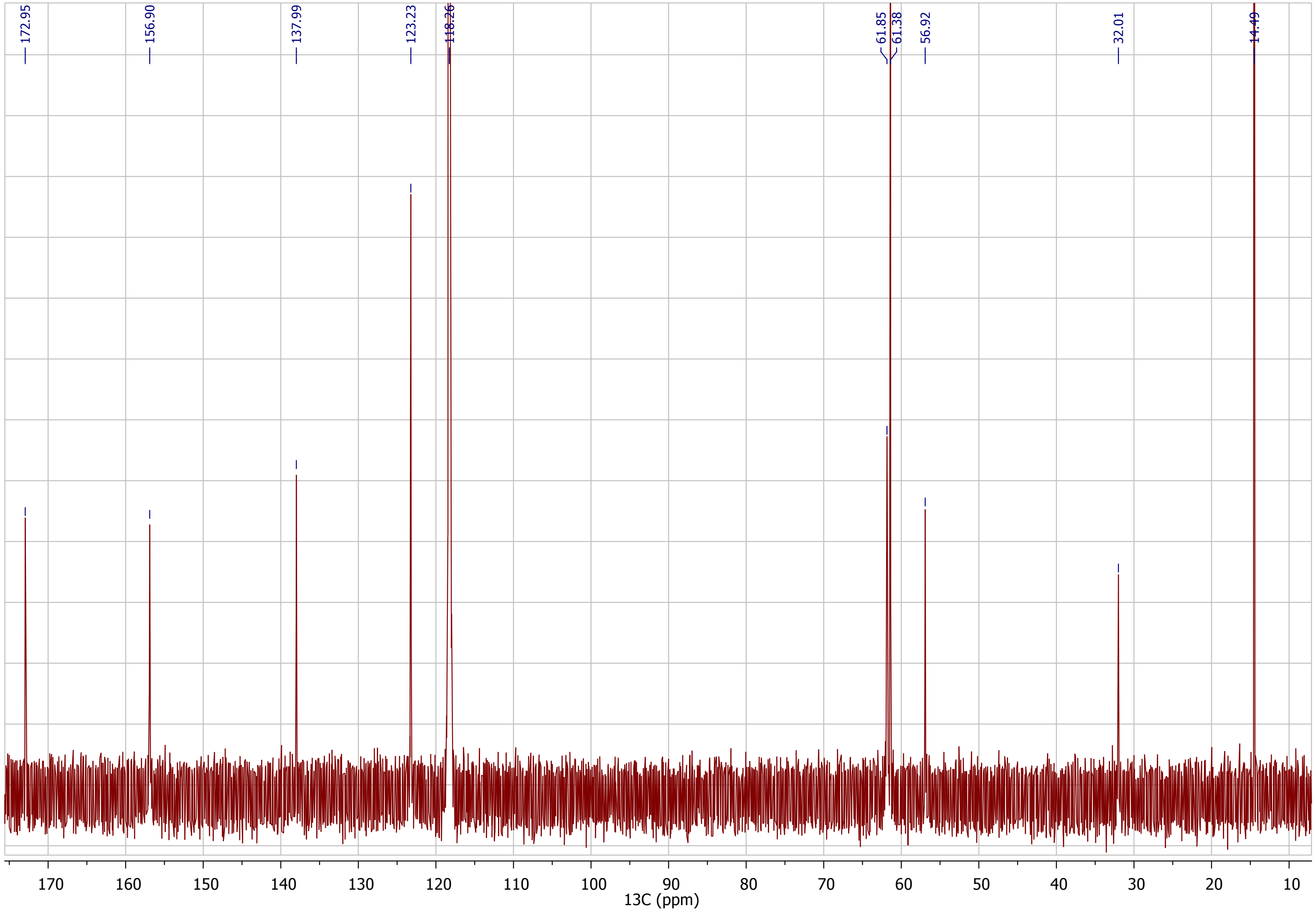

Figure S15. ^{13}C spectrum of **2** in CD_3CN at 23 °C.

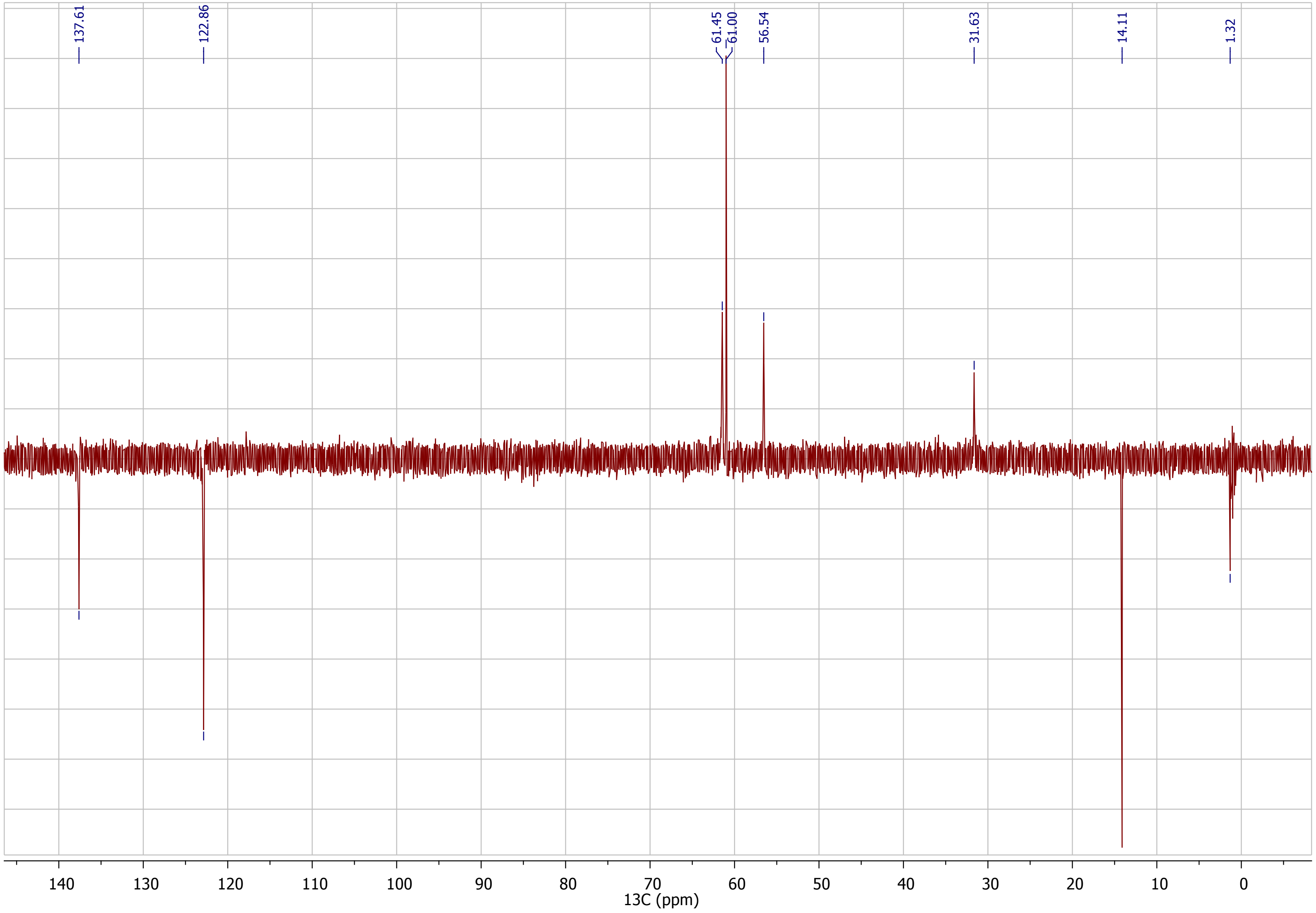

Figure S16. DEPT135 spectrum of **2** in CD_3CN at 23 °C.

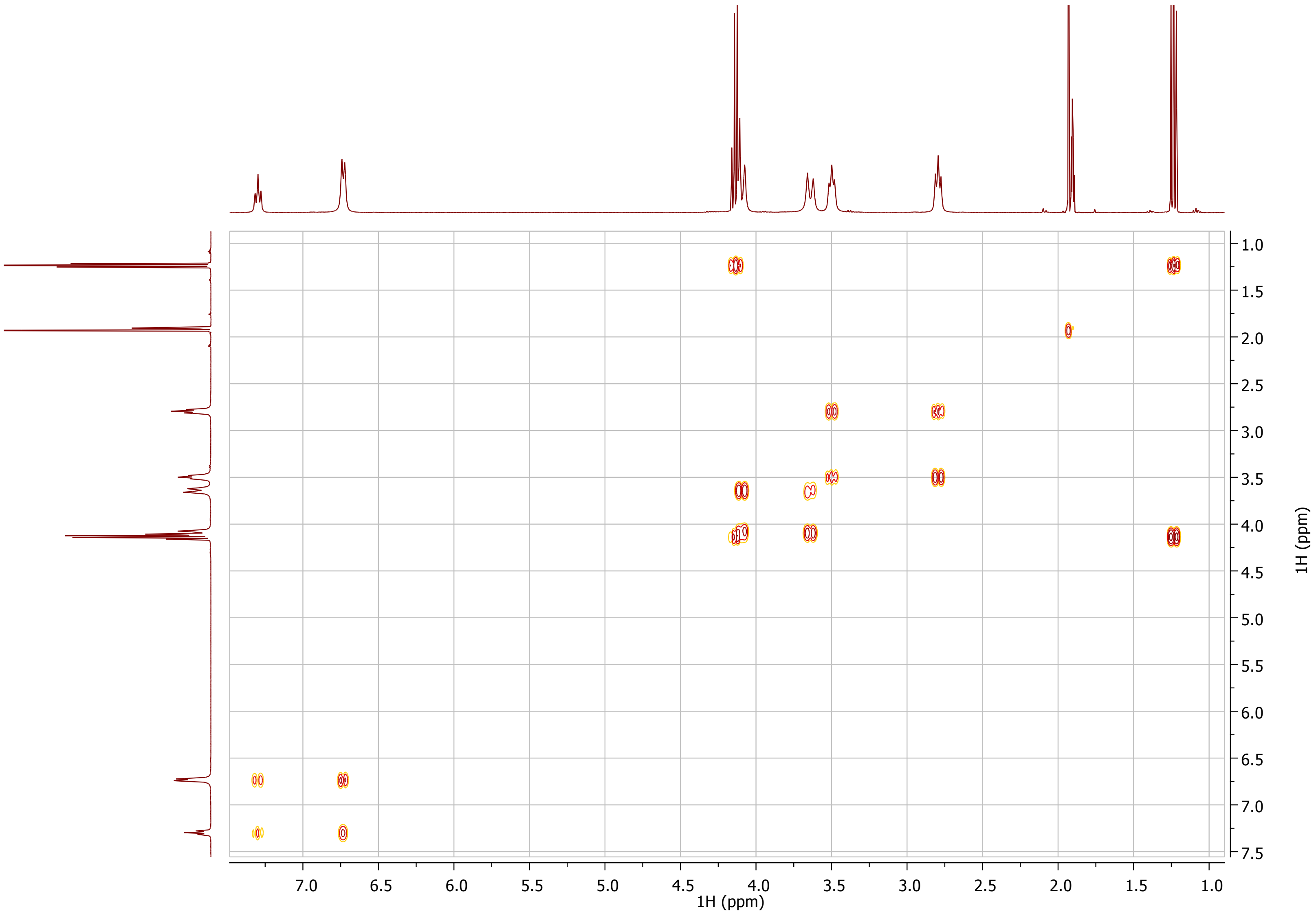

Figure S17. gCOSY spectrum of **2** in CD_3CN at 23 °C

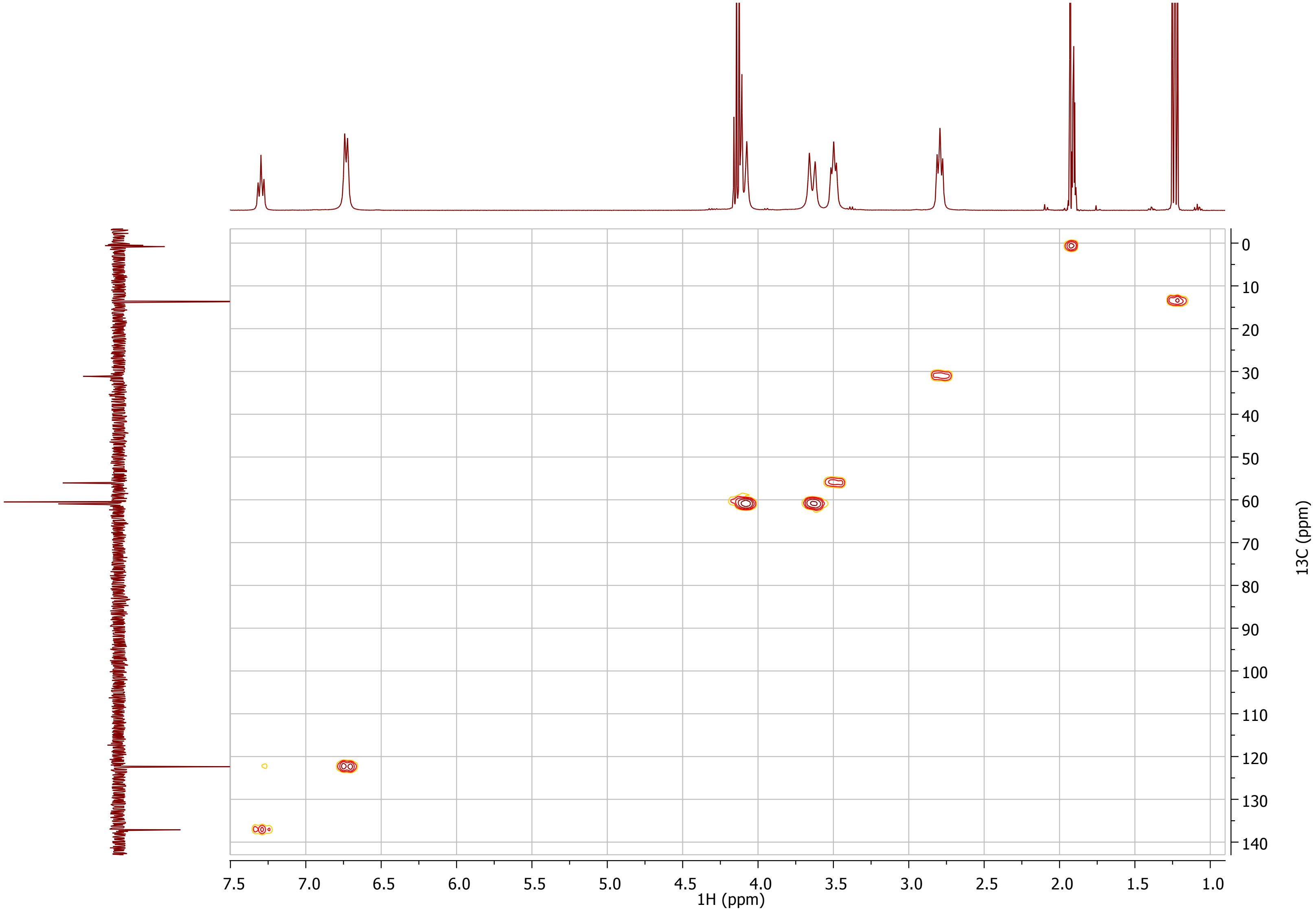

Figure S18. gHMQC spectrum of **2** in CD_3CN at 23 °C

Complex 3:

3

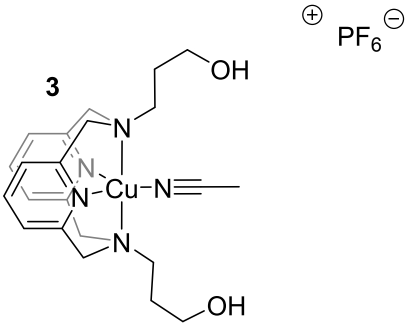

Identical synthetic procedure as for complexes **1** on the same (0.1 mmol) scale. Recrystallization from MeCN/Et$_2$O yields red-orange crystalline scales. Yield: 41 mg (67%) of analytically pure solid. The sample for X-ray diffraction prepared by recrystallization from EtOH/benzene.

^{1}H NMR (400 MHz, CD$_3$CN) δ 7.31 (t, $^3J_{HH}$ = 7.3 Hz, *p*-H$_{Py}$, 1H), 6.75 (d, $^3J_{HH}$ = 6.9 Hz, *m*-H$_{Py}$, 2H), 4.14 (d, $^2J_{HH}$ = 15.0 Hz, Py-C***H***$_2$-N, 2H), 3.64 (overlap m and d, 3H, -N-CH$_2$-CH$_2$-C***H***$_2$-OH and Py-C***H***$_2$-N,), 3.23 (m, -N-C***H***$_2$-CH$_2$-CH$_2$-OH, 2H), 2.70 (s, -CH$_2$-O***H***, 1H), 2.00 (m, -N-CH$_2$-C***H***$_2$-CH$_2$-OH, 2H).

^{13}C NMR (101 MHz, CD$_3$CN) δ 157.69 (Py-C$_q$), 138.23 (*p*-C$_{Py}$), 123.51 (*m*-C$_{Py}$), 62.74 (-Py-***C***H$_2$-N-), 61.23 (-N-***C***H$_2$-CH$_2$-CH$_2$-OH), 59.17 (-N-CH$_2$-CH$_2$-***C***H$_2$-OH), 30.53 (-N-CH$_2$-***C***H$_2$-CH$_2$-OH).

EA Found (Calcd): $C_{22}H_{31}N_5O_2CuPF_6$: C 43.77 (43.60), H 5.05 (5.16), N 11.39 (11.56)

IR(ATR, cm^{-1}): υ 3416(br, -OH, H-bonded), 3593 (-OH)

QY (Solid, 400 nm) 2.49%

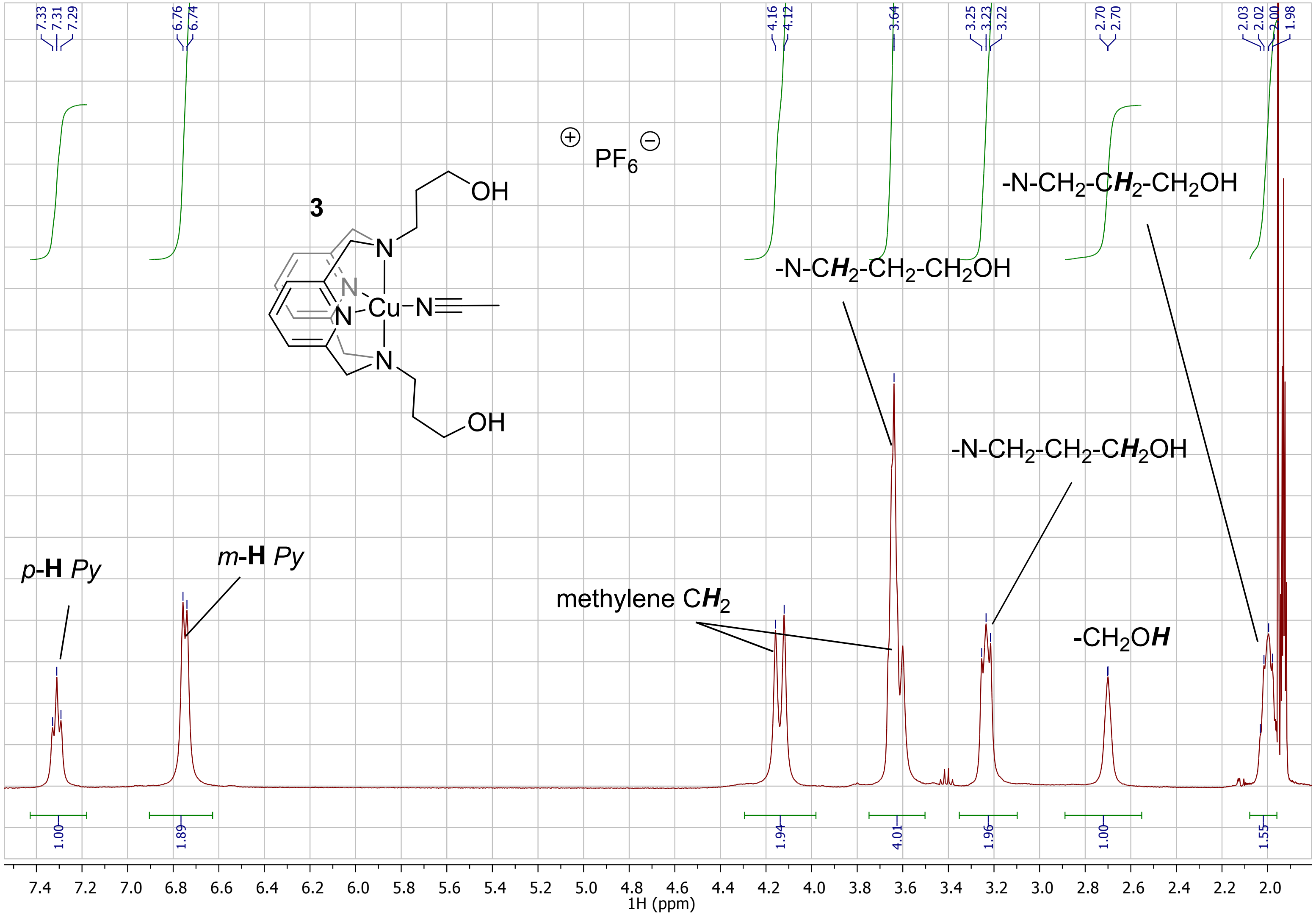

Figure S19. ^{1}H NMR spectrum of **3** in CD_3CN at 23 °C

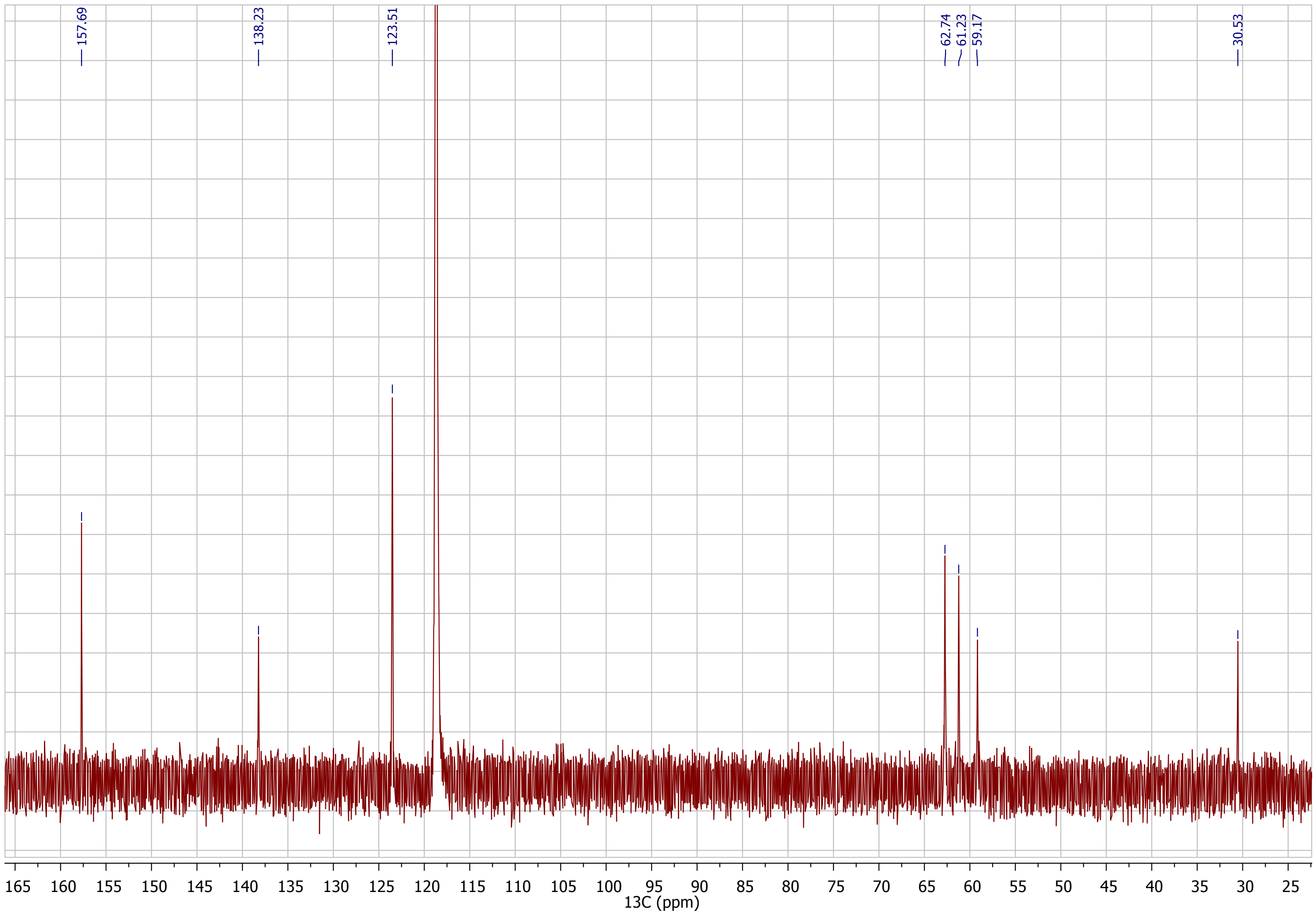

Figure S20. ^{13}C spectrum of **3** in CD_3CN at 23 °C.

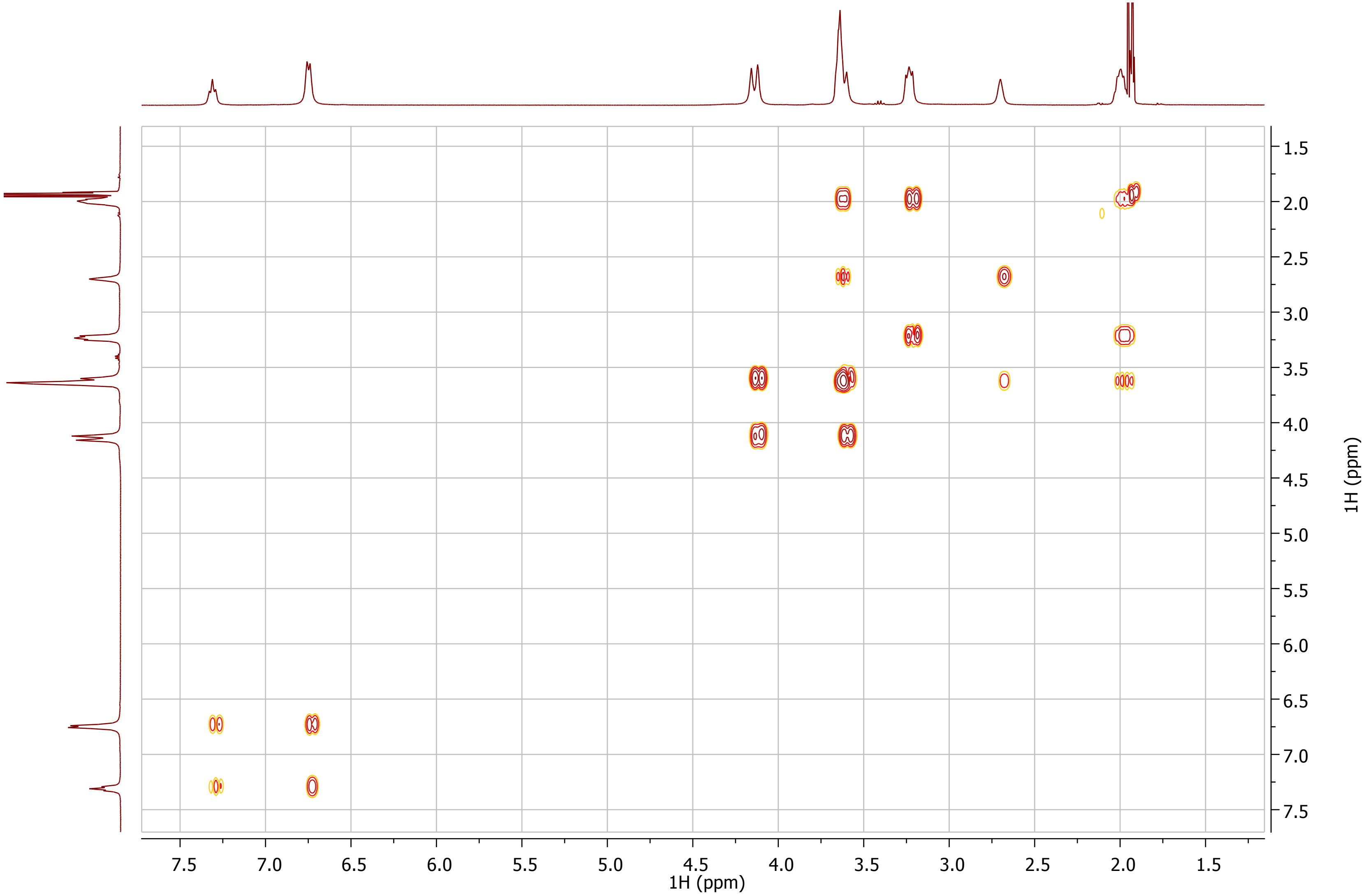

Figure S21. gCOSY spectrum of **3** in CD_3CN at 23 °C

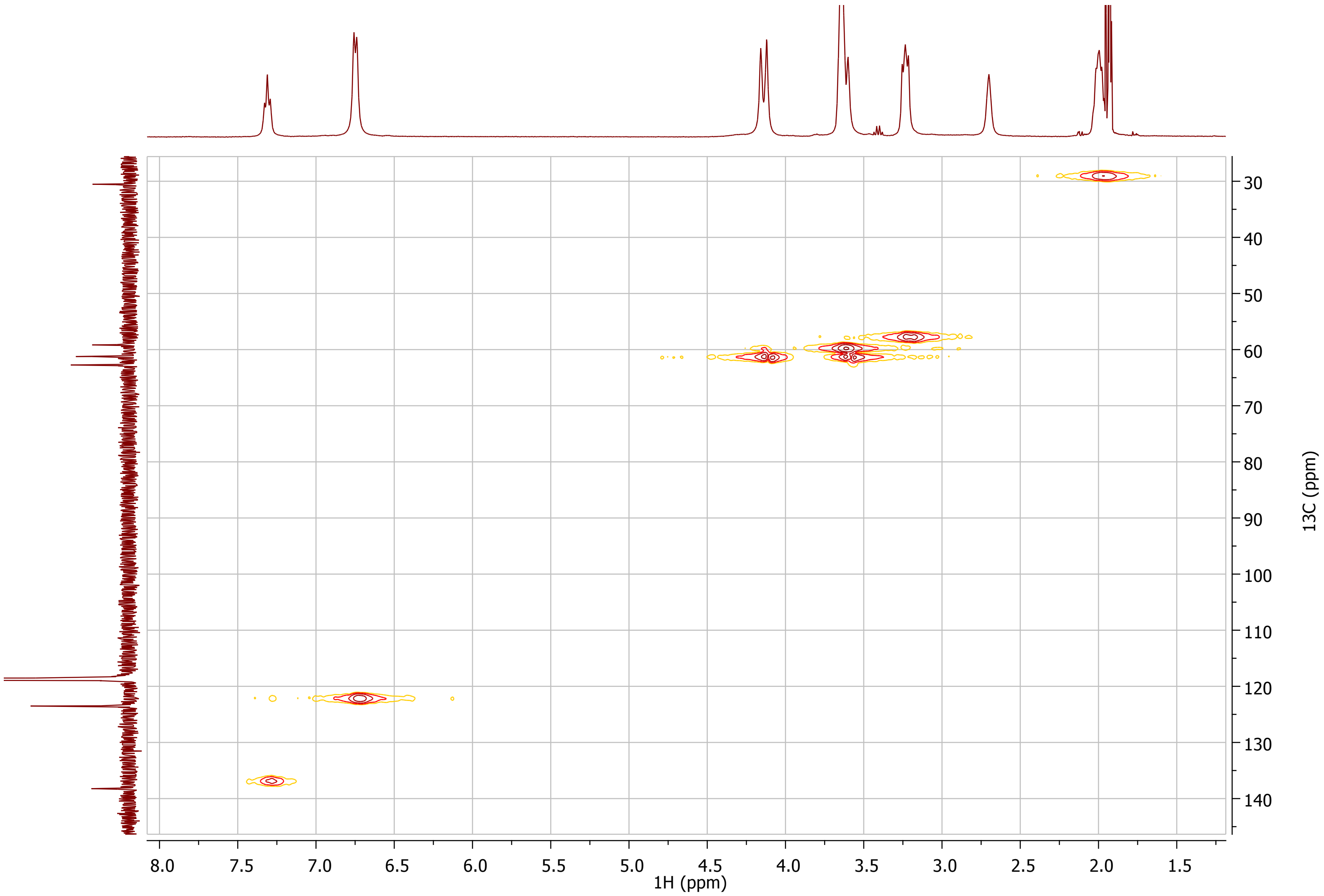

Figure S22. gHMQC spectrum of **3** in CD_3CN at 23 °C

Complex 4:

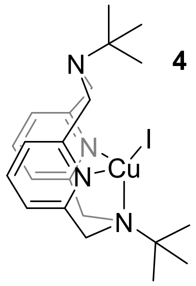

4

A vial was charged with 70.6 mg of ligand **L1** (0.200 mmol, 1 eq.) dissolved in 3 mL THF. 38 mg of CuI (0.200 mmol, 1 eq.) were added as solid and vigorously stirred reaction mixture gradually turned bright yellow. Within 10 minutes suspended solids dissolved and after 2h a crop of bright yellow solid appeared. Precipitation was completed by adding 10 mL of Et_2O, solids were separated, washed with ether and extracted with minimum CH_2Cl_2 (ca. 0.7 mL). The dichloromethane solution was passed through celite plug and allowed to crystallize by ether vapour diffusion over 20-30 hours. Bright orange crystals of X-ray quality were collected, washed with ether and dried in vacuum. Yield: 85.1 mg (78.3%).

In our hands crystalline **4** was stable under aerial conditions for at least a month with no detectible change in the ^{1}H NMR spectrum after this period of time.

In CD_2Cl_2 complex **4** features a tetragonal geometry with **L1** coordinated in a κ^3 fashion as the only detected conformer. The observed dynamics implies the absence of a conformer with κ^4-bound ligand. Possible sources of exchange in **4** include restricted rotation of ^{t}Bu group of metal-bound amine donor[5] and/or exchange between N-^{t}Bu groups of **L1** in a κ^3 conformer. The effects of chemical exchange in complex **4** are largely mitigated at -35 °C.

^{1}H NMR (600 MHz, CD_2Cl_2, -35 °C): δ 7.25 (t, $^3J_{HH}$ =7.7 Hz, *p*-H_{Py}, 1H), 6.86 (d, $^3J_{HH}$ = 7.7 Hz, *m*-H_{Py}, 1H), 6.65 (d, $^3J_{HH}$ = 7.5 Hz, *m*-H_{Py}, 1H), 4.76 (d, $^2J_{HH}$ = 12.9 Hz, methylene CH_2, 1H), 4.65 (d, $^2J_{HH}$ = 14.7 Hz, 1H), 4.30 (d, $^2J_{HH}$ = 12.7 Hz, methylene CH_2, 1H), 3.42 (d, $^2J_{HH}$ = 14.7 Hz, methylene CH_2, 1H), 1.75 (br s, ^{t}Bu-C$\boldsymbol{H}_3$, 4.5H), 1.29 (s, ^{t}Bu-C$\boldsymbol{H}_3$, 4.5H).

^{13}C NMR (151 MHz, CD_2Cl_2, -35 °C): δ 160.45 (quaternary C_{Py}), 155.04 (quaternary C_{Py}), 136.39 (*p*-C_{Py}), 123.98 (*m*-C_{Py}), 121.09 (*m*-C_{Py}), 59.03 (C_q-^{t}Bu), 58.66 (methylene *C*H_2), 57.57 (methylene *C*H_2), 56.45 (C_q-^{t}Bu), 30.32 (br s, *C*H_3-^{t}Bu), 27.70 (*C*H_3-^{t}Bu).

EA Found (Calcd): $C_{22}H_{32}N_4CuI$: C 48.19 (48.67), H 5.78 (5.94), N 10.03 (10.32)

QY (Solid, 400 nm) 78.01%

QY (Solution, 400 nm) 28.55%

QY (PMMA film, 400 nm) 28.78%

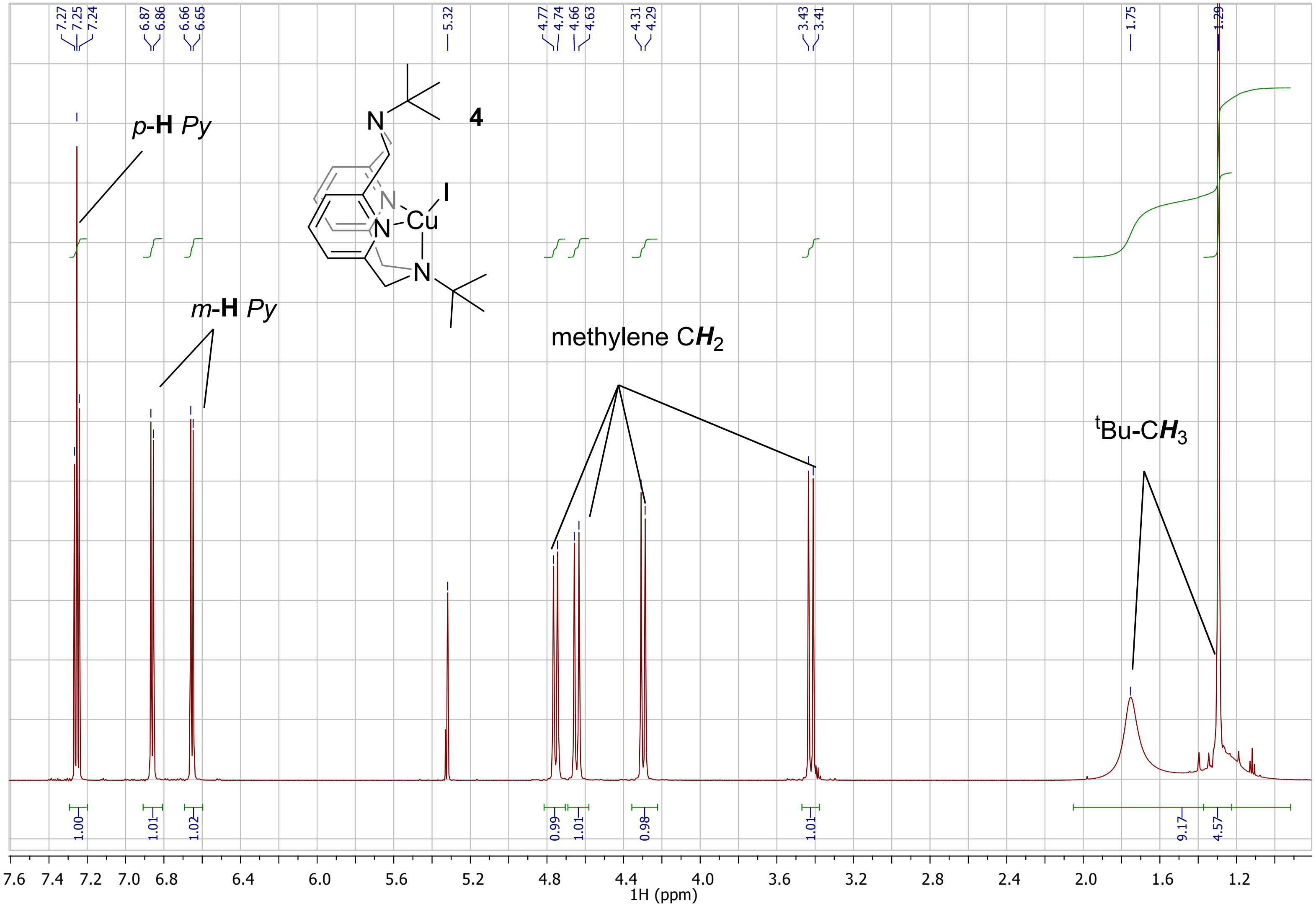

Figure S23. ^{1}H NMR spectrum of **4** in CD_2Cl_2 at -35 °C.

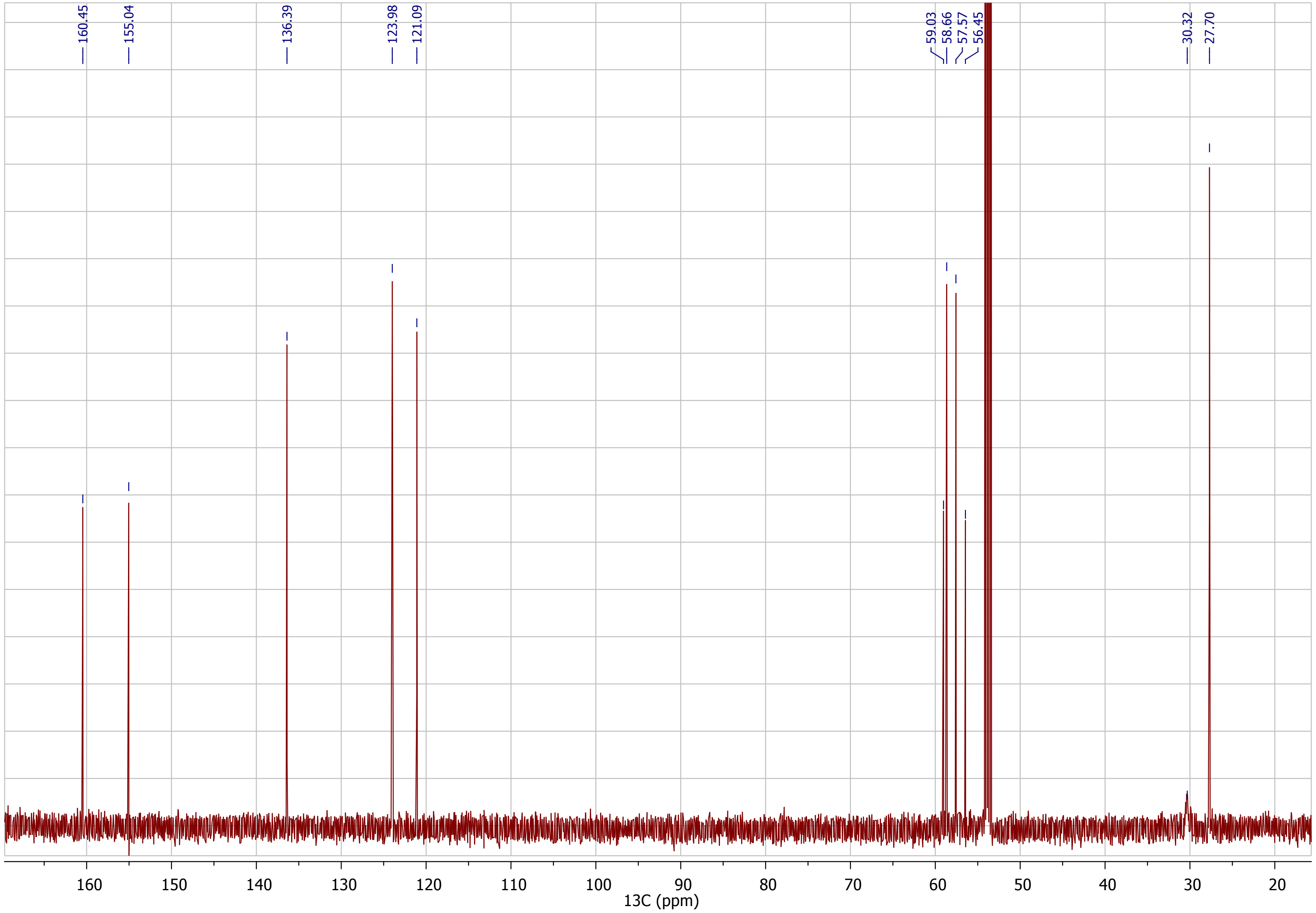

Figure S24. ^{13}C spectrum of **4** in CD_2Cl_2 at -35 °C.

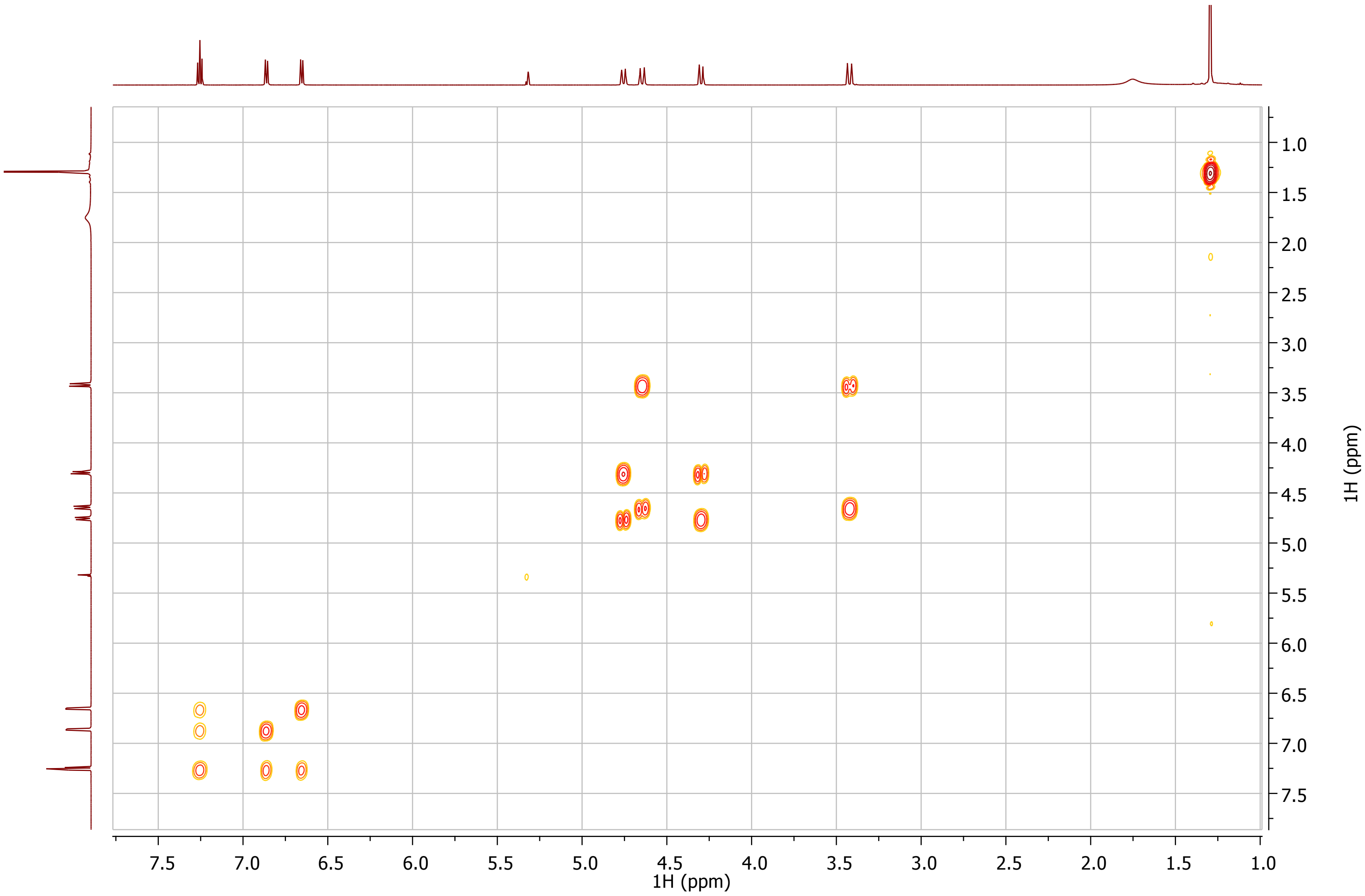

Figure S25. gCOSY spectrum of **4** in CD_2Cl_2 at -35 °C

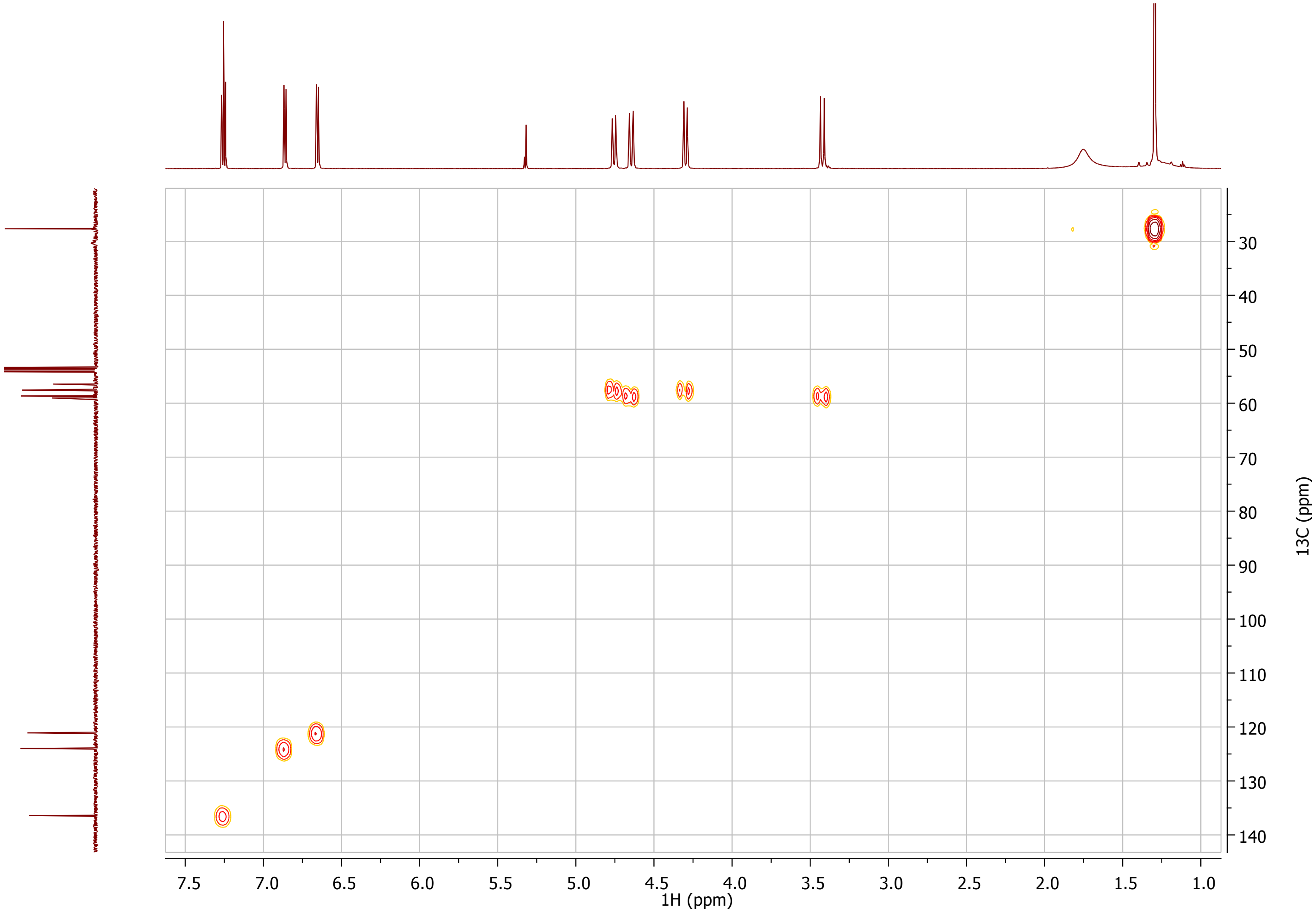

Figure S26. gHMQC spectrum of **4** in CD_2Cl_2 at -35 °C

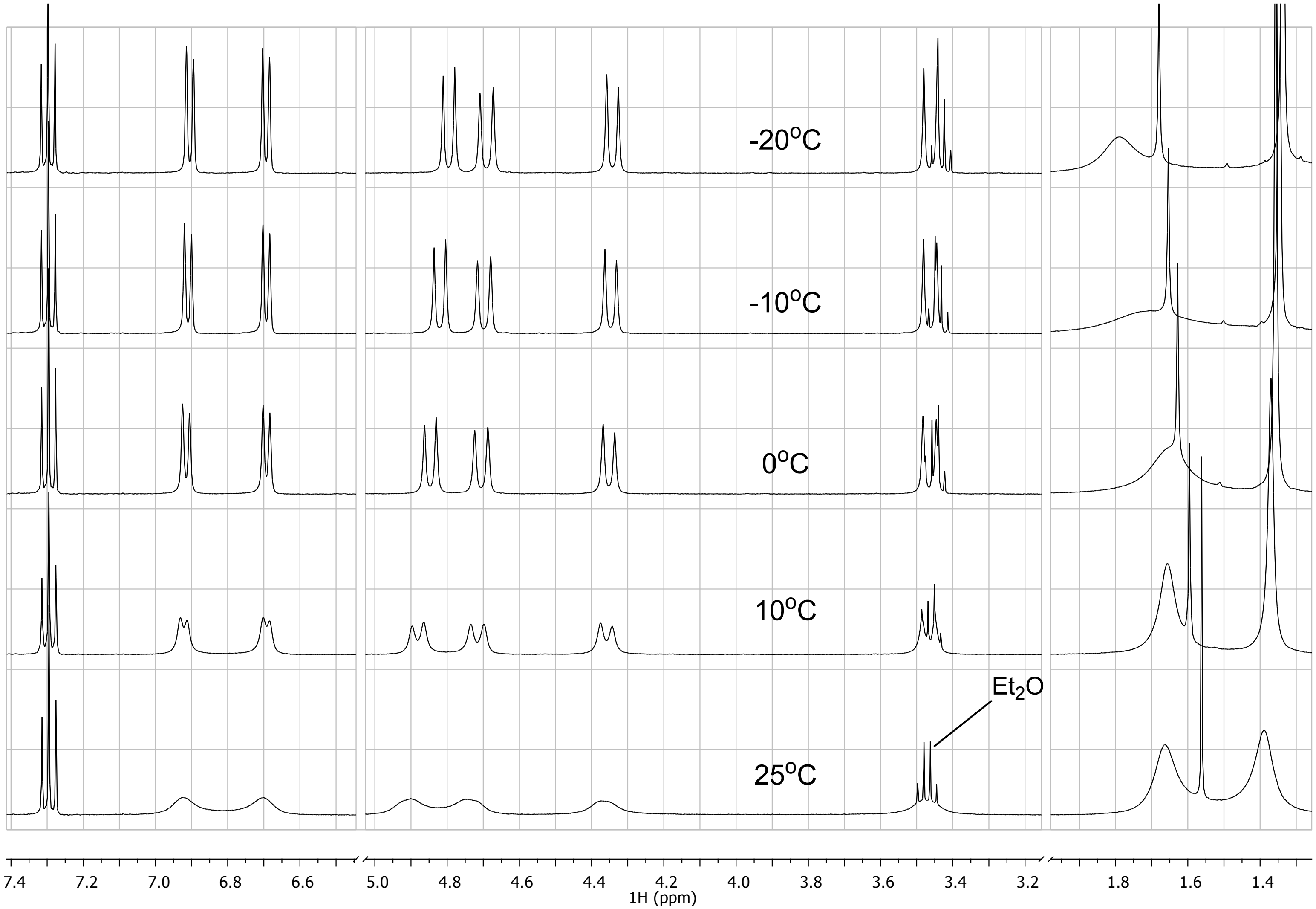

Figure S27. ^{1}H VT NMR spectra of **4** in CD_2Cl_2.

Complex 5:

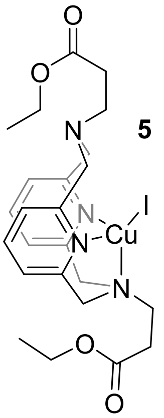

5

A vial was charged with 88.1 mg of ligand **L2** (0.200 mmol, 1 eq.) dissolved in 3 mL of THF. 38 mg of CuI (0.200 mmol, 1 eq.) were added as solid and the vigorously stirred reaction mixture gradually turned bright yellow-orange. Within 10 minutes suspended solids dissolved and the stirring was continued for 2 hours. The THF was removed in vacuum and resulting solids were extracted with minimum CH_2Cl_2 (ca. 1 mL). The dichloromethane solution was passed through celite plug and allowed to crystallize by ether vapour diffusion over several days. Yellow rod-like crystals of X-ray quality were collected, washed with ether and dried in vacuum. Yield: 108 mg (85.6%) of pure crystalline solid.

NOTE: Complex **4** is highly dynamic in CD_3CN on the NMR timescale and reacts vigorously with chloroform.

In CD_2Cl_2 complex **4** exists as a mixture of major tetragonal complex (κ^3-**L2**)CuI and minor trigonal bipyramidal complex (κ^4-**L2**)CuI similar to behaviour of **2**. Conformers of **L2** are readily distinguishable at -35 °C.

Notations are given per complex equivalent. Assignments are based on 2D homo- and heteronuclear measurements.

^{1}H NMR (600 MHz, CD_2Cl_2, -35 ^{o}C) (κ^3-**L2**)CuI: δ 7.27 (t, J = 7.7 Hz, p-H_{Py} 2H), 6.87 (d, J = 7.7 Hz, , m-H_{Py} 2H), 6.69 (d, J = 7.5 Hz, m-H_{Py}, 2H), 4.86 and 4.04 (d, J = 13.0 Hz, Py-C$\boldsymbol{H}_2$-N, each 2H), 4.29 and 3.58 (d, J = 14.7 Hz, Py-C$\boldsymbol{H}_2$-N, each 2H), 4.08 (m, overlap containing –C(O)-C$\boldsymbol{H}_2$-CH_3, 4H), 3.48 (overlap contains PyN-C$\boldsymbol{H}_2$-CH_2-C(O)-, 2H), 3.08 (m, overlap of PyN-C$\boldsymbol{H}_2$-CH_2-C(O)- and PyN-CH_2-C$\boldsymbol{H}_2$-C(O)- each 2H) 2.64 (t, J = 6.6 Hz, PyN-CH_2-C$\boldsymbol{H}_2$-C(O)-, 2H), 1.23 (m, overlap of – C(O)-CH_2-C$\boldsymbol{H}_3$, 6H).

(κ^4-**L2**)CuI: 7.19 (t, J = 7.6 Hz, 2H), 6.61 (d, J = 7.6 Hz, 2H), 4.08 (m, overlap containing –C(O)-C$\boldsymbol{H}_2$-CH_3, 4H and , Py-C$\boldsymbol{H}_2$-N, 2H), 3.51 (m, overlap contains PyN-C$\boldsymbol{H}_2$-CH_2-C(O), 2H and , Py-C$\boldsymbol{H}_2$-N, 2H), 2.81 (t, J = 7.2 Hz, PyN-CH_2-C$\boldsymbol{H}_2$-C(O), 2H), 1.23 (m, overlap contains of –C(O)-CH_2-C$\boldsymbol{H}_3$, 6H).

^{13}C NMR (101 MHz, CD_2Cl_2, -35 ^{o}C): (κ^3-**L2**)CuI: 157.53 and 154.13 (Py-C_q), 136.85 (p-C_{Py}), 124.51 (m-C_{Py}), 121.63 (m-C_{Py}), 63.77 and 63.36 (Py-$\boldsymbol{C}H_2$-N), 56.83 and 53.50 (PyN-$\boldsymbol{C}H_2$-CH_2-C(O)), 33.51 and 32.78 (PyN-CH_2-$\boldsymbol{C}H_2$-C(O)),

(κ^4-**L2**)CuI: 156.06 (Py-C_q), 136.29 (p-C_{Py}), 122.25 (m-C_{Py}), 57.67 (PyN-$\boldsymbol{C}H_2$-CH_2-C(O)), 61.27 (Py-$\boldsymbol{C}H_2$-N), 31.17 (PyN-CH_2-$\boldsymbol{C}H_2$-C(O))

Groups of resonances that cannot be assigned accurately to specific conformation

1) 172.80, 172.62 and 172.11 belonging to quaternary carbons of carboxylic group
2) 61.02, 60.87 and 60.68 belonging to –C(O)-$\boldsymbol{C}H_2$-CH_3 unit

3) 14.30, 14.17 and 14.14 belonging to –C(O)-CH$_2$-$\boldsymbol{C}$H$_3$ unit

EA Found (Calcd): $C_{22}H_{32}N_4O_4CuI$: C 45.38 (45.68), H 4.95 (5.11), N 8.60 (8.88)

IR(ATR, cm^{-1}): υ 1718 (ester -C=O)

QY (Solid, 400 nm) 7.67%

QY (PMMA film, 400 nm) 8.51%

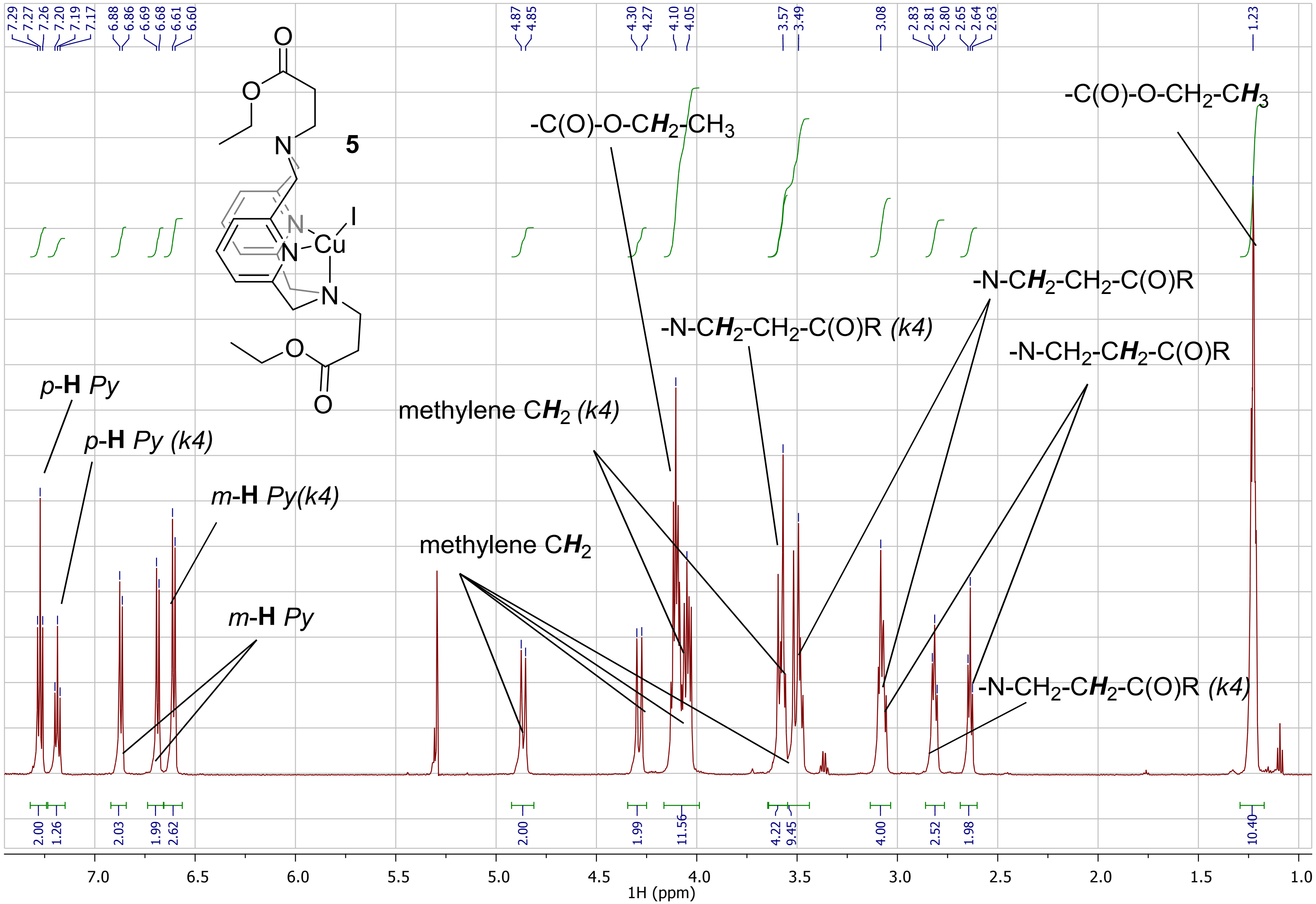

Figure S28. ^{1}H NMR spectrum of **5** in CD_2Cl_2 at -35 °C.

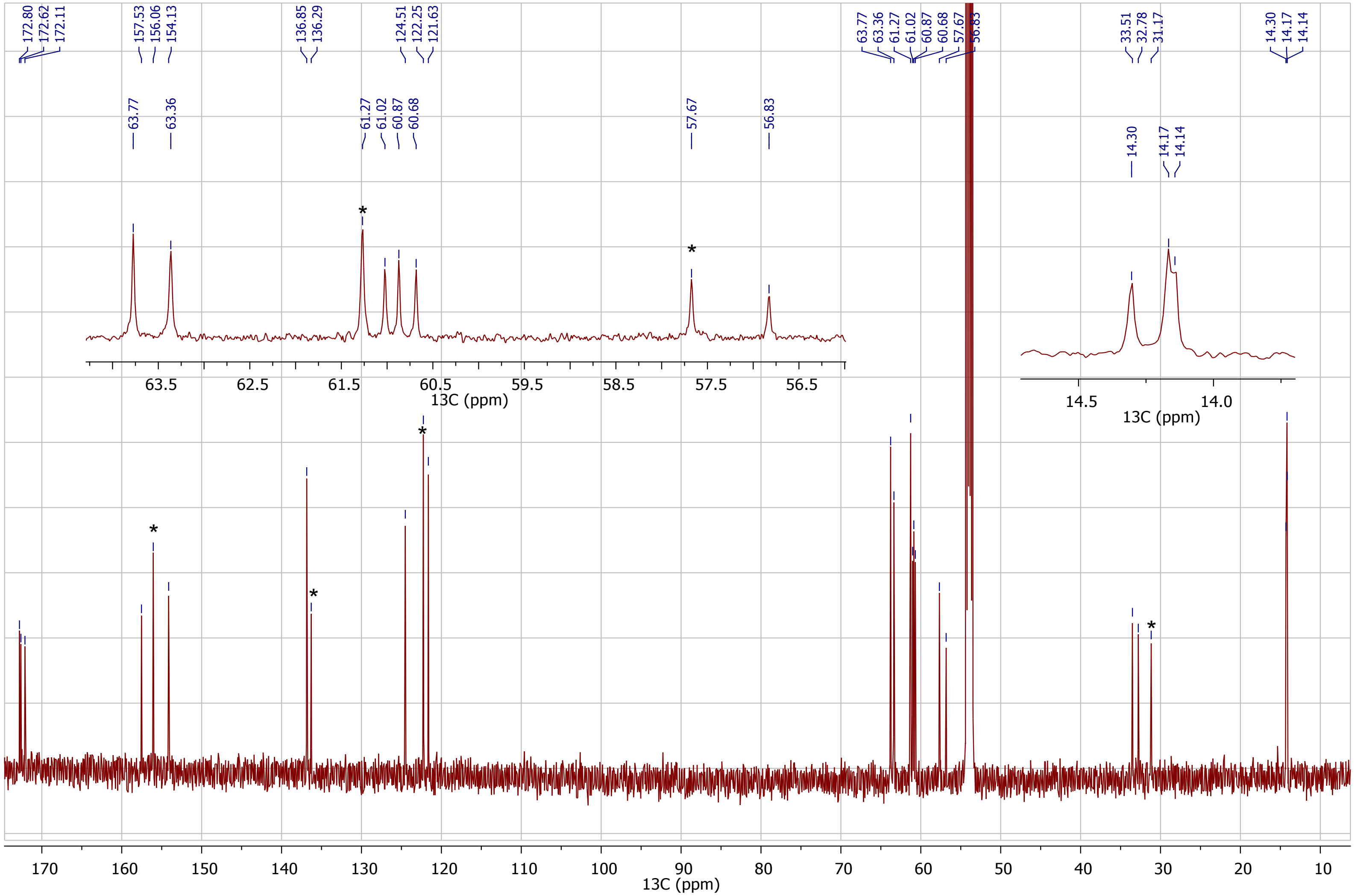

Figure S29. ^{13}C spectrum of **5** in CD_2Cl_2 at -35 °C. Peaks of minor conformer (κ^4-**L2**)CuI are labelled with an asterisk where possible.

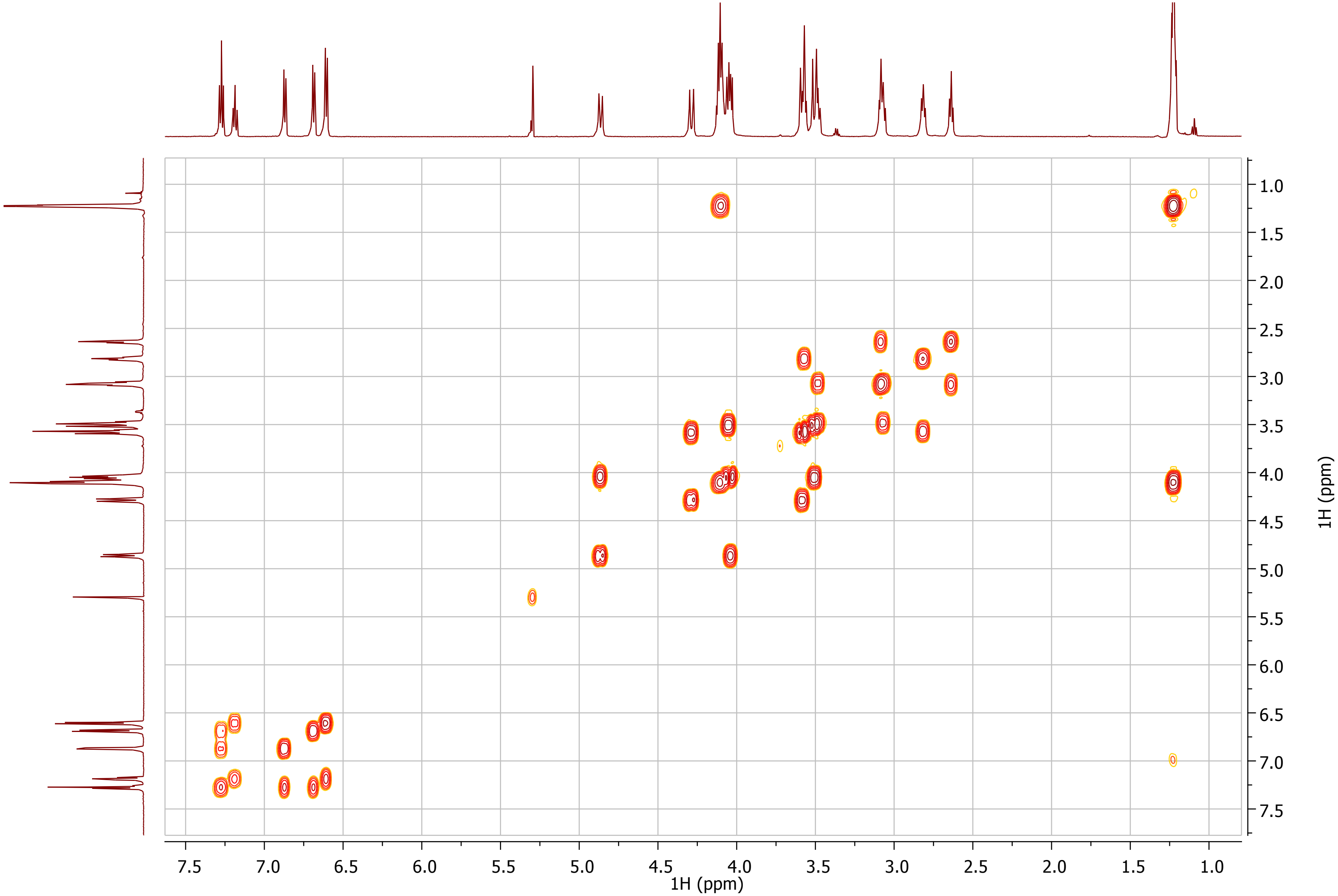

Figure S30. gCOSY spectrum of **5** in CD_2Cl_2 at -35 °C

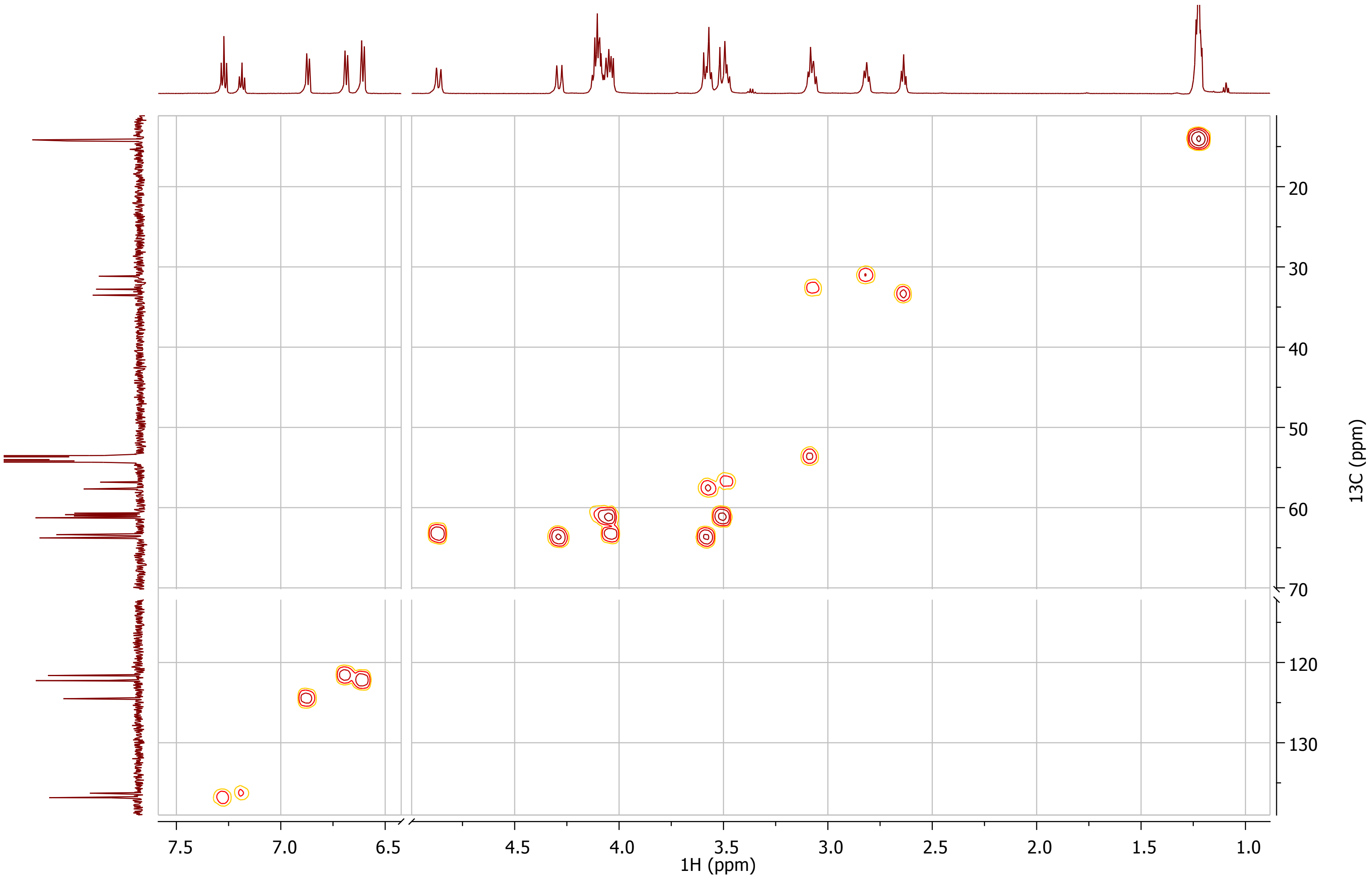

Figure S31. gHMQC spectrum of **5** in CD_2Cl_2 at -35 °C

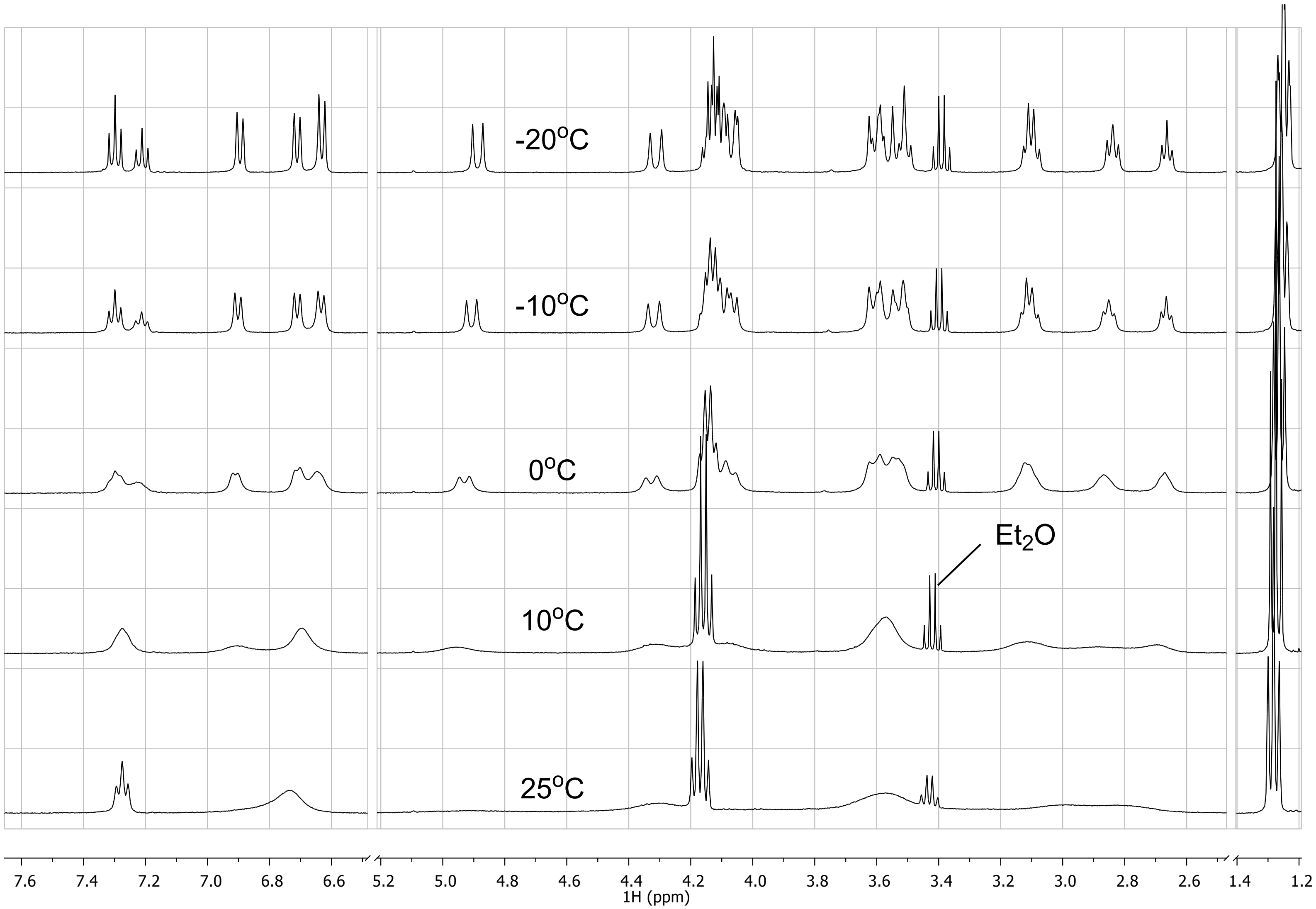

Figure S32. ^{1}H VT NMR spectra of **5** in CD_2Cl_2.

Complex 6:

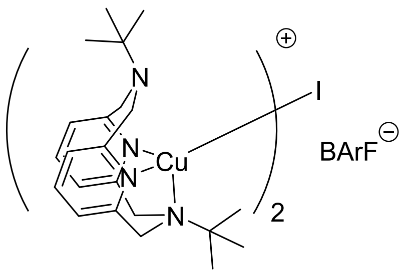

6

Complex **4** (44.6 mg, 0.1 mmol) was dissolved in 2 mL CH_2Cl_2 and treated with 43.6 mg of NaBARF (0.05 mmol) (BARF = $((3,5\text{-}(CF_3)_2C_6H_3)_4B^-$; tetrakis[3,5-bis(trifluoromethyl) phenyl]borate). The solution colour changed from orange to pale yellow-green within 5 minutes and the stirring was continued for 1 hour. The white precipitate of NaI was separated by filtration and the dichloromethane solution was slowly treated with 2.5-3 mL of hexane and set aside. Within 30 minutes a crop of pale-green needles formed and the solution was treated with the same amount of hexane to complete crystallization. The solvent was decanted and the green crystalline material was washed twice with a little hexane and dried in vacuum. This yields 56 mg of analytically pure solid (72 %).

For preparation of X-ray quality crystalline samples the needle crystals were treated with a minimal amount of benzene (ca. 1 mL per 10 mg), the solution was quickly filtered through celite plug and set aside in an opened vial. After evaporation of ca. 20 % of the solvent large green prisms suitable for X-ray diffraction were formed.

^{1}H NMR (600 MHz, -35°C, CD_2Cl_2): δ 7.71 (s, $C\boldsymbol{H}_{\mathrm{BARF}}$, 8H), 7.54 (s, $C\boldsymbol{H}_{\mathrm{BARF}}$, 4H), 7.29 (t, $^3J_{\mathrm{HH}}$ =7.6 Hz, p-$\mathrm{H_{Py}}$, 4H), 6.87 (d, $^3J_{\mathrm{HH}}$ = 7.7 Hz, m-$\mathrm{H_{Py}}$, 4H), 6.71 (d, $^3J_{\mathrm{HH}}$ = 7.5 Hz, m-$\mathrm{H_{Py}}$, 4H), 4.62 (d, $^2J_{\mathrm{HH}}$ =14.8 Hz, methylene CH_2, 4H), 4.51 (d, $^2J_{\mathrm{HH}}$ =12.8 Hz, methylene CH_2, 4H), 4.18 (d, $^2J_{\mathrm{HH}}$ =12.8 Hz, methylene CH_2, 4H), 3.46 (d, $^2J_{\mathrm{HH}}$ =14.9 Hz, methylene CH_2, 4H), similar to the complex **4**, the following resonances of the $C\boldsymbol{H}_3$-^{t}Bu are broadened - δ 1.62 (m, ^{t}Bu-$C\boldsymbol{H}_3$, 18H), 1.08 (m, ^{t}Bu-$C\boldsymbol{H}_3$, 18H).

^{13}C NMR (151 MHz , -35°C, CD_2Cl_2) quaternary boron-coupled C_{BARF} was observed as a broad feature at δ 167.7 due to low solubility; 160.04 (quaternary C_{Py}), 155.00 (quaternary C_{Py}), 137.13 (p-C_{Py}), 134.77 ($\boldsymbol{C}\mathrm{H}_{\mathrm{BARF}}$), 128.77 (d observed instead of q due to low concentration, $^2J_{\mathrm{CF}}$ = 28.7 Hz, $\mathrm{Cq}_{\mathrm{BARF}}$), 124.56 (d observed instead of q due to low concentration, $^1J_{\mathrm{CF}}$ = 273.3 Hz, $\boldsymbol{C}\mathrm{F}_{3\mathrm{BARF}}$), 124.34 ($m$-$C_{\mathrm{Py}}$), 121.57 ($m$-$C_{\mathrm{Py}}$), 117.57 ($\boldsymbol{C}\mathrm{H}_{\mathrm{BARF}}$), 59.29 ($C_q$-^{t}Bu), 58.91 (methylene CH_2), 58.61 (methylene CH_2), 57.05 (C_q-^{t}Bu), 27.60 (CH_3-^{t}Bu). The resonance at δ 30.7 assigned to the dynamic CH_3-^{t}Bu group is severely broadened and could not be reported reliably.

EA: Found(Calcd): $C_{76}H_{76}BCu_2F_{24}IN_8\cdot CH_2Cl_2$: C 48.46 (48.49), H 3.95 (4.12), N 5.95 (5.88)

QY (Solid, 400 nm) 53.0%

QY (Solution, 400 nm) 15.4%

QY (PMMA film, 400 nm) 26.0%

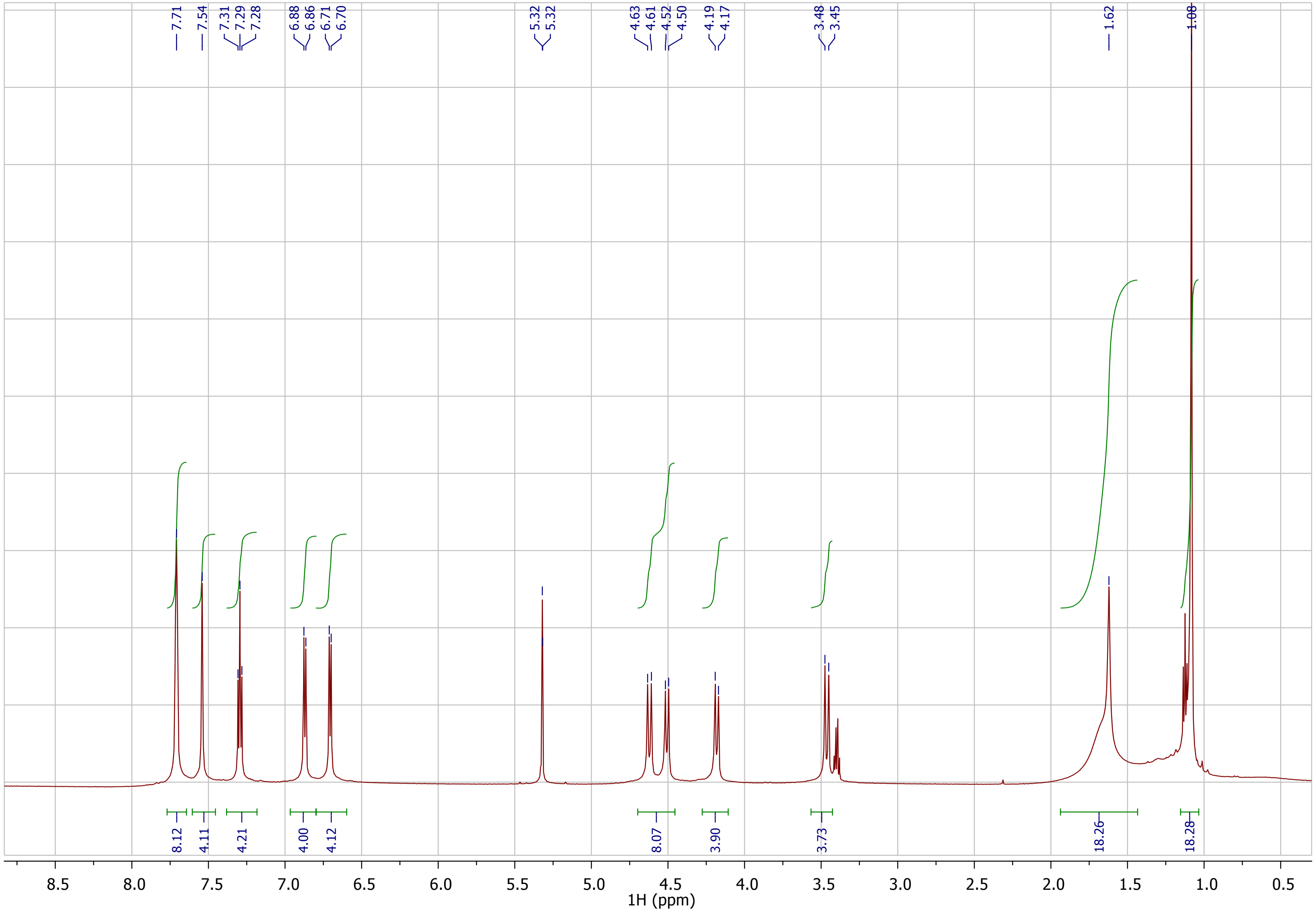

Figure S33. ^{1}H NMR spectrum of **6** in CD_2Cl_2 at -30 °C.

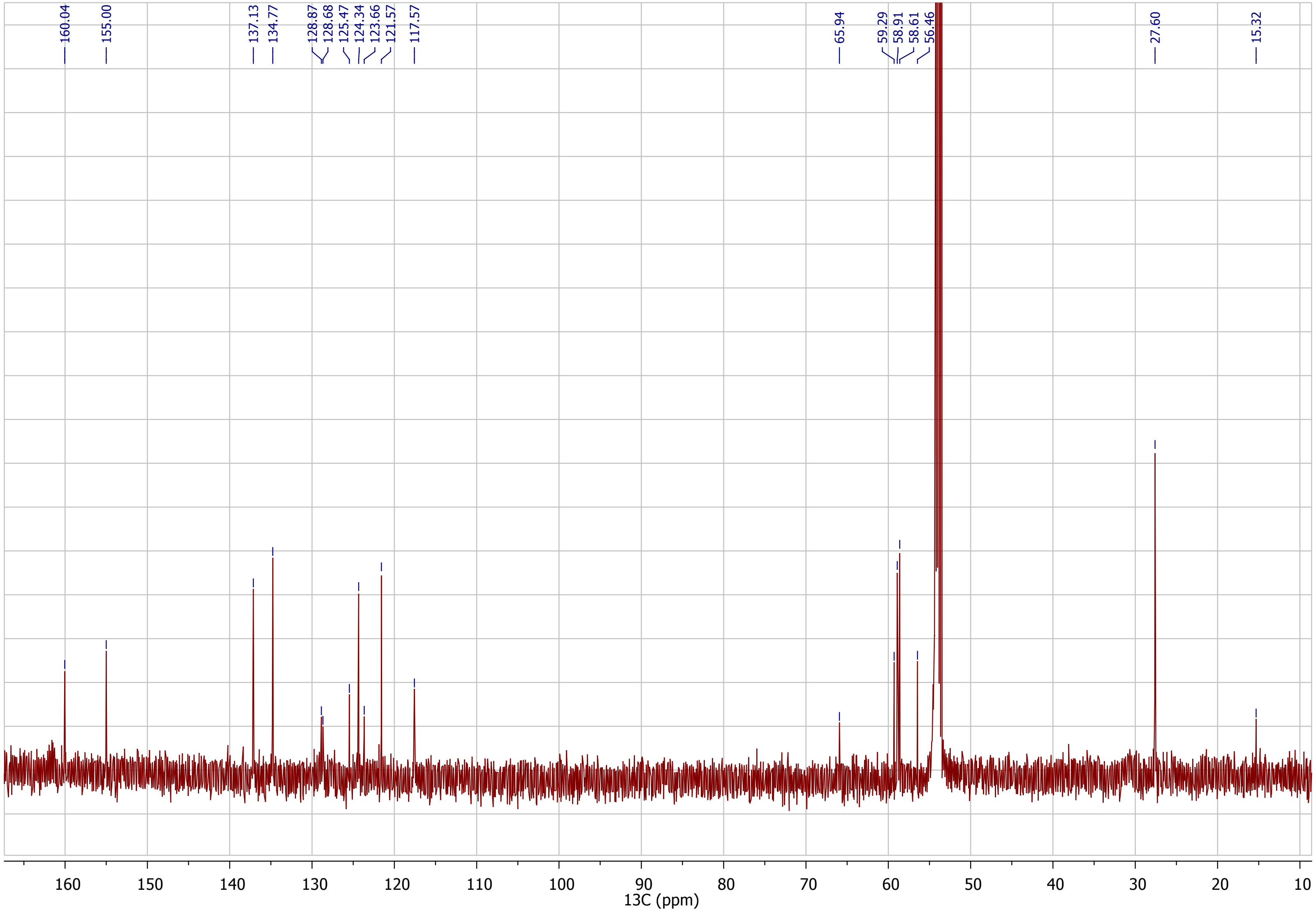

Figure S34. ^{13}C spectrum of **6** in CD_2Cl_2 at -30 °C.

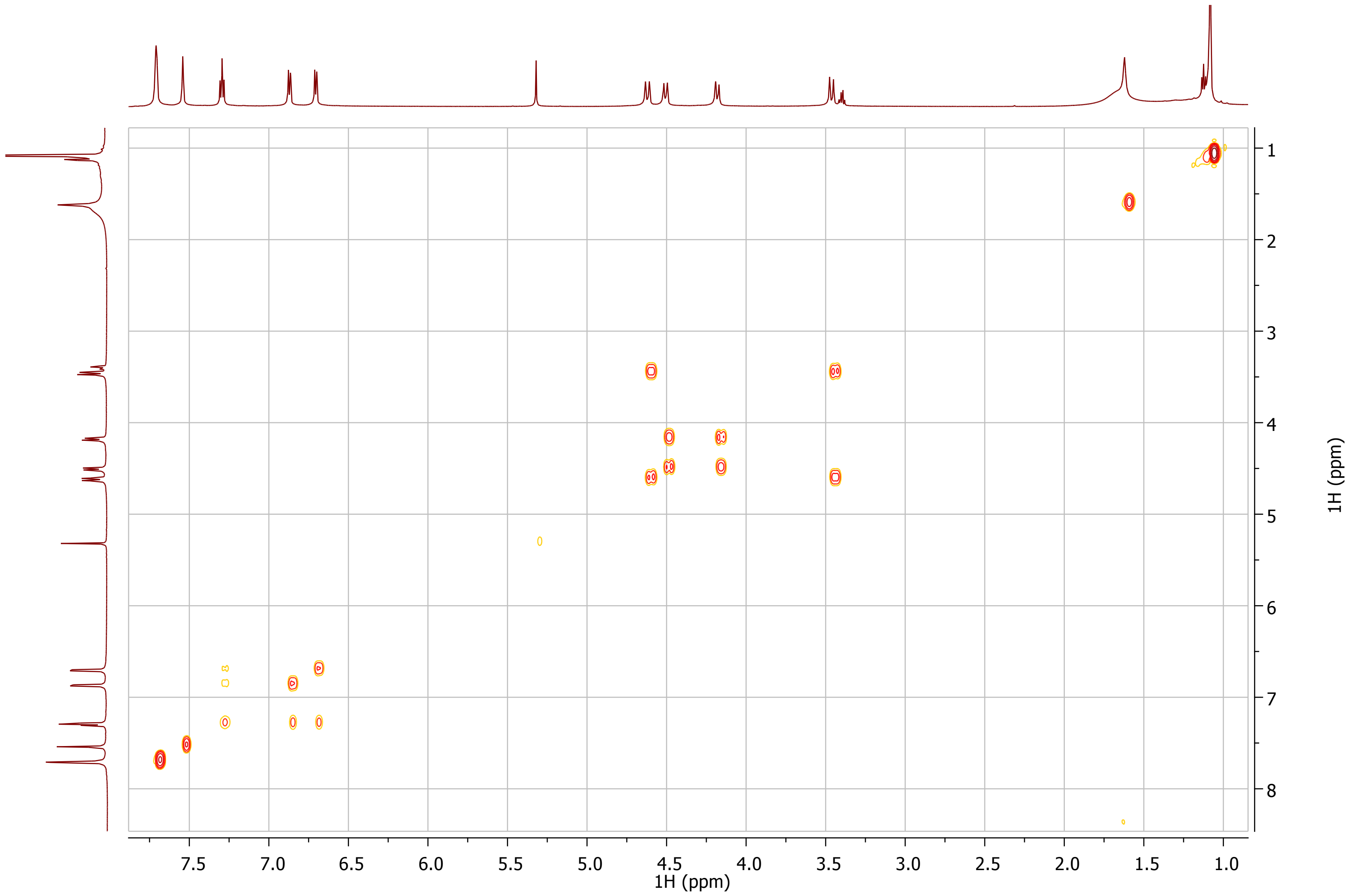

Figure S35. gCOSY spectrum of **6** in CD_2Cl_2 at -30 °C

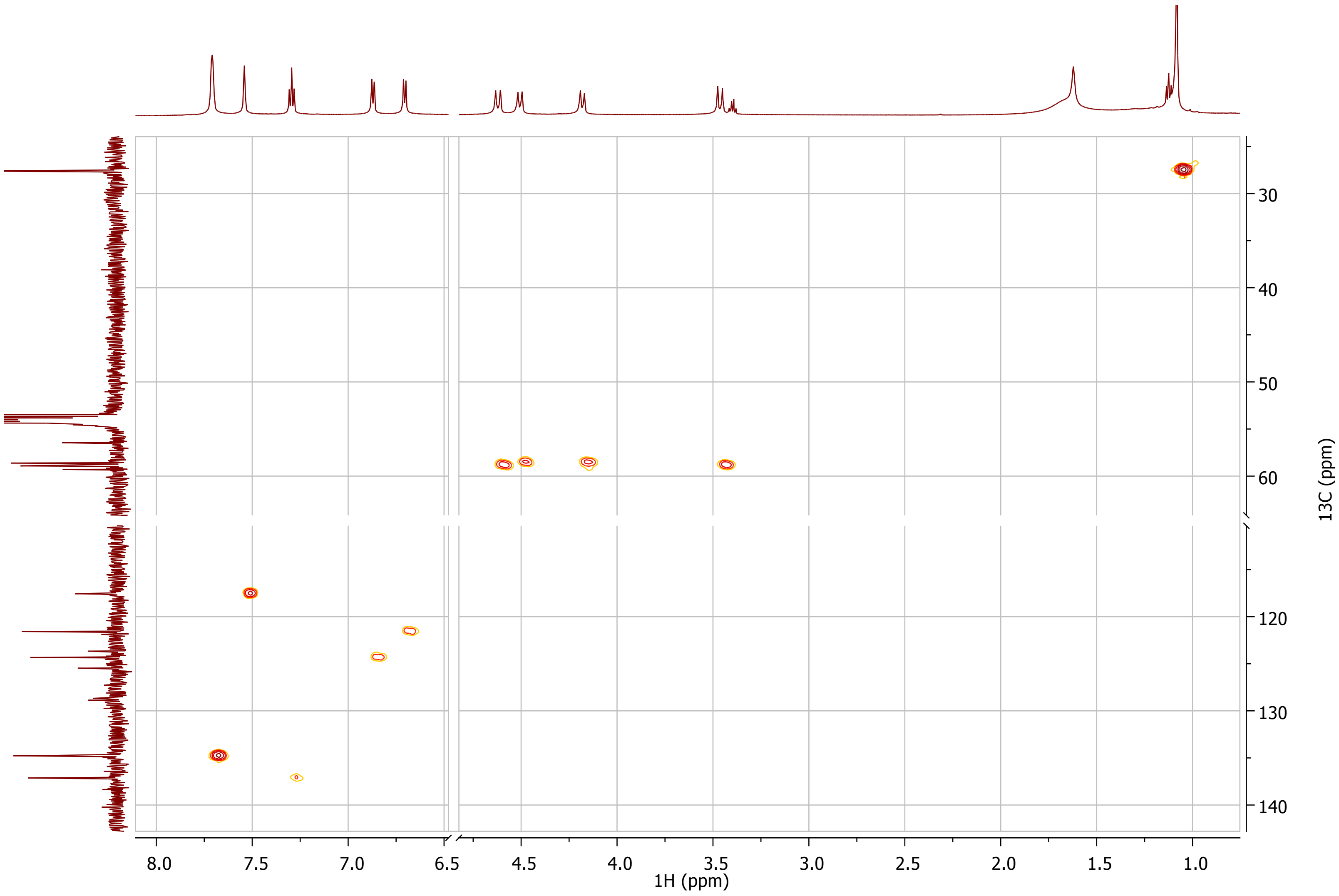

Figure S36. gHMQC spectrum of **6** in CD_2Cl_2 at -35 °C

S2. Photophysical properties of complexes 1-6 in solid and solution state.

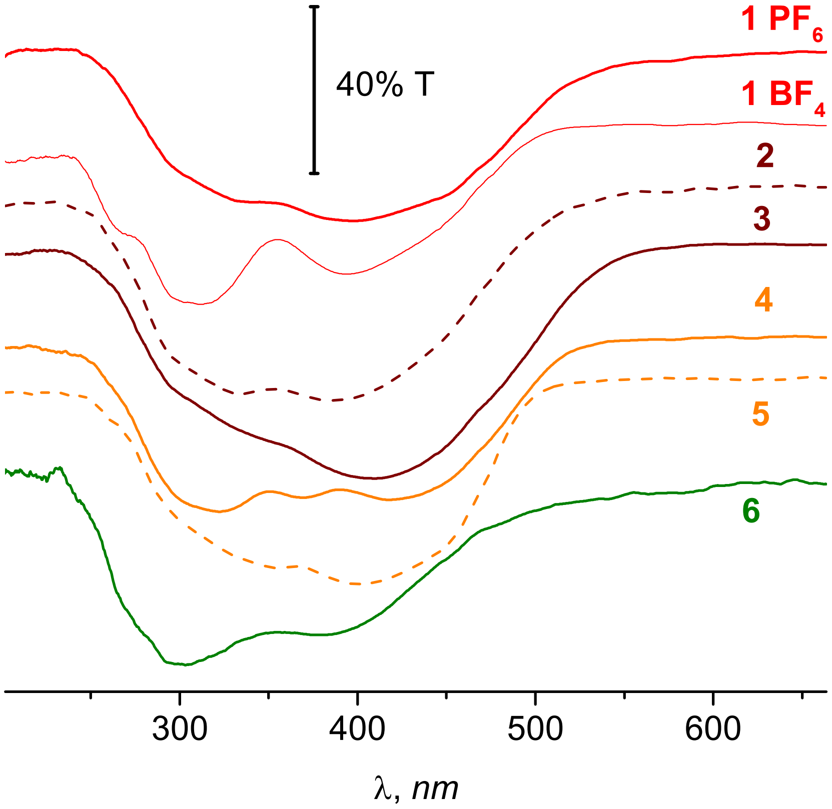

Figure S37. Transmittance of crystalline **1-6**. Curves are translated in the vertical direction for clarity, scale bar corresponding to 40% transmittance is placed on the graph.

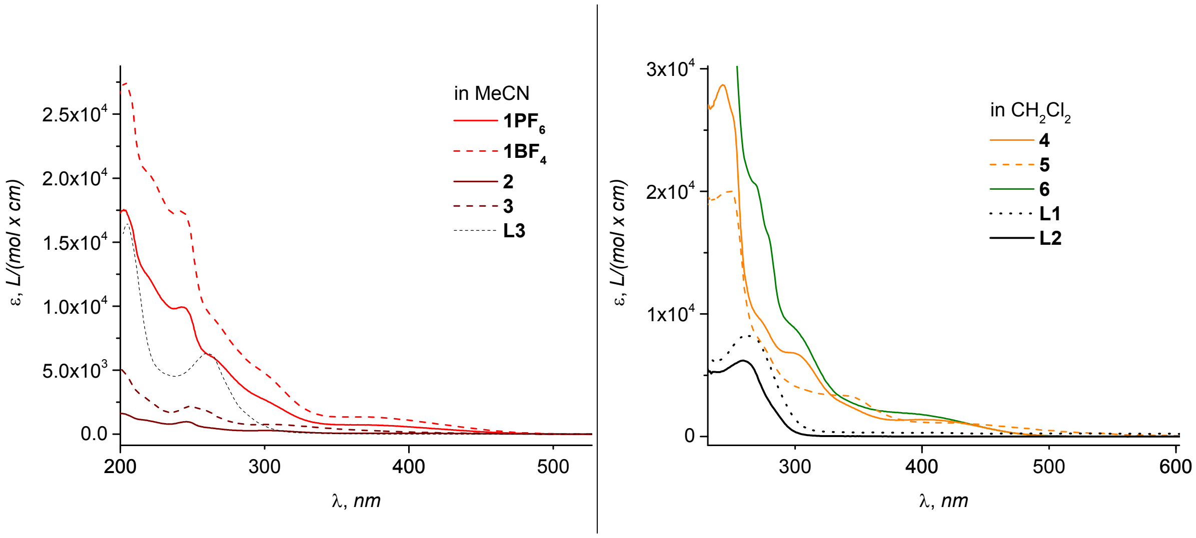

Figure S38. UV-Vis absorbance spectra for complexes **1-6** and ligands **L1-L3** in dichloromethane and acetonitrile

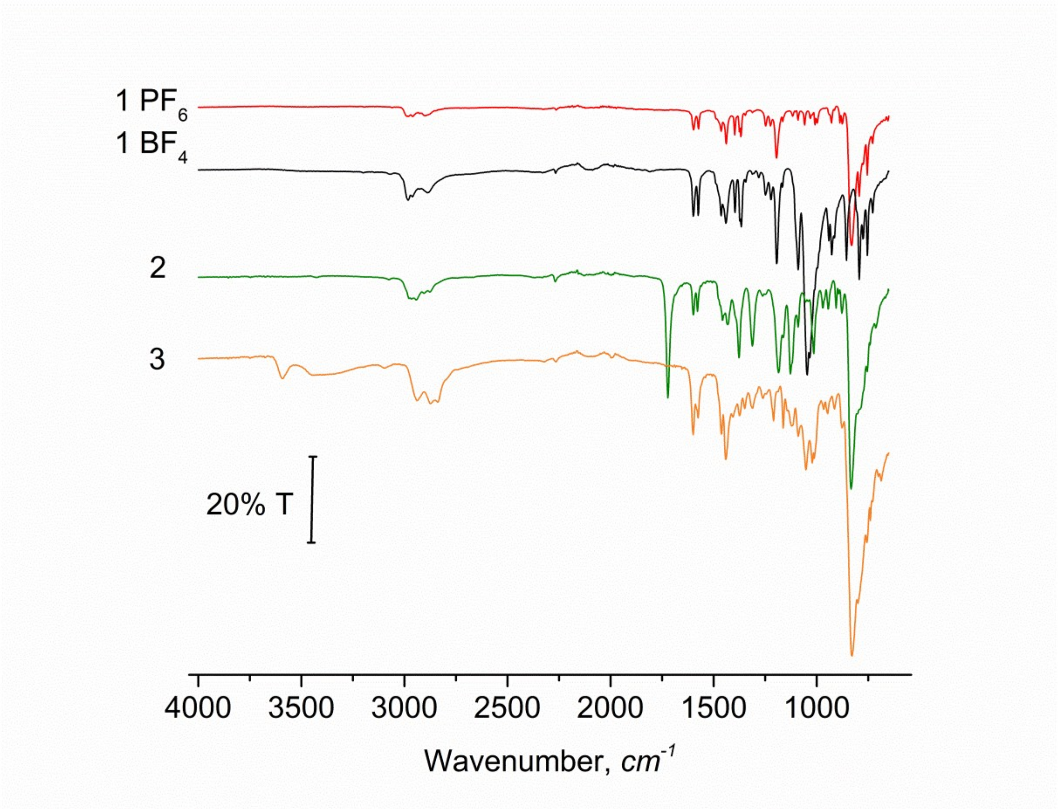

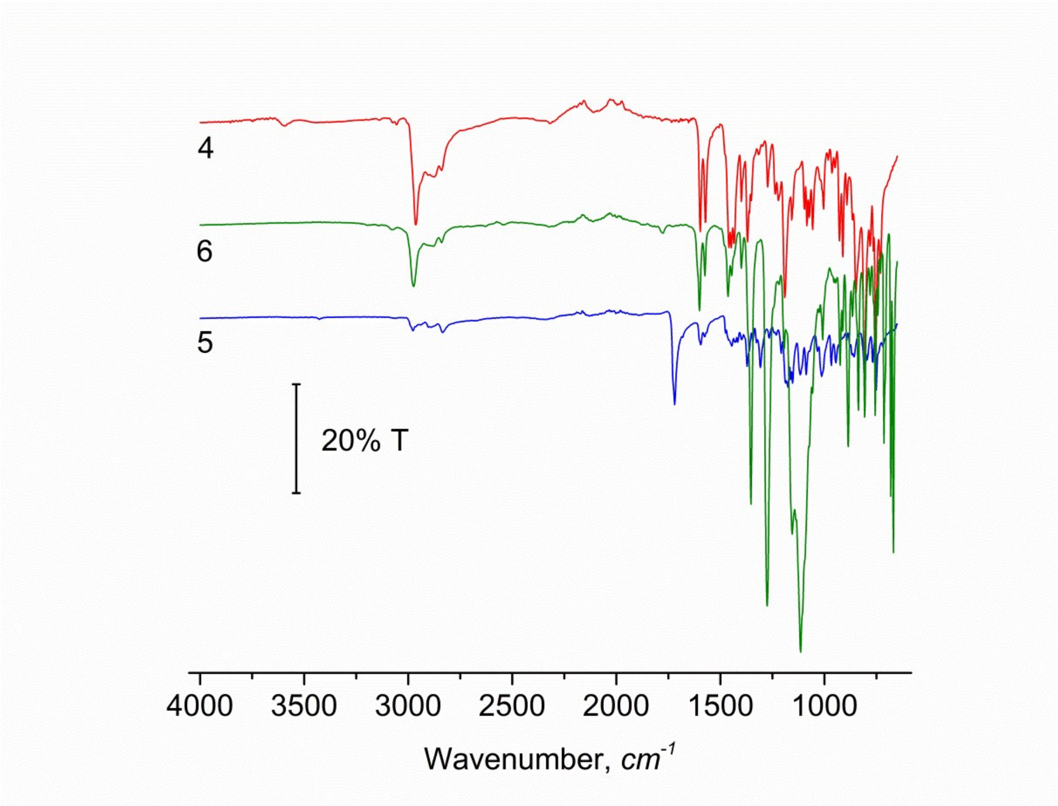

Figure S39. ATR FT-IR transmittance spectra of crystalline **1-6**. Curves are translated in the vertical direction for clarity, 20% transmittance scale bar is placed on the graph.

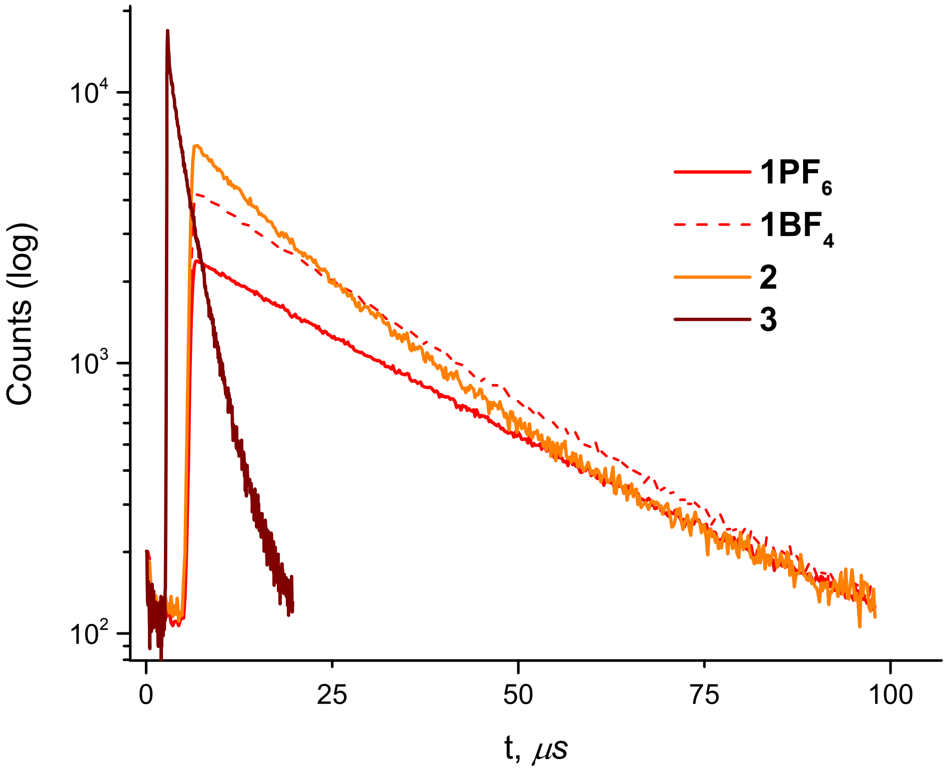

Figure S40. Photoluminescence decay profiles for complexes **1-2** (500-800 nm range) and **3** (550-850 nm range) in the solid state. Excitation at 400 nm.

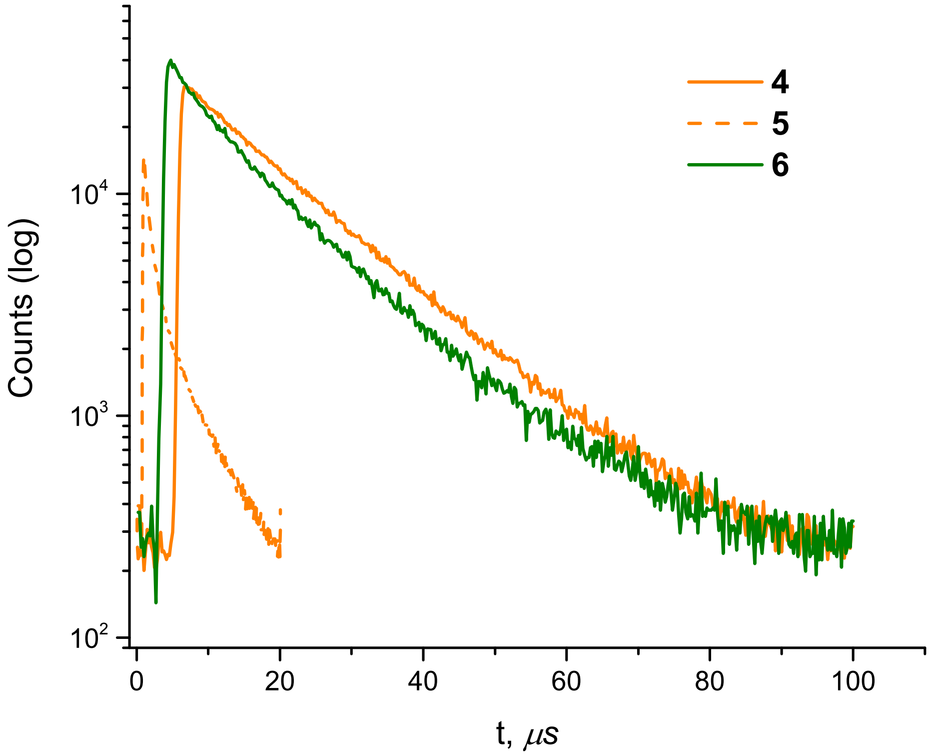

Figure S41. Photoluminescence decay profiles for complexes **4** and **5** (450-750 nm range) and **6** (400-700 nm range) in the solid state. Excitation at 400 nm.

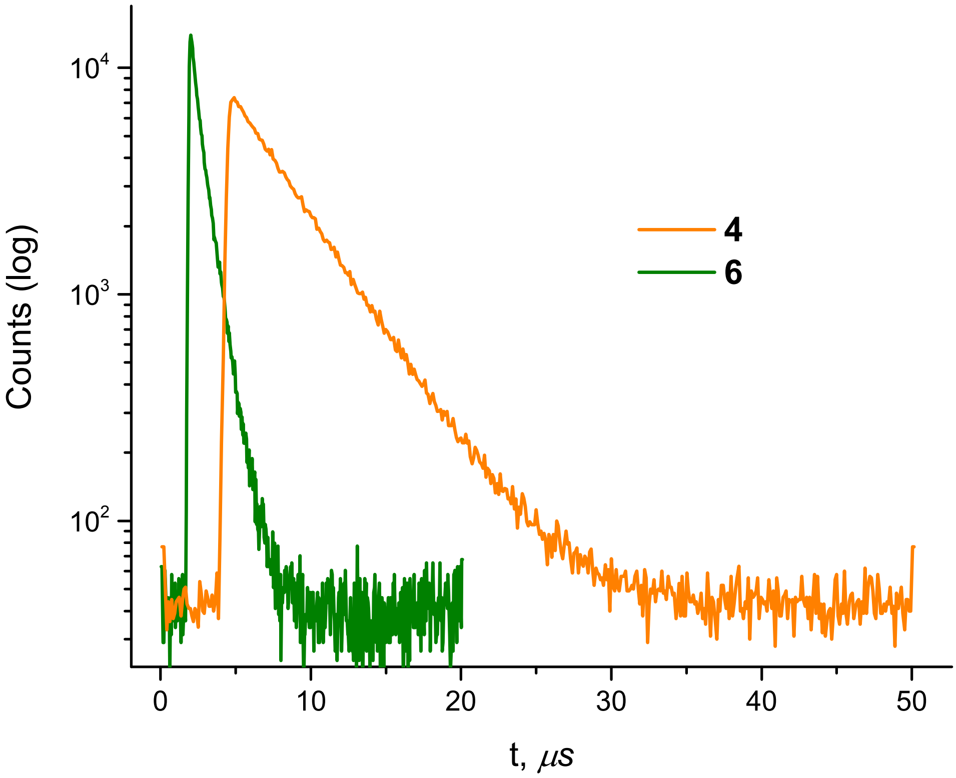

Figure S42. Photoluminescence decay profiles for complexes **4** and **6** (450-750 nm range) in CH_2Cl_2. Excitation at 400 nm.

PL decay profile processing:

All profiles except those for complex **5** were fitted with a monoexponential decay function:

$$I = Ae^{-kt} = Ae^{\frac{-t}{\tau}},$$

where k is the apparent PL decay rate constant and $\tau = \frac{1}{k}$ is the photoluminescence lifetime.

Constant k can be expressed as a sum of radiative and non-radiative decay rate constants k^{rad} and k^{nrad}.

Assuming that the quantum yield is:

$$\Phi = \frac{k^{rad}}{k^{rad} + k^{nrad}}, \text{ where } \tau = \frac{1}{k^{rad} + k^{nrad}},$$

one can derive the k^{rad} as the Φ/τ using the Φ values obtained from direct measurements and τ values derived from decay profile fitting.

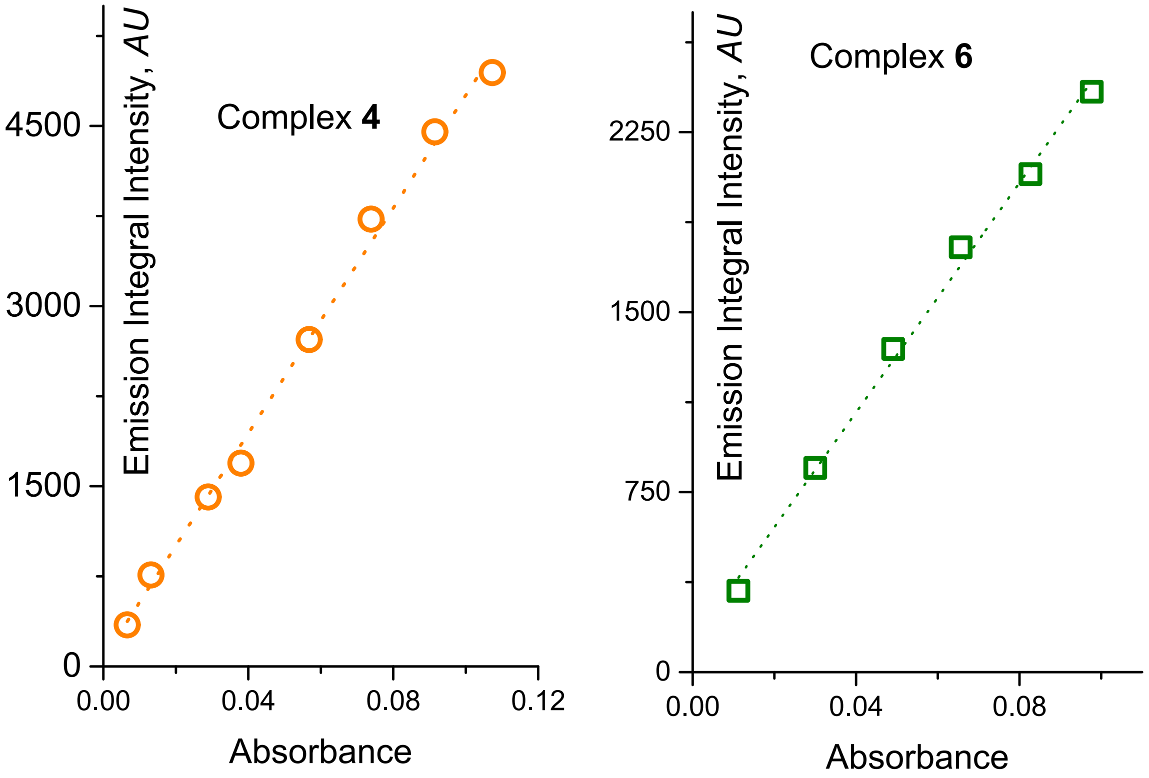

Figure S43. Integral photoluminescence intensity vs absorbance curves for complexes **4** and **6** in dichloromethane. Maximal concentrations 0.078 µmol/mL (**4**) and 0.053 µmol/mL (**6**). Excitation at 400 nm, integral emission in 450-750 nm range

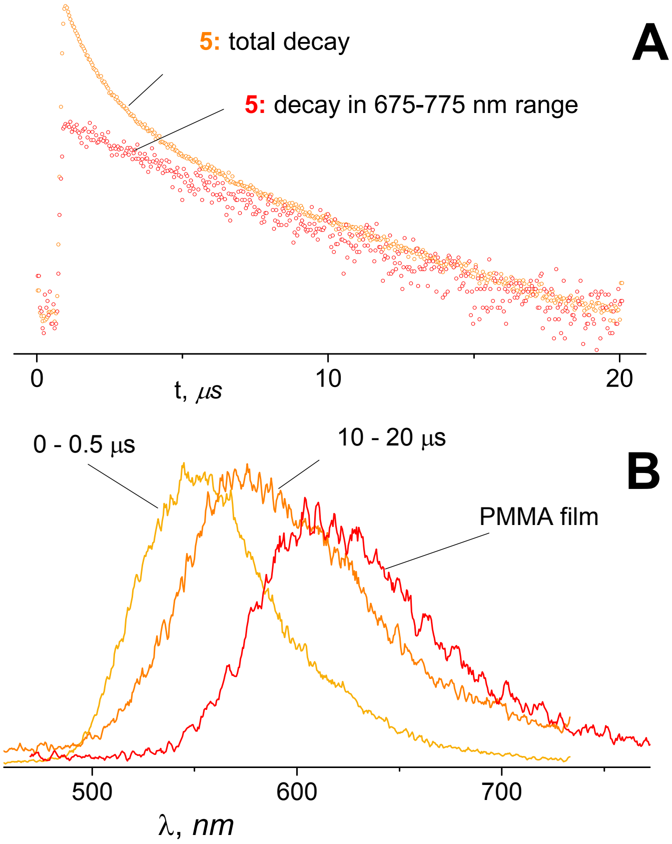

Figure S44. A) Full (450 - 775 nm, orange circles) and partial spectral range (675 - 775 nm, red circles) PL decay curves of crystalline **5** in logarithmic coordinates; curves translated in the vertical direction and overlaid for clarity and B) normalized emission spectra of a short and long decaying components of crystalline **5** and emission of PMMA film doped with **5**. Excitation at 400 nm.

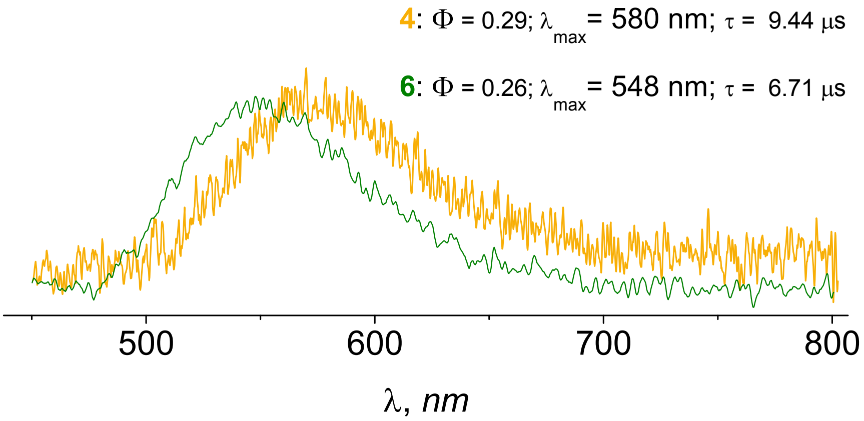

Figure S45. Normalized emission spectra and properties of PMMA films doped with **4** and **6**. Excitation at 400 nm.

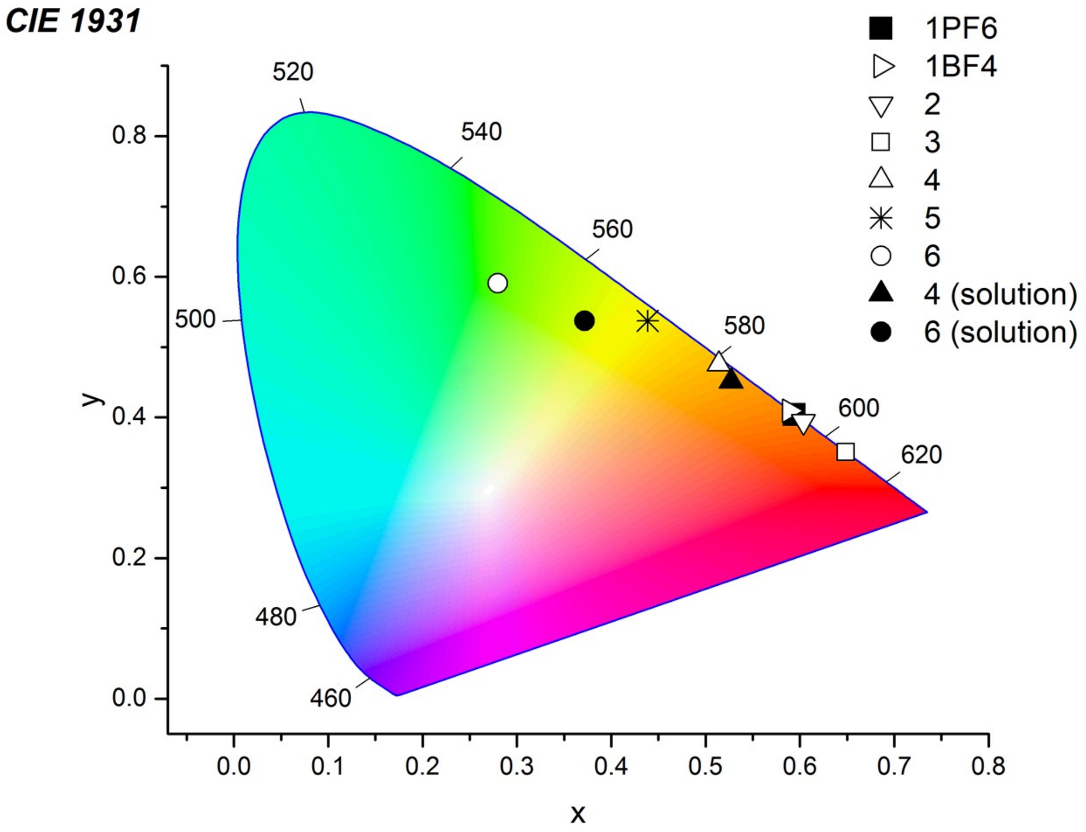

Figure S46 CIE 1931 colour space chromaticity diagram containing data points for complexes **1-6** in crystalline state and CH_2Cl_2 solutions.

S3 Cyclic voltammetry data.

CV curves were referenced against ferrocene standard at every temperature indicated.

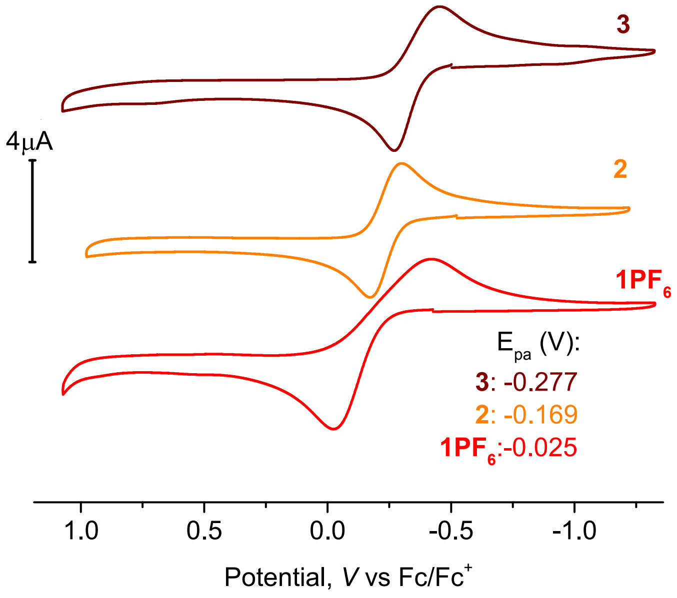

Figure S47. Cyclic voltammograms for complexes **1PF$_6$** (1.2 mM), **2** (1 mM) and **3** (1 mM) in 0.1M solution of NBu_4ClO_4 in acetonitrile at 23°C; 100 mV/s scan rate, glassy carbon disk electrode (*d* = 1.6 mm).

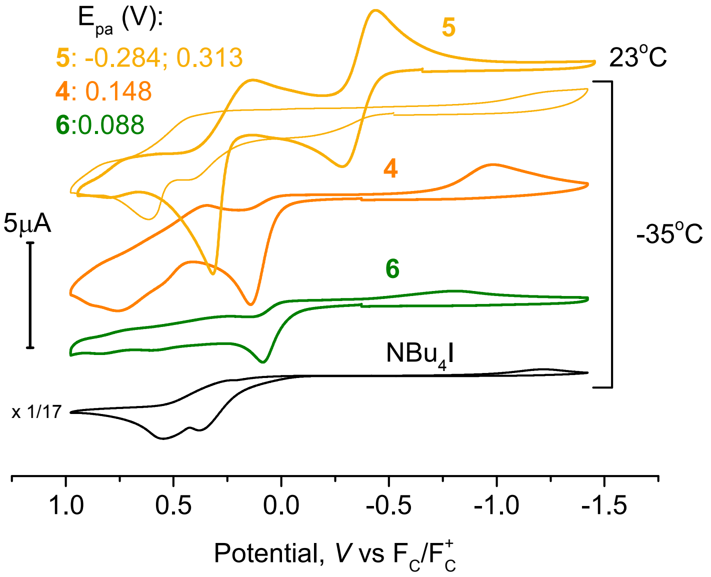

Figure S48. Cyclic voltammograms for complexes **4** (-35 °C, 1 mM), **5** (23 °C, 2 mM) and **6** (-35 °C, 1 mM) and NBu_4I (-35 °C, 16.9 mM) in 0.1M solution of NBu_4ClO_4 in CH_2Cl_2; 100 mV/s scan rate, glassy carbon disk working electrode (*d* = 1.6 mm). Oxidation of complex **5** at -35 °C was not analysed due to severe broadening of oxidation waves and overlap with iodide oxidation features.

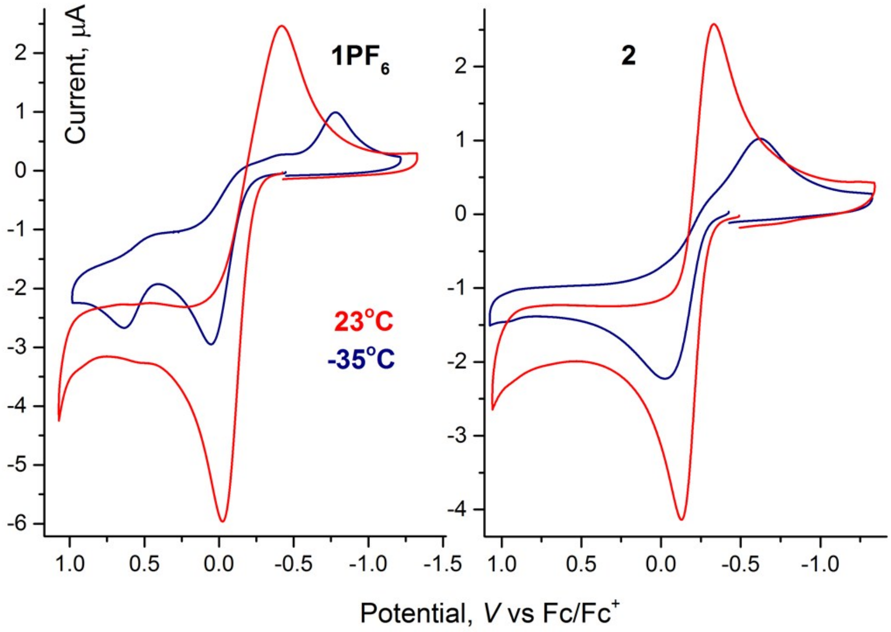

Figure S49 is a duplicate of Figure 4 of the manuscript given here for comparison. Cyclic voltammograms for complexes **1PF$_6$** (1.2 mM) and **2** (1 mM) in 0.1M solution of NBu_4ClO_4 in acetonitrile at 23 and -35 °C; 100 mV/s scan rate, glassy carbon disk electrode (*d* = 1.6 mm). Referencing vs Fc standard performed at both temperatures.

Table S1. Summary of electrochemical features of complexes **1-6**.*

Complex	Solvent	T, °C	E_{pa}, *mV*	E_{pc}, *mV*
1PF$_6$	MeCN	23 °C	-25	-420
		-35 °C	59, 640	-778
1BF$_4$		23 °C	-48	-383
2		23 °C	-127	-332
		-35 °C	0	-609
3		23 °C	-277	-455
4	CH_2Cl_2	-35 °C	148	-977
5		23 °C	-284, 313	142, -437
6		-35 °C	88	-811

* conditions identical to that given above for Figures S45-47; 100 mV/s scan rate, glassy carbon disk electrode (*d* = 1.6 mm), 0.1M solution of NBu_4ClO_4 used as supporting electrolyte; potentials are referenced against Fc/Fc$^+$.

S4 Density functional theory calculations.

All DFT calculations were carried out using the hybrid PBE0[6] exchange-correlation functional as implemented in the Gaussian 09 program, revision E01.[7] The 6-311G(d,p) basis was set for all atoms except copper and iodine for which the LanL2DZ basis set was employed. To account for solvation effects the polarized continuum model (PCM) was employed in all calculations. For all calculations, an empirical dispersion correction was employed using the GD3 model. The nature of the stationary points was confirmed for all ground and triplet states using frequency calculations. TD-DFT method as implemented in the Gaussian package was used for calculation of singlet excited states with at least 30 states analyzed. Chemcraft software was used for MO visualization. GaussSum software[8] was used for partial density of states (PDOS) analysis to assign the contributions to frontier orbitals.

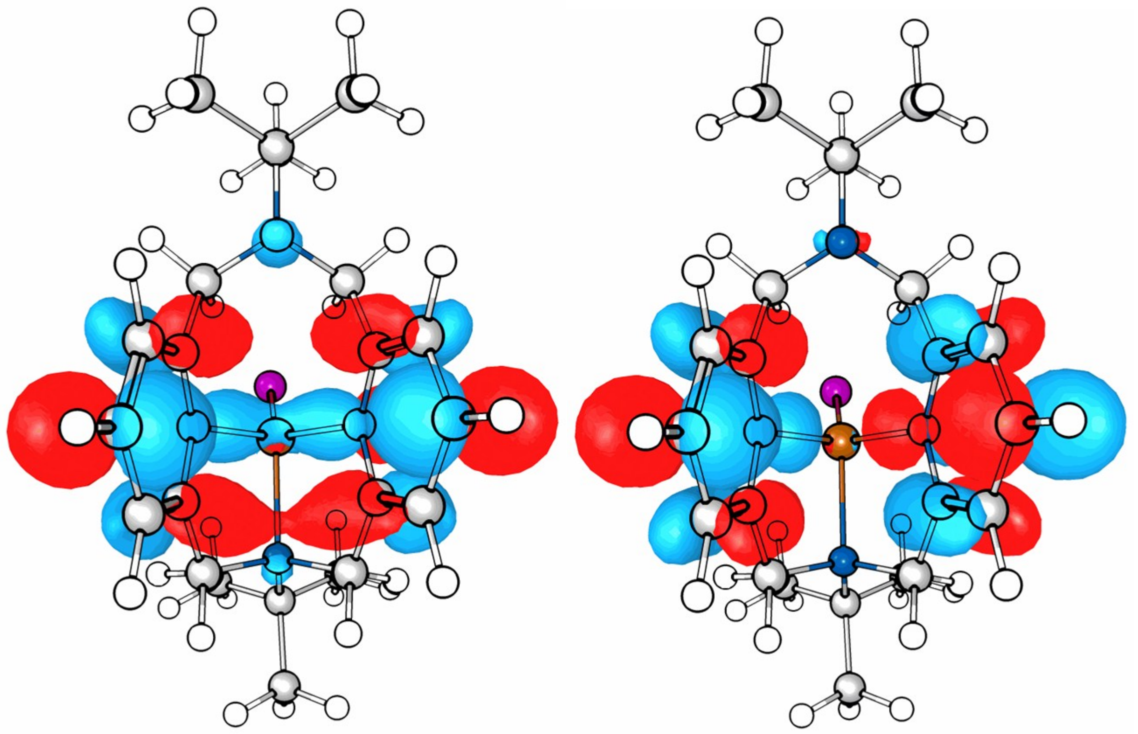

Figure S50. Additional frontier orbitals of **4** in S_0 state: LUMO+1 (left) and LUMO+2 (right).

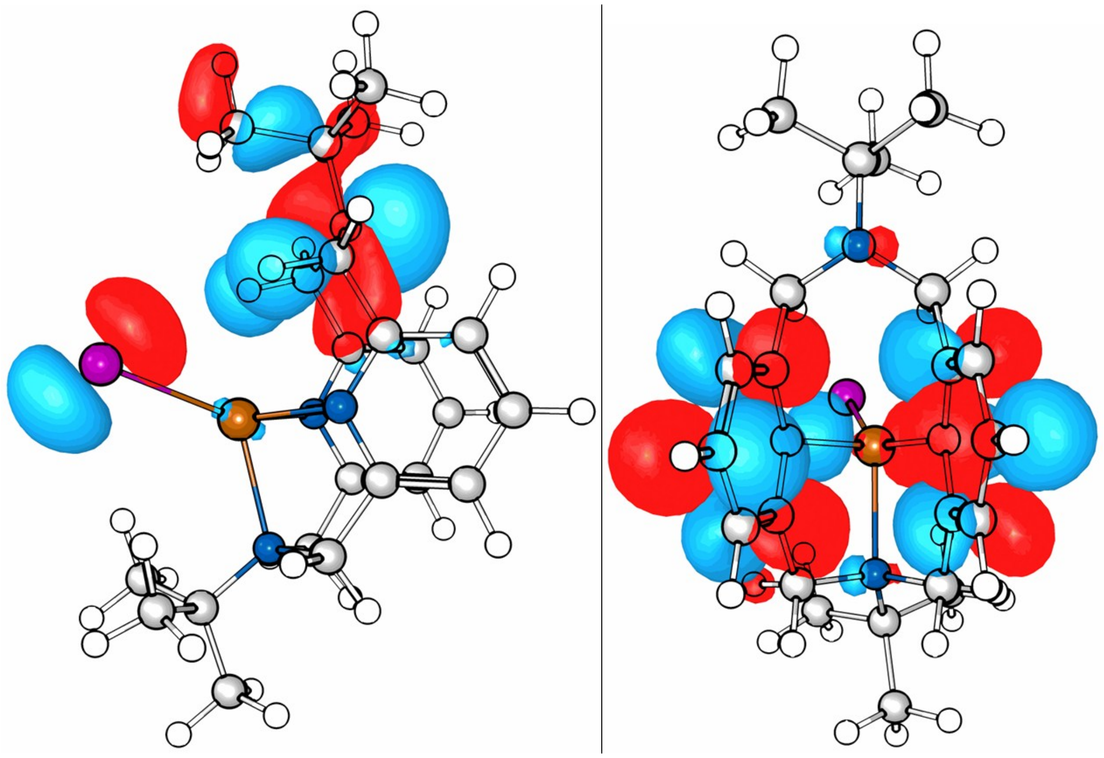

Figure S51. Additional frontier orbitals of **4** in T_1 state: lower energy SOMO (left) and LUMO (right).

XYZ coordinates of optimized structures are listed below:

4; ground state:

Total energy -1283.2511779 A.U.

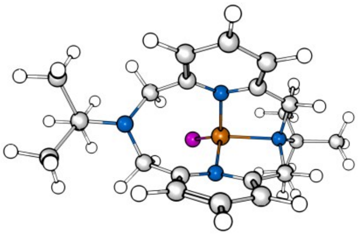

Cu	-0.83328000	0.54029500	-0.00625800
N	0.03318500	-0.92841400	-1.32871200
N	0.02323500	-0.86491000	1.40966600
N	-2.47146400	-0.99210800	0.01912500
C	1.35134100	-1.01842500	-1.53102100
C	1.94172000	-2.19862600	-1.97496100
H	3.01427100	-2.23709000	-2.12571500
C	-0.77112400	-1.93185800	1.56970600
C	-0.73454200	-2.01549000	-1.46685500
C	-3.90753700	0.53639500	-1.29420600
H	-3.07878400	1.25103700	-1.29666000
H	-4.84486100	1.09763600	-1.27843100
H	-3.89190000	-0.02579900	-2.23031700
C	-4.95665700	-1.39476000	-0.08528600
H	-4.89369000	-2.02783900	-0.97468000
H	-5.92687600	-0.89152000	-0.10731900
H	-4.93871500	-2.03654200	0.80018900
C	1.09567100	-3.29444600	2.17414000
H	1.51482000	-4.24649800	2.48174500
C	-0.27387200	-3.16338000	1.96563600
H	-0.94289800	-4.00831600	2.08294000
C	1.14268300	-3.31003200	-2.18458900
H	1.57450500	-4.24318900	-2.53024200
C	-0.21650500	-3.22544100	-1.90632800
H	-0.86350100	-4.08976700	-2.00550400
C	1.91720700	-2.20427600	1.94616900
H	2.99394100	-2.27749900	2.04527900
C	-2.23591100	-1.71651200	1.27998300
H	-2.75165000	-2.68642700	1.29298600
H	-2.63878900	-1.11956800	2.09808400
C	-4.02369200	0.56545700	1.16277700
H	-4.20230800	0.01816200	2.09102700
H	-4.89627100	1.20107000	0.99648500
H	-3.14969100	1.21298900	1.28699900
C	1.34381900	-0.99631100	1.55303600
C	-3.83701100	-0.35123800	-0.04899600
C	-2.20051400	-1.87095200	-1.12929200
H	-2.68893000	-1.45108200	-2.00922900
H	-2.62709100	-2.87168100	-0.97682200
I	-0.80057600	3.11862900	-0.00048900
C	2.19009600	0.18901000	-1.19395600
H	2.84664300	0.38870200	-2.03971100
H	1.51931400	1.05521300	-1.08871100
C	2.20377600	0.19715400	1.21509000
H	1.54717800	1.07580600	1.12351400
H	2.87084900	0.37346800	2.05748200
N	3.00232400	-0.02627400	0.00747100
C	4.31716400	0.67272400	-0.01185200
C	4.16073400	2.19538300	-0.09652800
H	5.13879100	2.68557300	-0.08925500
H	3.64425600	2.49110500	-1.01432600
H	3.58620300	2.57708500	0.75283800
C	5.11016200	0.30564300	1.24750200
H	5.10812700	-0.77796600	1.39809000
H	6.14569000	0.63377800	1.12950900
H	4.72989600	0.78691300	2.15124200
C	5.13526800	0.15944500	-1.20239600
H	4.73262900	0.46795100	-2.16956100
H	6.15179600	0.55646100	-1.14405200
H	5.18807900	-0.93291400	-1.17995500

4, optimized S_1 geometry:

Total energy -1283.23685297A.U.

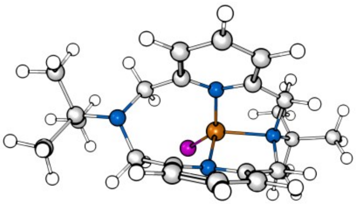

Cu	0.79030900	0.46331500	0.18088400
N	-0.00484300	-1.05719300	1.24671400
N	-0.06235000	-0.78854400	-1.40109200
N	2.48211700	-0.83530800	0.00496900
C	-1.33494700	-1.16097700	1.38326400
C	-1.90762700	-2.41589100	1.70120000
H	-2.97977100	-2.49001100	1.83287300
C	0.81527700	-1.78722500	-1.57265800
C	0.79927400	-2.12120500	1.29142600
C	3.81205600	0.67124800	1.44626600
H	3.02947200	1.43492800	1.41044900
H	4.77186100	1.18223000	1.55259400
H	3.66751400	0.06709800	2.34378400
C	4.96373200	-1.17955200	0.20464200
H	4.90975200	-1.81734500	1.08991900
H	5.91858600	-0.64922300	0.23765300
H	4.97025900	-1.81452300	-0.68528600
C	-0.96581200	-3.28122600	-2.14127100
H	-1.32343700	-4.26080000	-2.44440000
C	0.39936600	-3.06461200	-1.98079700
H	1.12401300	-3.85371800	-2.14015000
C	-1.08025400	-3.51692800	1.81141200
H	-1.50490900	-4.48870200	2.04585100
C	0.29462400	-3.39819500	1.59950700
H	0.95783600	-4.25227900	1.64228700
C	-1.87201000	-2.26019500	-1.89418000
H	-2.94091100	-2.41191700	-1.97872000
C	2.25700200	-1.42735800	-1.34250000
H	2.88736500	-2.31382700	-1.47497500
H	2.55415000	-0.68658800	-2.08488000
C	4.06021300	0.80359500	-1.01052500
H	4.32360800	0.28400600	-1.93388300
H	4.89503400	1.46201100	-0.76026500
H	3.18407900	1.43267800	-1.19054300
C	-1.37382900	-0.99922900	-1.50124600
C	3.82710000	-0.15463200	0.15860400
C	2.25356100	-1.87739400	1.03528800
H	2.73494500	-1.56005400	1.96250600
H	2.73125600	-2.81661800	0.73213200
I	0.75267200	3.01356600	-0.08637700
C	-2.18814300	0.05511800	1.18769400
H	-2.80340900	0.17953300	2.08099700
H	-1.54421900	0.95124200	1.13555000
C	-2.29353600	0.15031800	-1.20085600
H	-1.68571200	1.06978200	-1.15959300
H	-2.98291900	0.25235900	-2.03915900
N	-3.06959400	-0.05094400	0.02380300
C	-4.31115600	0.76454700	0.12208300
C	-4.01688000	2.26099900	0.28955700
H	-4.94875100	2.83328000	0.32570700
H	-3.46814200	2.45925500	1.21485400
H	-3.42213000	2.64126900	-0.54640600
C	-5.16362000	0.55094400	-1.13338000
H	-5.25088100	-0.51616700	-1.35873300

H	-6.16675300	0.94948900	-0.96165000
H	-4.76381600	1.06404100	-2.01093000
C	-5.14194300	0.25999900	1.30750000
H	-4.68068300	0.46961700	2.27511900
H	-6.11728900	0.75405200	1.30785300
H	-5.29856300	-0.81918900	1.22487500

4; optimized T_1 geometry:

Total energy -1283.15889659 A.U.

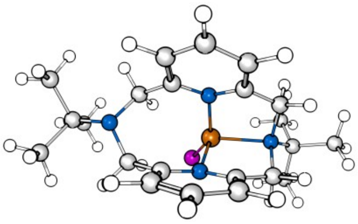

Cu	-0.66991755	0.44292152	-0.21059083
N	-0.02463814	-1.07490511	-1.25806651
N	-0.00465599	-0.71345339	1.31136696
N	-2.54187930	-0.77772706	-0.05087236
C	1.32297271	-1.29827720	-1.35996166
C	1.81501257	-2.56148903	-1.59430039
H	2.88792627	-2.68883472	-1.68879027
C	-0.90307602	-1.70575705	1.56293878
C	-0.87794888	-2.14708575	-1.25453906
C	-3.78737844	0.77717907	-1.50165060
H	-2.94311080	1.47238876	-1.46334660
H	-4.70410481	1.36369700	-1.60083799
H	-3.69661212	0.16791532	-2.40299889
C	-5.03371137	-1.02679695	-0.28142740
H	-4.99131358	-1.66763773	-1.16564173
H	-5.96795433	-0.46142885	-0.32865129
H	-5.07682104	-1.66197412	0.60801937
C	0.84361801	-3.14840317	2.35306405
H	1.17471864	-4.09385605	2.76583511
C	-0.51114437	-2.91316761	2.09782429
H	-1.26040230	-3.67216065	2.29541453
C	0.94460899	-3.65803884	-1.66630273
H	1.32097333	-4.65942096	-1.83609702
C	-0.42298542	-3.42585430	-1.47384188
H	-1.13504924	-4.24433177	-1.47452672
C	1.75955947	-2.14378748	2.03462894
H	2.82455347	-2.28706321	2.18150879
C	-2.34245071	-1.36648294	1.29072838
H	-2.95897456	-2.26316376	1.43048405
H	-2.64846257	-0.62446251	2.02882885
C	-4.06158471	0.91562108	0.94750053
H	-4.35488760	0.40880936	1.86953876
H	-4.86708949	1.60741531	0.69087357
H	-3.15910787	1.50452105	1.13203069
C	1.32147207	-0.94974006	1.49536749
C	-3.85368545	-0.05313929	-0.21813050
C	-2.32739056	-1.81440735	-1.08123828
H	-2.70482000	-1.42628561	-2.02975034
H	-2.88769700	-2.72822107	-0.84952250
I	-0.65486925	2.99368745	0.12335336
C	2.22818009	-0.10132284	-1.23903249
H	2.85840080	-0.06937846	-2.12771836
H	1.60879226	0.81483184	-1.27142211
C	2.28498195	0.15243001	1.13919467
H	1.70860513	1.08736803	1.03593921
H	2.95749249	0.27996147	1.98557132
N	3.08064608	-0.13661171	-0.05374030
C	4.31973933	0.68034593	-0.18614172
C	4.02639449	2.15158339	-0.50804486
H	4.95655103	2.72640767	-0.54292891
H	3.53225858	2.26046464	-1.47761466
H	3.38269289	2.60146915	0.25389710
C	5.12850494	0.59931622	1.11269906
H	5.20823989	-0.43806218	1.45134114
H	6.13703869	0.97940985	0.93265334
H	4.70061207	1.20160474	1.91745736
C	5.19161185	0.06654420	-1.28723715
H	4.74928595	0.15131549	-2.28232119
H	6.15422785	0.58340000	-1.32349705
H	5.37160528	-0.99159631	-1.07772076

S5. X-ray structure determination details.

Crystallographic data for the investigated compounds have been deposited in the Cambridge Crystallographic Data Centre as supplementary publication numbers CCDC 1513688 (**1PF$_6$**), 1513667 (**1BF$_4$**), 1513689 (**2**), 1513690 (**3**), 1513669 (**4**), 1513670 (**5**), 1513671 (**6**).

The X-ray diffraction data for the single crystals were collected on a Rigaku XtaLab PRO instrument (ω-scan mode) using graphite monochromated MoKα radiation (0.71073 Å). The diffractometer was equipped with a Rigaku GN2 low temperature system (air cooling type) and data were collected at -180 °C. The performance mode of the microfocus sealed X-ray tube was 50 kV, 0.60 mA. Suitable crystals of appropriate dimensions were mounted on loops in random orientations. Preliminary unit cell parameters were determined with three sets of total 30 narrow frame scans. Data collection: images were indexed and integrated using CrysAlisPro data reduction package (version 1.171.39.7b, Rigaku Oxford Diffraction, 2015). Analysis of the integrated data did not show any decay. Final cell constants were determined by global refinement of reflections from the complete data set. Data were corrected for systematic errors and absorption using the ABSPACK module. The structures were solved by the intrinsic phasing method using SHELXT-2014/5 and refined by the full matrix least-squares on F^2 using SHELXL-2014/7.[9] Non-hydrogen atoms were refined anisotropically. Hydrogen atoms were inserted at the calculated positions and refined as riding atoms. The crystal data, data collection and structure refinement details for the seven investigated crystals are summarized in Table S2. Some packing details of crystals **2** and **5** are shown in Fig. S54. Molecular structures of investigated complexes in the crystalline phase and accepted partial numbering are presented as ORTEP diagrams in Figures S53-S59.

Interestingly, achiral **1PF$_6$** and **1BF$_4$** crystallize in the Sohncke space group $P2_12_12_1$ of the orthorhombic crystal system. Their crystals are almost isostructural.

Complex **2** crystallizes with an acetonitrile molecule (1:1) (Fig. S55).

Complex **3** is characterized with two molecules A and B in the asymmetric cell (Fig. S56). The cations (two molecules A and two molecules B) form H-bonded tetramers in the crystals.

Fragments of the main residues of **2**, **3**, and **6** and anions of **3** and **6** are disordered. The disorder was resolved using the PART instructions, free variables, and restraints on geometry and anisotropic displacement parameters. In the case of **2** (Fig. S55), both side arms of the ligand are disordered on two (C32-C33(O32)-O31-C34-C35 with occupancy of 0.874(3) and C36-C37(O34)-O33-C38-C39) and three (C142-C143(O142)-O141-C144-C145 with occupancy of 0.575(3), C242-C243(O242)-O241-C244-C245 with occupancy of 0.262(3) and C342-C343(O342)-O341-C344-C345) components.

In the case of **3**, one of two side chains of both main residues are disordered (Fig. S56). The alcohol fragment of the symmetrically independent molecule A is disordered on three components (C43A-O41A with occupancy of 0.473(3), C44A-O42A with occupancy of 0.280(3) and C45A-O43A). The analogous fragment of the symmetrically independent molecule B is disordered on four components (C42B-C43B-O41B with occupancy of 0.346(3), C44B-C45B-O42B with occupancy of 0.314(3), C46B-C47B-O43B with occupancy of 0.208(3) and C48B-C49B-O44B). One of two hexafluorophosphate anions is almost equally disordered on four components.

In the case of binuclear complex **6** (Fig. S59), the pyridinophane ligand chemically bound to Cu2 is disordered on two components (their atoms are marked with number 1 or 2 as last symbol in labels, respectively). Occupancy of main component is 0.550(15). The two aryl rings and trifluoromethyl groups of the BArF anion are highly disordered as well.

Table S2. Crystallographic data summary for complexes **1**-**6**.

Compound	**1PF$_6$**	**1BF$_4$**	**2**	**3**	**4**	**5**	**6**
File name	gfe097	gfe094	jk108	jk091	jk068	jk069	jk107
Formula	$C_{24}H_{35}CuF_6N_5P$	$C_{24}H_{35}BCuF_4N_5$	$C_{28}H_{38}CuF_6N_6O_4P$	$C_{22}H_{31}CuF_6N_5O_2P$	$C_{22}H_{32}CuIN_4$	$C_{24}H_{32}CuIN_4O_4$	$C_{76}H_{76}BCu_2F_{24}IN_8$
Colour	orange	orange	yellow	orange	orange	yellow	green
Formula weight	602.08	543.92	731.15	606.03	542.95	630.97	1822.23
Crystal system	orthorhombic	orthorhombic	triclinic	monoclinic	monoclinic	triclinic	triclinic
Space group	$P2_12_12_1$	$P2_12_12_1$	P-1	$P2_1/c$	$I2/a$	P-1	P-1
Cell parameters: *a*, *b*, *c* (Å) and α, β, γ (deg)	9.21714(18), 11.1644(2), 25.8510(6) and 90, 90, 90	9.2282(3), 10.7038(3), 25.8222(8) and 90, 90, 90	10.3221(8), 12.5539(11), 13.3412(9) and 96.242(6), 97.713(6), 111.660(8)	20.8422(5), 22.3058(5), 11.2544(3) and 90, 94.493(3), 90	18.0389(4), 10.7179(3), 23.2190(6) and 90, 95.190(2), 90	9.8894(3), 11.0273(3), 12.5448(3) and 76.939(2), 71.011(2), 82.147(2)	12.58365(19), 17.6541(3), 18.0319(3) and 79.3917(14), 84.4139(13), 87.6240(13)
Volume, Å^3	2660.17(10)	2550.63(14)	1568.5(2)	5216.1(2)	4470.75(19)	1257.18(6)	3917.54(11)
Z and *Z′*	4 and 1	4 and 1	2 and 1	8 and 2	8 and 1	2 and 1	2 and 1
Calculated density, g cm^{-3}	1.503	1.416	1.548	1.543	1.613	1.667	1.545
Absorption coefficient, mm^{-1}	0.947	0.908	0.828	0.972	2.373	2.134	1.042
F(000)	1248	1136	756	2496	2192	636	1840
Crystal size, mm^3	0.160 x 0.190 x 0.200	0.170 x 0.180 x 0.300	0.056 x 0.088 x 0.186	0.128 x 0.140 x 0.248	0.082 x 0.114 x 0.140	0.086 x 0.117 x 0.132	0.041 x 0.088 x 0.098

Table S2 (continues). Crystallographic data summary for complexes **1**-**6**.

Θ range, deg	2.346 to 25.449	2.914 to 25.548	2.757 to 25.599	2.910 to 26.049	2.743 to 25.598	2.345 to 25.799	2.700 to 26.398
Index ranges	$-10 \le h \le 11$, $-12 \le k \le 13$, $-31 \le l \le 31$	$-11 \le h \le 10$, $-12 \le k \le 12$, $-30 \le l \le 31$	$-12 \le h \le 12$, $-15 \le k \le 15$, $-16 \le l \le 16$	$-25 \le h \le 25$, $-27 \le k \le 27$, $-13 \le l \le 13$	$-21 \le h \le 21$, $-13 \le k \le 13$, $-28 \le l \le 28$	$-11 \le h \le 12$, $-13 \le k \le 13$, $-15 \le l \le 15$	$-15 \le h \le 15$, $-22 \le k \le 22$, $-22 \le l \le 22$
Measured and independent reflections [R(int)]	27476 and 4918 [0.0322]	17024 and 4708 [0.0266]	24976 and 5879 [0.0497]	60210 and 10274 [0.0559]	18307 and 4204 [0.0364]	16037 and 4819 [0.0334]	78129 and 16040 [0.0334]
Observed Data [$I > 2\sigma(I)$]	4818	4627	5153	9063	3989	4540	14404
Completeness to Θ = 25.242°, %	99.9	99.2	99.8	99.8	99.8	99.8	99.8
Data, restraints, parameters	4918, 15, 341	4708, 0, 323	5879, 767, 577	10274, 1901, 976	4204, 0, 259	4819, 0, 309	16040, 2795, 1497
Goodness-of-fit on F^2	1.043	1.050	1.059	1.030	1.055	1.041	1.032
$R1$ and $wR2$ indices [$I > 2\sigma(I)$]	0.0244 and 0.0631	0.0195 and 0.0508	0.0435 and 0.1171	0.0356 and 0.0880	0.0202 and 0.0495	0.0210 and 0.0513	0.0238 and 0.0572
$R1$ and $wR2$ indices (all data)	0.0249 and 0.0634	0.0199 and 0.0510	0.0501 and 0.1219	0.0414 and 0.0909	0.0218 and 0.0502	0.0226 and 0.0520	0.0282 and 0.0589
Absolute structure parameter	-0.003(3)	-0.007(4)	n/a	n/a	n/a	n/a	n/a
Largest diff. hole and peak, e Å^{-3}	-0.397 and 0.607	-0.194 and 0.255	-0.670 and 0.784	-0.404 and 0.723	-0.437 and 0.344	-0.473 and 0.405	-0.440 and 0.624

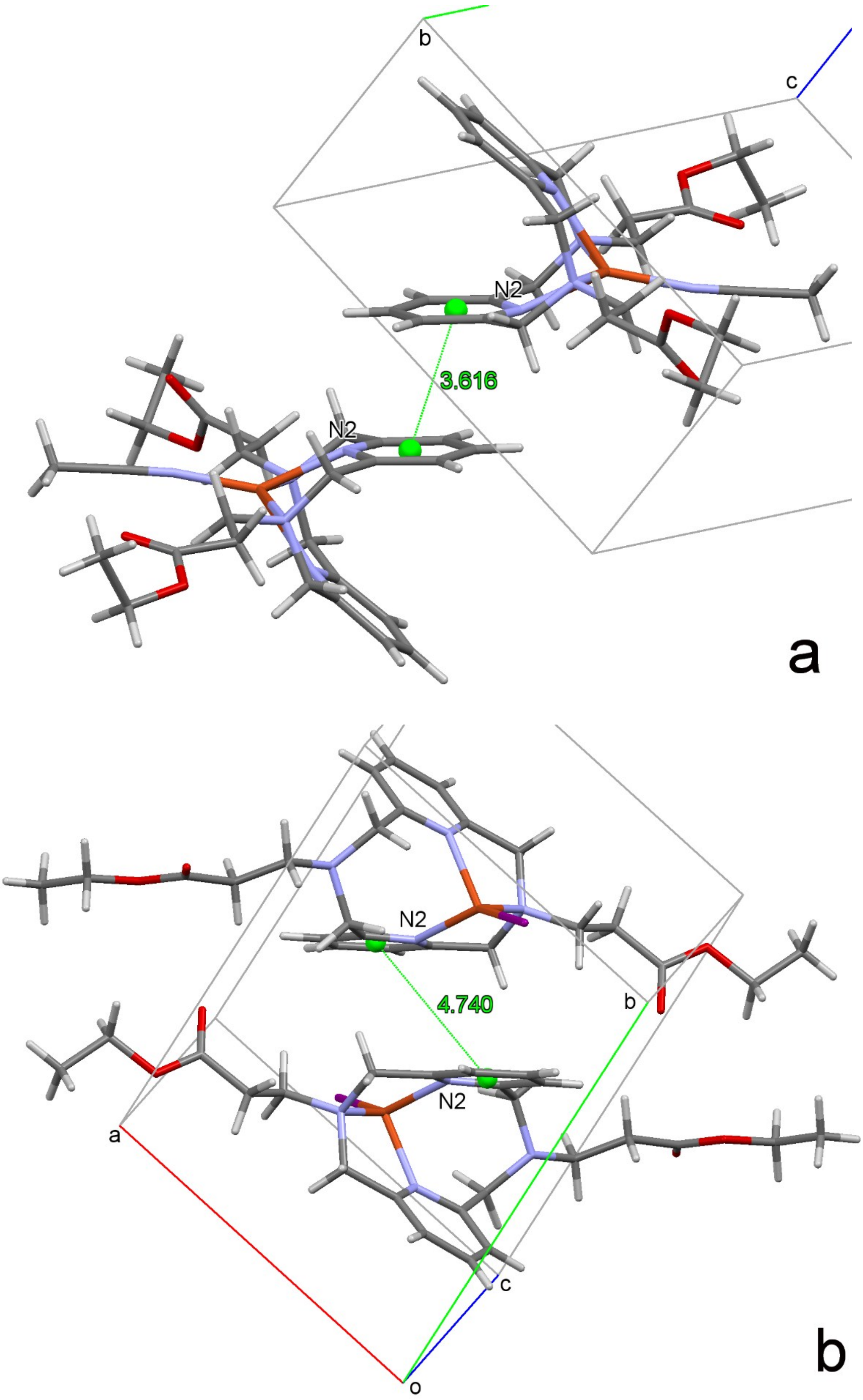

Figure S52. Illustration of the shortest intermolecular Py-Py distances in complexes **2** (a) and **5** (b). Centroids of pyridine rings and distances between them are indicated. Minor components of disordered moieties, anions and acetonitrile molecules are omitted in the case of compound **2**.

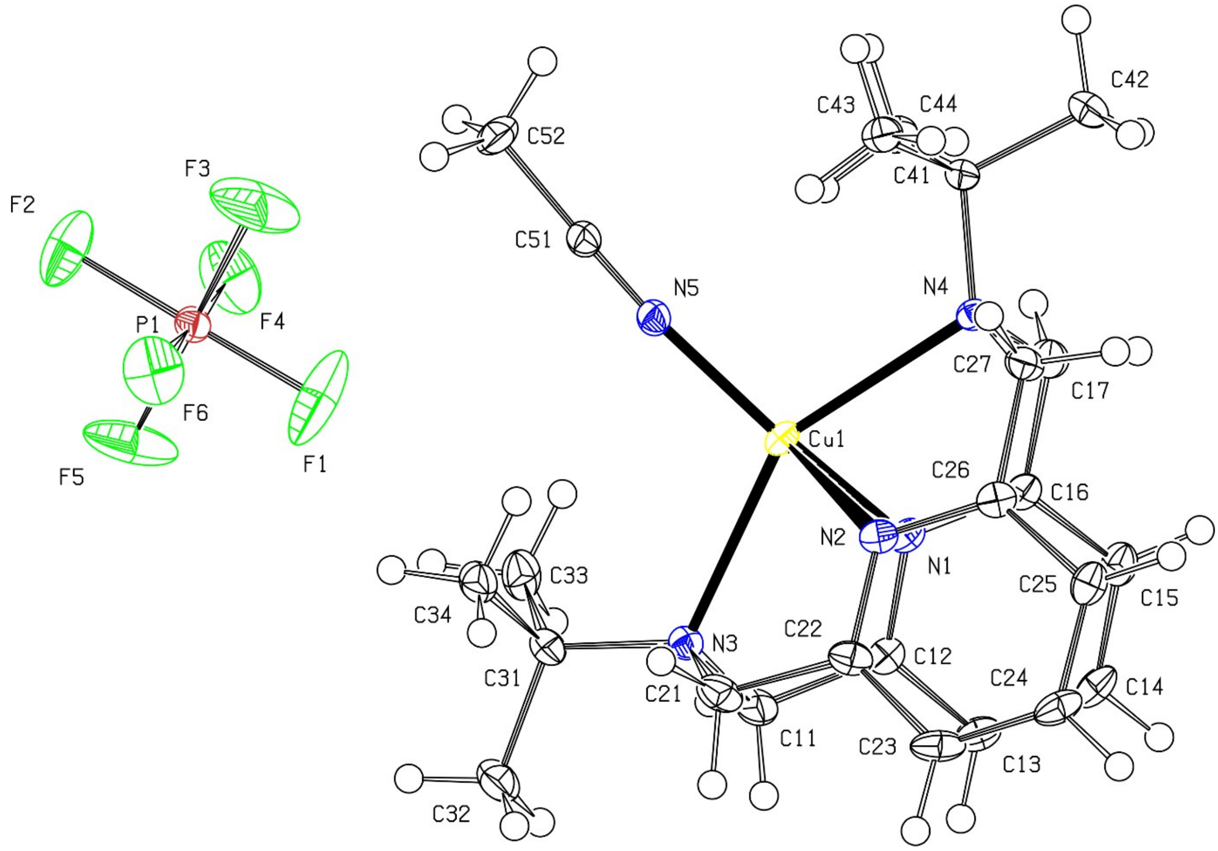

Figure S53. ORTEP diagram showing 50 % probability anisotropic displacement ellipsoids of non-hydrogen atoms for complex **1PF$_6$** in crystals.

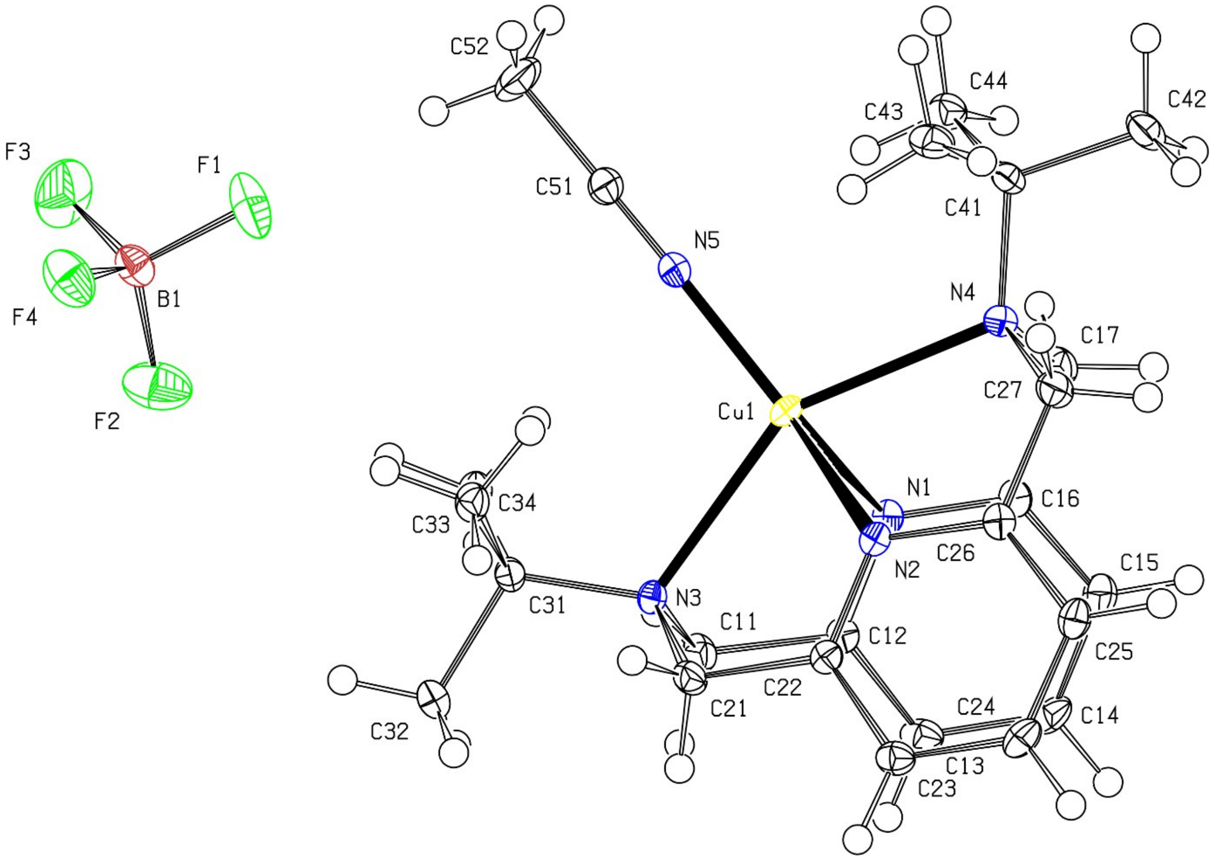

Figure S54. ORTEP diagram showing 50 % probability anisotropic displacement ellipsoids of non-hydrogen atoms for complex **1BF$_4$** in crystals.

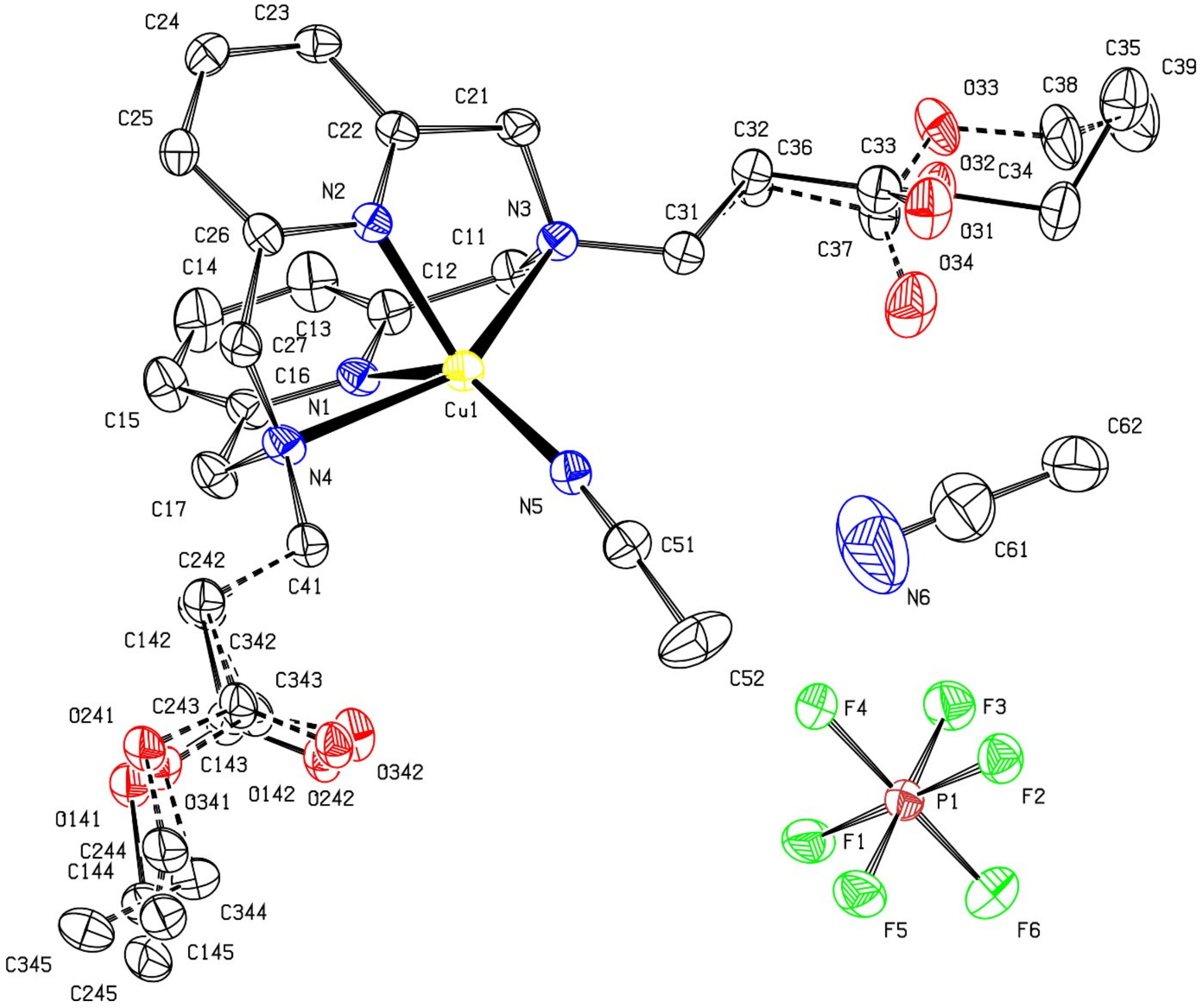

Figure S55. ORTEP diagram showing 50 % probability anisotropic displacement ellipsoids of atoms for acetonitrile solvate of complex **2** in crystals. The hydrogen atoms are omitted for clarity.

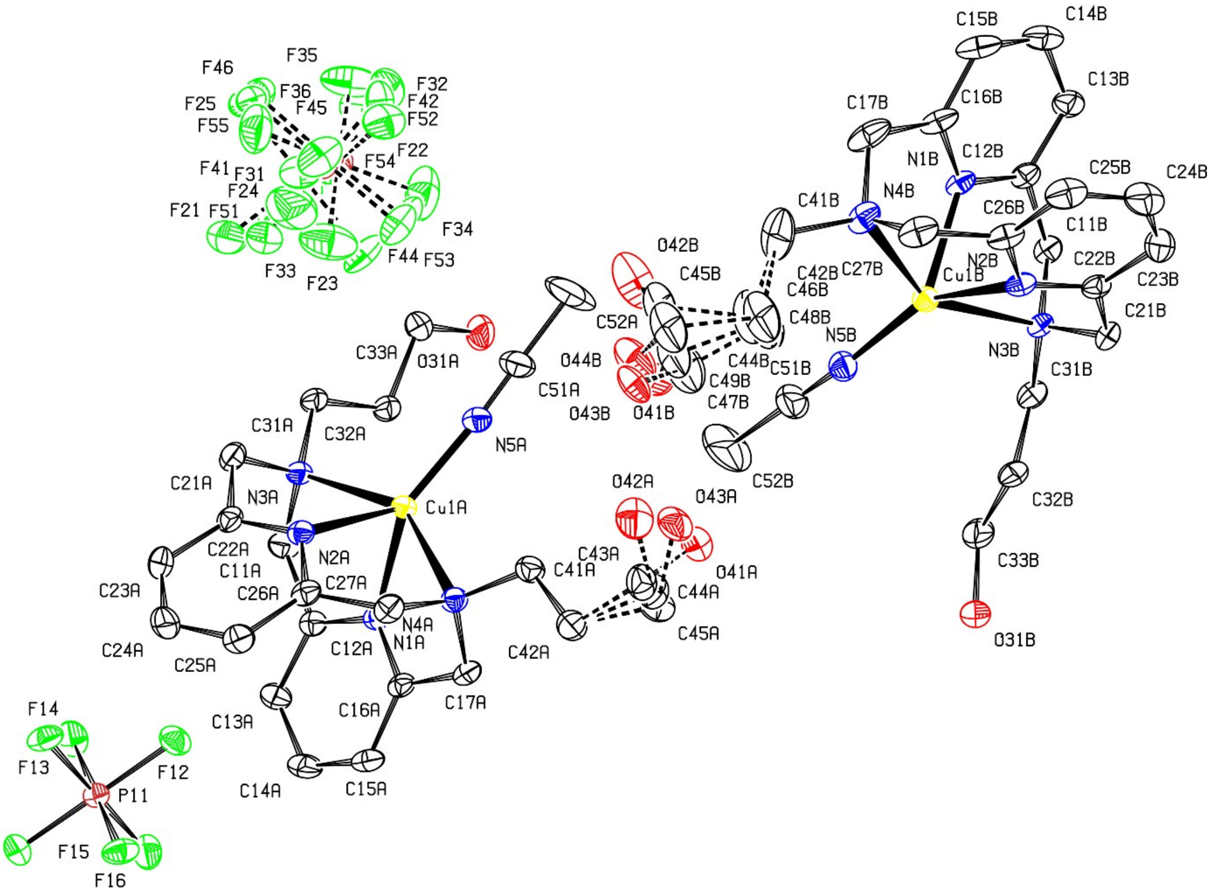

Figure S56. ORTEP diagram showing 50 % probability anisotropic displacement ellipsoids of atoms for both symmetrically independent molecules of the unit cell in complex **3** crystals. The hydrogen atoms are omitted for clarity.

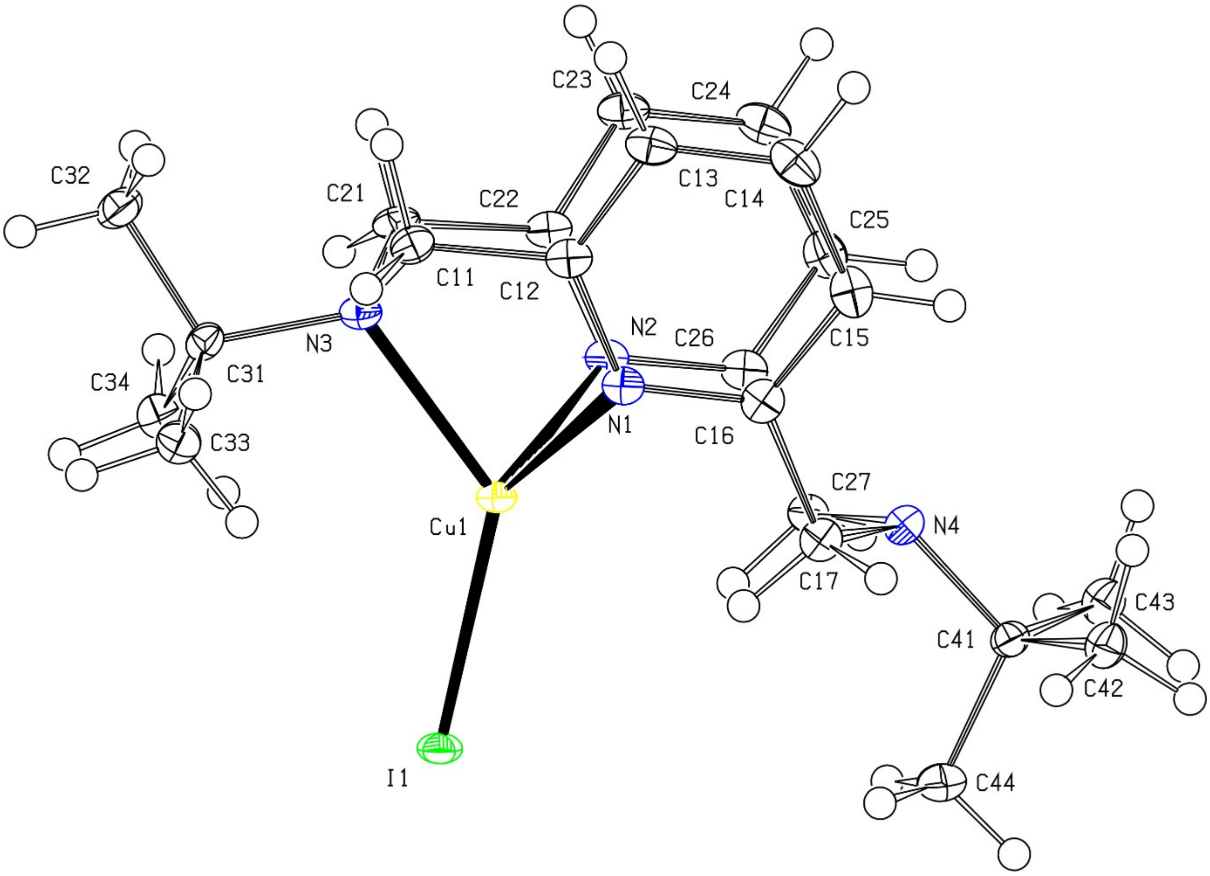

Figure S57. ORTEP diagram showing 50 % probability anisotropic displacement ellipsoids of non-hydrogen atoms for complex **4** in crystals.

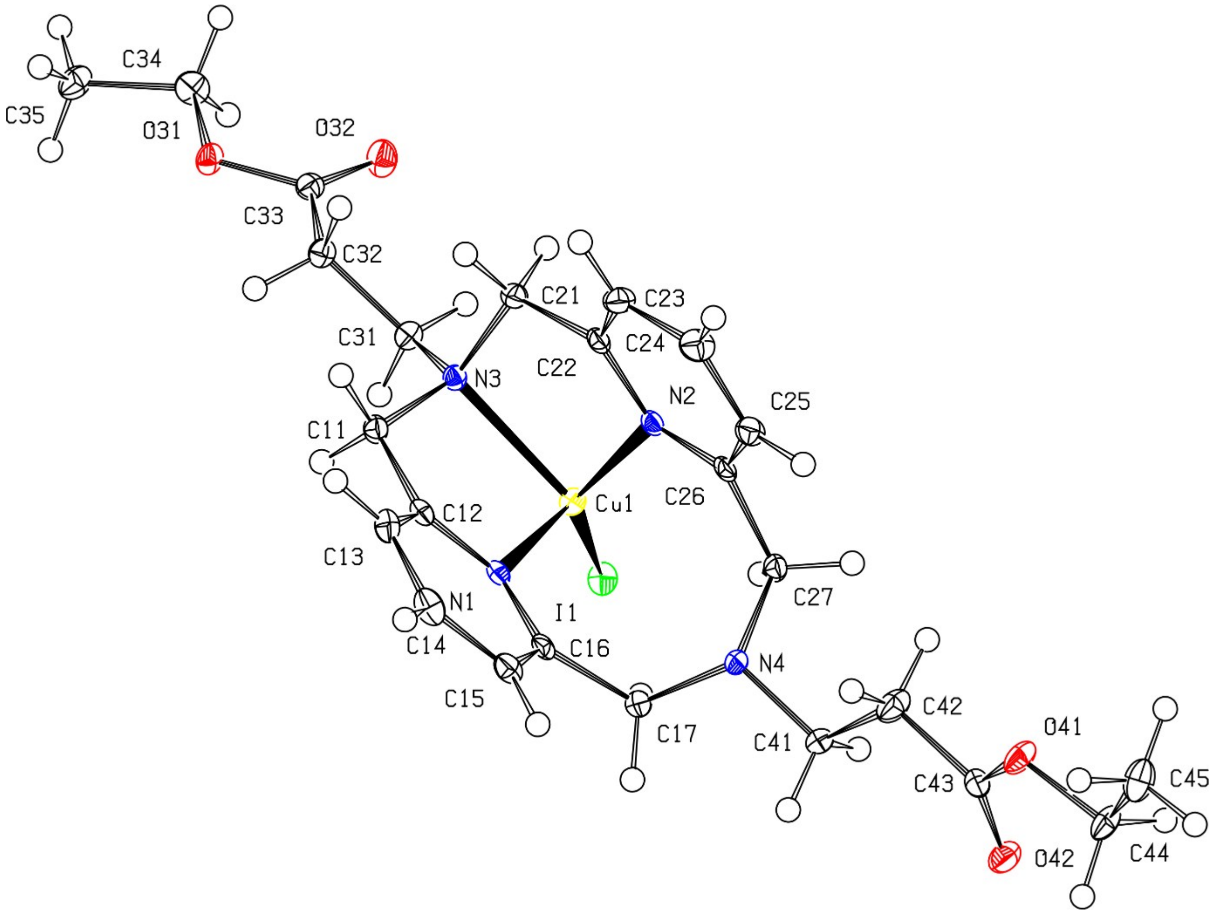

Figure S58. ORTEP diagram showing 50 % probability anisotropic displacement ellipsoids of non-hydrogen atoms for complex **5** in crystals.

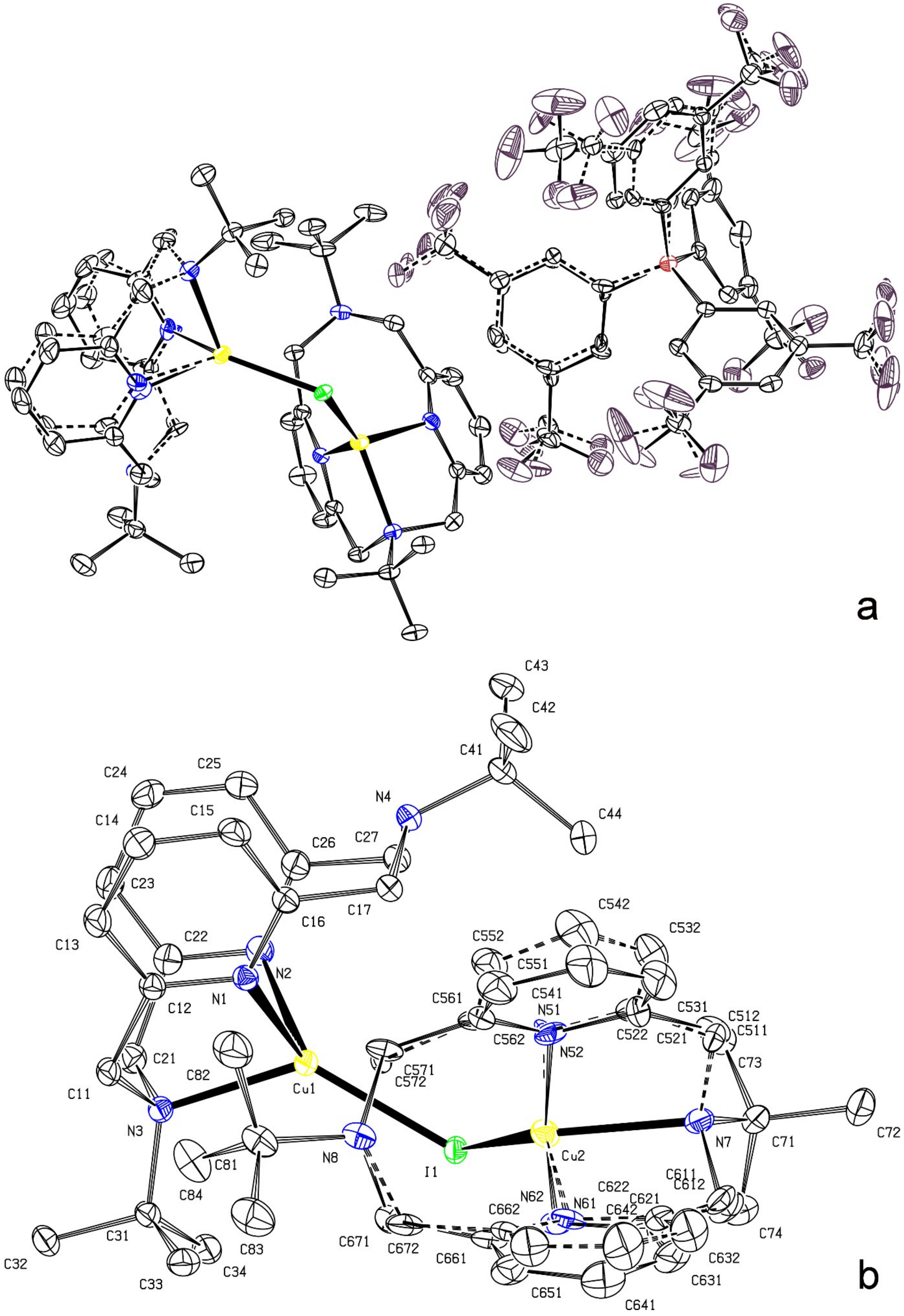

Figure S59. ORTEP diagram showing 50 % probability anisotropic displacement ellipsoids of atoms for complex **6** (a) and binuclear cation (b) in crystals. The hydrogen atoms are omitted for clarity.

S6. References:

1) Che, C.-M.; Li, Z.-Y.; Wong, K.-Y.; Poon, C.-K.; Mak, T. C. W.; Peng, S.-M. *Polyhedron* **1994**, *13*, 771.

2) Bottino, F.; Di Grazia, M.; Finocchiaro, P.; Fronczek, F. R.; Mamo, A.; Pappalardo, S. *J. Org. Chem.* **1988**, *53*, 3521.

3) Yakelis, N. A.; Bergman, R. G. *Organometallics* **2005**, *24*, 3579.

4) Kubas, G. J.; Monzyk, B.; Crumblis, A. L. In *Inor. Synth.*; John Wiley & Sons, Inc.: **2007**, 68.

5) Meneghetti, S. P.; Lutz, P. J.; Kress, J. *Organometallics* **2001**, *20*, 5050.

6) Adamo, C.; Barone, V. *J. Chem. Phys.* **1999**, *110*, 6158.

7) Frisch, M. J.; Trucks, G. W.; Schlegel, H. B.; Scuseria, G. E.; Robb, M. A.; Cheeseman, J. R.; Scalmani, G.; Barone, V.; Mennucci, B.; Petersson, G. A.; Nakatsuji, H.; Caricato, M.; Li, X.; Hratchian, H. P.; Izmaylov, A. F.; Bloino, J.; Zheng, G.; Sonnenberg, J. L.; Hada, M.; Ehara, M.; Toyota, K.; Fukuda, R.; Hasegawa, J.; Ishida, M.; Nakajima, T.; Honda, Y.; Kitao, O.; Nakai, H.; Vreven, T.; Montgomery, J. A., Jr.; Peralta, J. E.; Ogliaro, F.; Bearpark, M.; Heyd, J. J.; Brothers, E.; Kudin, K. N.; Staroverov, V. N.; Kobayashi, R.; Normand, J.; Raghavachari, K.; Rendell, A.; Burant, J. C.; Iyengar, S. S.; Tomasi, J.; Cossi, M.; Rega, N.; Millam, N. J.; Klene, M.; Knox, J. E.; Cross, J. B.; Bakken, V.; Adamo, C.; Jaramillo, J.; Gomperts, R.; Stratmann, R. E.; Yazyev, O.; Austin, A. J.; Cammi, R.; Pomelli, C.; Ochterski, J. W.; Martin, R. L.; Morokuma, K.; Zakrzewski, V. G.; Voth, G. A.; Salvador, P.; Dannenberg, J. J.; Dapprich, S.; Daniels, A. D.; Farkas, Ö.; Foresman, J. B.; Ortiz, J. V.; Cioslowski, J.; Fox, D. J.; Gaussian, Inc.: Wallingford CT, 2009.

8) O'Boyle, N. M.; Tenderholt, A. L.; Langner, K. M. *J. Comput. Chem.* **2008**, *29*, 839.

9) Sheldrick, G. M. *Acta Cryst. A* **2008**, *64*, 112.